Università degli studi di Napoli

"Federico II"

SCUOLA DI DOTTORATO IN INGEGNERIA NAVALE, AEROSPAZIALE E DELLA QUALITA'

XXIV CICLO

Experimental Study on Interceptor's Effectiveness

TUTOR CANDIDATE

Prof. CLAUDIO PENSA *Eng. FABIO DE LUCA*

NOVEMBER 2011

Contents

List of figures

List of tables

1. Introduction

The use of Interceptor on both partial or total dynamic lift crafts has been widespread for some time now. It has always been considered as an alternative to flaps and there is large evidence in literature about its higher effectiveness. The interceptor consists of a thin plate jutting out of the craft of a percentage generally between 1.5 and 4 ‰ of the L_{WL} and it's located on the sternmost part of the bottom. Its role is to exert an overpressure able to lift the stern and consequently to change the trim. It's often used as regular device on crafts sailing at a low relative speed and as a movable device on speed boats.

The usual area of applicability is the one of partial or total hydrodynamic lift. During recent years, relevant advantages have been reported about its use at lower relative speeds, such as those of speed crafts with hydrostatic buoyancy.

Although already quite widespread, there is no sound evidence in literature reporting a quantitative evaluation of the advantages of the use of Interceptors, in terms of hull resistance.

The work carried out for this thesis conveys a great number of experimental data based on the variation of speed, trim, displacement, deadrise angle, considering different dimensions of the device. Furthermore, new geometries of interceptors are proposed that have lead to significant results.

An attempt is here made to go deep into the knowledge of the dynamics of the physical model and to propose explanatory observations.

2. Structure of the Thesis

Chapter 3

Chapter 3 shows some useful strategies to deal with the problem and the study tools traditionally used in literature for the assessment of the Interceptor's effectiveness.

Chapter 4

This chapter gives an outline of the physical principles behind the planing hulls, through the linear theory of planing applied to indefinite flat plate. Thus, based on the knowledge acquired through the several experimental tests carried out, the base principles behind the functioning of interceptors are described. Starting from the knowledge of the basic mechanisms we've proven the experimental tests carried out on non conventional geometries, thus enhancing the same features of the interceptor for some working conditions of the hulls.

Chapter 5

Ch 5 briefly describes the towing tank and the tools used.

Chapter 6

This Chapter introduces the models chosen for the tests, the choice criteria and the strategies for correlation and comparison of data.

Chapter 7

Chapter 7 presents the data collected through experimental tests carried out on models equipped with conventional interceptors.

Chapter 8

This chapter shows the two non-conventional geometries introduced in chapter 4.

Chapter 9

The test on prismatic models has been based on models with a very low Lcg/Lwl ratio, this could lead us to imagine that the good effectiveness reported may be due to unfavourable reference conditions of the bare hull. In this chapter we've introduced a new reference word, that is BPE. BPE (Best Performance Envelope) is the curve of token resistance that takes into account the best possible performances of the bare hull (in function of the Lcg) at any speed. This virtual feature of the functioning of the hull, as for standard tests, has been used as reference point, in this case a stricter one, of the performance of hulls with interceptors.

Chapter 10

The work accomplished has shown that the interceptor affects the hull, both in terms of lift and of change of trim. Tests have been thus carried out constraining first the trim and then both trim and draught. In this way, it was made possible to study the two effects separately and to quantify their influence.

Chapter 11

This chapter briefly describes the main experimental troubles usually encountered whit standard towing trials and the standard procedures proposed by ITTC for the evaluation of mistakes. Then, the problem of the unreliability of the tests made on interceptors has been outlined by carrying out an analysis of the quality of tests with interceptors set on. The non fully conventional tests introduced in the previous chapter, can be dealt with by using different strategies. These different modes that can be used to perform this kind of test are then described as well as the related difficulties. In conclusion, the choices made during the tests are explained.

Chapter 12

As already explained in the introduction, interceptor is widely used on displacement hulls. The functioning principles of this kind of hulls are different, since they're not affected by the increase of lift.

The part of the study on displacement hulls is quite less thorough than that on hydrodynamic lift hulls. Since data used for the analysis come from the DIN data bank, no specific tests have been performed.

Nevertheless, the analysis proposed conveys a reliable evidence of the higher effectiveness of interceptors compared to that of the flaps and of ducktails.

Chapter 13

In chapter 13 a comment is made about the reference articles relevant to this work.

3. Study tools

Two different approaches can be used in order to deal with the problem of evaluation of the effects of this kind of device, a numerical and an experimental one.

Several are the possible numerical procedures, although those mainly used in the naval sector are the panel model or the RANSE codes: the panel model makes it possible to solve the potential flow around the hull, but it is not suitable for the evaluation of the effects of viscosity and so those of interceptor, since it operates within the boundary layer where phenomena of viscosity occur. This is the reason why the best suitable solution when choosing a numerical approach is to use RANSE (Reynolds Averaged Navier-Stokes Equations) codes, which are based on the numerical solution of Navier-Stokes equations, thus allowing a calculation of the effects of viscosity to detriment of the time required for calculation that is considerably longer with this kind of codes.

When solving a naval problem by using computational fluid dynamics, it's indispensable to deal with the description of the separation of the two liquids, air-water. In order to solve this kind of problems the VOF (volume of fluid method) is applied.

VOF is a numerical method to trace and localize the free-flowing surface (or liquid-liquid interface) and belongs to the class of Euler methods, that feature a fixed mesh or movable one in a certain prefixed way, in order to follow the evolving shape of the interface between different liquids. As such, VOF is defined as an advection scheme, that is a numerical tool enabling the programmers to monitor shape and position of the free-flowing

surface. The solution of the advection algorithms requires the solution of the Nevier-Stokes equations separately, describing the movement of different fluids.

As previously mentioned, interceptor is a small size device located near the hull surface and, so, when choosing the numerical approach to describe the behaviours of this device, a near-wall approach is required in order to appropriately build the mesh close to the device.

An in-depth study of the effects of the interceptor applied to hulls by using the computational fluid dynamics would require the choice of a 3 DOF model (deg. of freedom) that, considered what mentioned so far, would demand higher power and calculation time.

The analysis of interceptor with RANSE codes has evidences in literature mainly through simplified 2D plate models, both orthogonal to the flow [3] and with the angles of incidence [18] in order to understand the physics of the device; successive developments have than introduced 3D constrained models allowing an assessment of the effects on geometries more similar to those actually used and allowing the assessment of the 3D effects of the flow field and the boundary effects, as well [5].

In this study we've chosen an experimental approach. The towing tank tests represent certainly the most reliable procedure for resistance prediction. Despite the many unsolved problems when dealing with the scale effect, they are frequently used (both in the field of research and industrial one) to assess the effectiveness of the trim correction devices, such as flaps, ducktails and interceptors.

In the industrial sector, very often, models for tank tests used for the assessment of the resistance of bare hull, are already available, thus

making it particularly cost-effective to set an interceptor to optimize its performances.

Mainly two are the articles [6] [7] dealing with the experimental study of the interceptors behaviour and introducing some interesting features, both in terms of efficacy and effectiveness, that have lead to the interest toward a more in-depth analysis of the behaviour of this device.

The need for a better knowledge of the physics of interceptors is confirmed by a research line on interceptors used to control pitching and yaw. Just as an example, in [14] M.J.H. , in order to direct the behaviour of interceptors employed to control the craft, had to use the Dawson and Blount [2] procedure to assess the action of the device, that, basically, compares these to the flaps. Nevertheless, this kind of procedure does not really take into account the main features of interceptors.

4. Physical model and functioning principle

This chapter roughs out the basic functioning of the planing hulls, in order to better describe the mechanisms the interceptor acts on. The basic principles of the device are then described.

4.1 Synthesis of the resistance models and the planing hulls

Before describing the physical behaviour of the flow field around the hulls with the interceptor, a brief introduction of the classical models may be useful to describe the behaviour of hulls, with a special focus on the partial or total hydrodynamic lift hulls, which are those reporting the highest advantages from the use of interceptors.

The nature of the forces operating in the flow around hulls is something quite articulated. Ships are actually means of transportation balanced between two liquids and, exactly because of this separation between the two liquids, resistances due to forces of a different nature are generated.

There are three main forces at play: viscous, inertial and gravitational. In order to simplify the complexity of the physical model, the forces due to the surface tension are not taken into account here. When evaluating resistances, usually a resolution of the effects is operated, which are matched to the fundamental values according to the nature of the forces at play. The resolution of resistances into different parts leads necessarily to some mistakes in terms of mutual interaction of forces of a different nature.

First, there should be a resolution of resistance into two parts: a component linked to viscosity phenomena, causing viscous resistance and a second one linked to gravitational phenomena and causing wave resistance.

The forces with a viscose nature depend, obviously, on viscosity as well as on the shape of the ship, as any other component of resistance. The wave drag is linked to the energy dispelled by the pressure gradients active close to the free surface and is released through the wave systems generated on the surface. It's evident that the two components are independent from each other: just considering the wave formation close to the hull initiating not only a variation of the wetted surface, but also of the speed ranges.

As already mentioned, the hull is a body balanced between two liquids, this means that an increase of the relative speed proportionally causes the pressures responsible of the wave resistance to impact on the balance of the hull, which shifts from a mere hydrostatic lift to a more and more dynamic equilibrium.

Once reached a status with a significant hydrodynamic lift, the dependence between the hull resistance and the lift is even higher. The reason for this is that the nature of the forces generating the wave drag and the lift is the same. And so an increase in speed corresponds to an increase of both the lift and the dynamic planing of the hull. In addition to this, a virtuous circle linked to the hull rise occurs: as said, the wave drag is correlated to the volumes close to the free surface and these are clearly reduced due to dynamic lift.

As a matter of fact, when dealing with pressures, the mechanisms above described depend not only on speed, but also on the shape, the size and the lying position of the surfaces of the hull; for instance, it's evident that a blade sailing on water, whatever its speed may be, will never enjoy a hydrodynamic lift, nor will generate a relevant wave system.

The contrary is true for a flat plate sailing on a liquid surface. Indeed, the first theory of planing has been developed from the study of the behaviour of an indefinite flat plate. Two theories are described in literature, a linear and a non-linear one; only the linear theory is here proposed because of its simplicity and efficacy.

The flat plate by definition has no volume and so it is in a purely hydrodynamic equilibrium: if W is the weight of the plate, L the hydrodynamic lift and Ry the vertical component of the integral of the pressures, then we'll have

$Ry = L = W$.

As mentioned for the general case, forces with a viscous nature act on the plate, alongside with forces linked to pressures initiated by the plate sailing on the free surface. By using the simplified model of the flat plate, the viscous forces are turned into pure friction forces, Rt, tangent to the plate and turn the resultant of the pressure range into a component orthogonal to the plate. This, in addition to the fact that the plate is intended to be fully lifted by hydrodynamic pressures, leads us to the Sottorf formula reported in 1 with reference to Figure 1.

1 Sottorf formula:

$$Rx = W\ tg\tau + Rt/cos\tau$$

The Sottorf formula clearly shows the effects of the longitudinal trim on the resistance due to the lift. It should also be considered that the Rt component depends on the size of the wetted surface; the smaller the trim, the higher it will be.

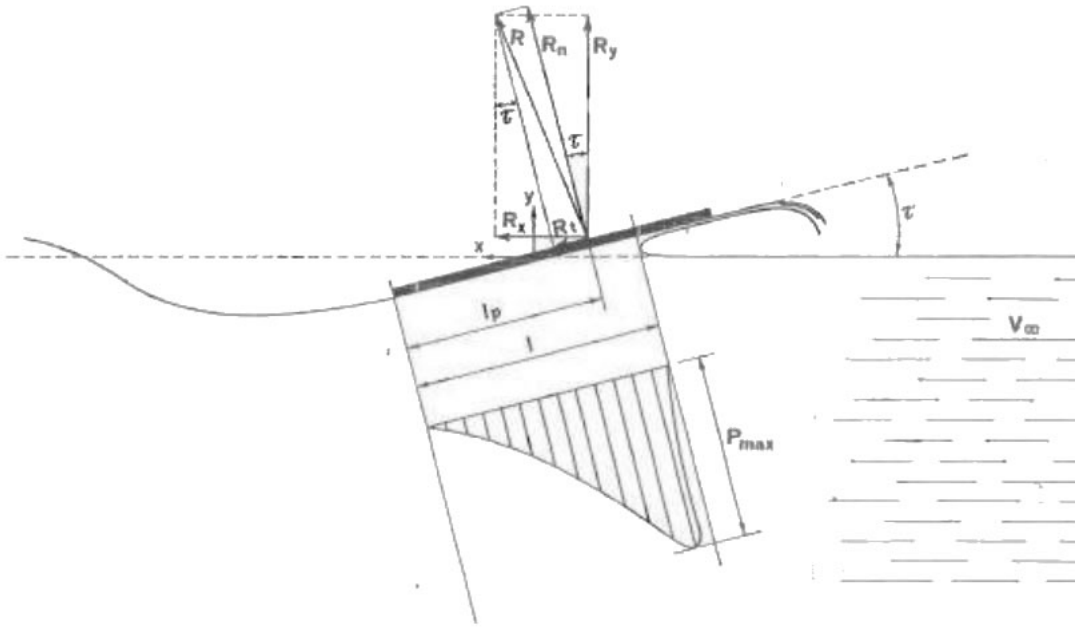

Figure 1 – Forces applied on a flat plate.

When shifting from an indefinite plate to a plate with definite size, a transversal pressure gradient due to the continuity and the congruency of the same on the edges of the plate is determined on its bottom. These gradients are responsible of the three-dimensional nature of the flow. In a kinematic perspective this leads to a divergent streamline, shown in the following figure.

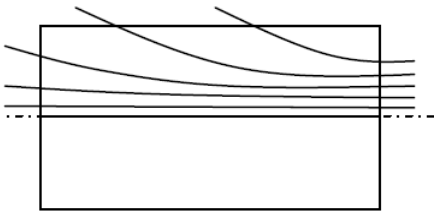

Figure 2 – Transversal flow scheme.

The simplified model of the flat plate, although not corresponding to the actual physics of planing hulls, is useful to describe the main dependence between resistance, lift and trims of a high speed craft, which are fundamental principles in order to understand the physical model behind the

hydrodynamic functioning of interceptor and its interactions with the dynamics of hull.

More structured models, similar to that of an hydrodynamic lift hull have been developed, such as the one with a V-shaped plate introducing a system allowing an evaluation of resistances and trims while solving the equilibrium between moments and forces with experimental formulas (Savitsky method, short form and long form).

4.2 Functioning Principle of interceptor

The functioning principle of interceptors consists in the generation of overpressures initiated by a sudden variation in the flow caused by the use of a thin plate. This, located orthogonally to the free flow by the transom, creates an area of stagnation with strong local increases in pressure.

.

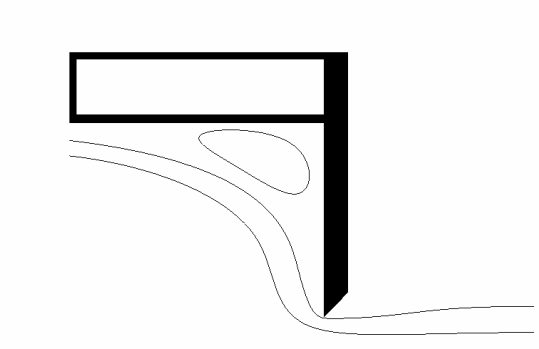

Figure 3 – Flow around the interceptor.

The idea behind this rises from a device used in aeronautics, whose name is Gurney flap; this device, geometrically totally similar to the interceptor, has the function of containing the pressures on the upstream side of the aerofoils, thus increasing the integral of the pressures

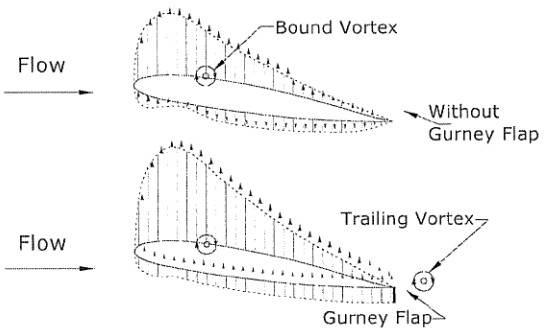

Figure 4 – Figure from Mancini Morioni [6].

The invention owes its name to Dan Gurney, a race car pilot during the 60's, and it was used to strengthen the adhesion of cars. There are also similar components dating back to the 30's and developed by E.F. Zaparka and Gruschwitz and Schrenk.

The principle behind it, is a variation of the Kutta-Joukowsky condition, obtained by creating a small gap and two counter-rotating vortices downstream the aerofoils. This device is often assigned the capacity to keep the flow adhering to surfaces of the aerofoil, thus allowing wider half entrance angles without determining a streamline separation and so a stall.

In the naval sector, the functioning principle is a different one, since we deal with a separation of the two liquids downstream the device.

The device is located orthogonally to the flow on the bottom of the hull by the stern. In order to understand its functioning, as already done previously, the 2D model of a flat plate should be considered, where the interceptors are set.

If we consider Figure 5 (from De Luca F. et al [18]), it shows an indefinite flat plate sailing on the free surface with a 2 deg half entrance angle. The figure shows what follows:

- a slowdown of the speed range near the hull,
- The generation of a closed vortex at the base of the device,

- a curvature and consequently a deviation downwards of the streamlines.

The slowdown of the speeds range is combined to an increase in pressures that will be added up to the natural trend of pressures on the bottom of the hull.

The pressure range exerted on the surface of the device will also generate some parasite drag, but of a limited extent, seen the small extension of the interceptor. The closed vortex will also contribute to dissipate energy and to the related increase in hull resistance.

The variation of the momentum due to the deviation of the streamline, causes a reaction leading to an increase in the pressures on the bottom of the hull. This increase in pressures will be responsible of the trim and lift variations.

It's worth here highlighting that both the effects lead, within a wider interest speed range, to a reduction of hull resistance:

- the reductions of trim produce some resistance reduction, as synthesized in the Sottorf formula.
- the increase of the dynamic lift produces a reduction of the immersed volume and subsequently the surface of interaction of the pressures (determining the wave formation) and of the tangential forces (friction).

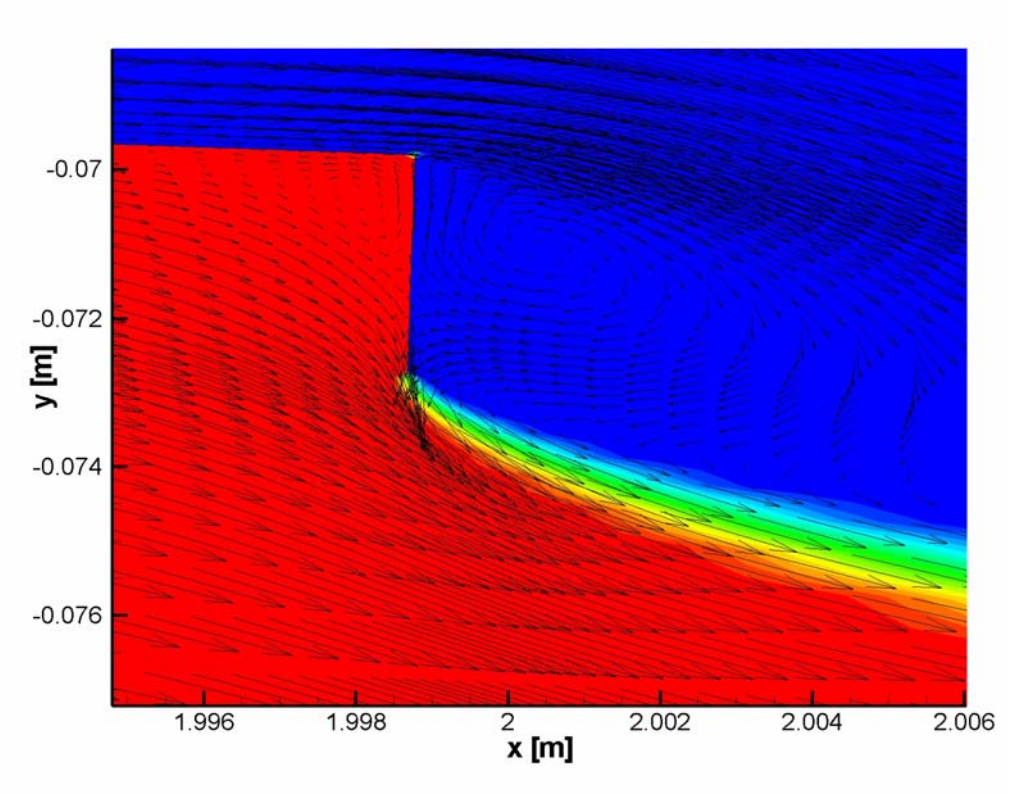

Figure 5 – Flow around the interceptor.

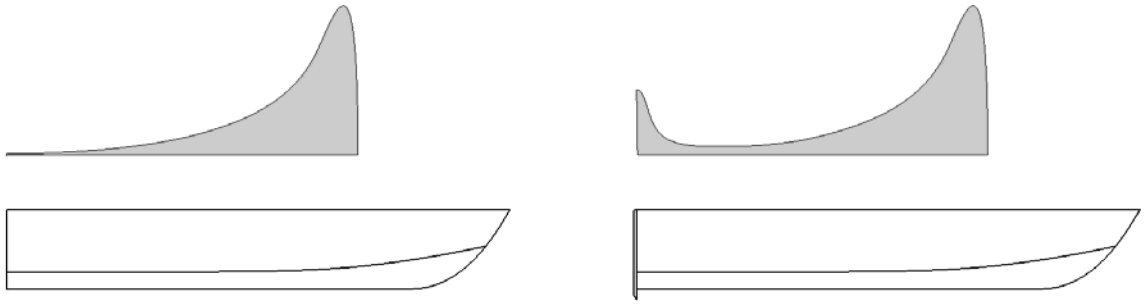

Figure 6 – Bottom pressure with and without interceptor.

What described so far, is clearly outlined in the results contained in Brizzolara, Villa [5] and in De luca, Pensa, Pranzitelli [18] showing that the device contributes to a significant variation of the pressure range upstream the device.

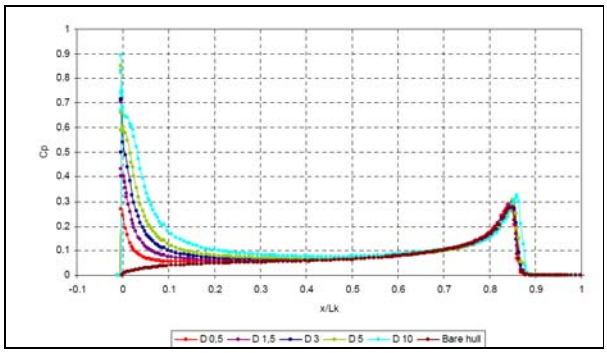

Figure 7 – C_P behaviour on a flat plate from Brizzolara et al [5].

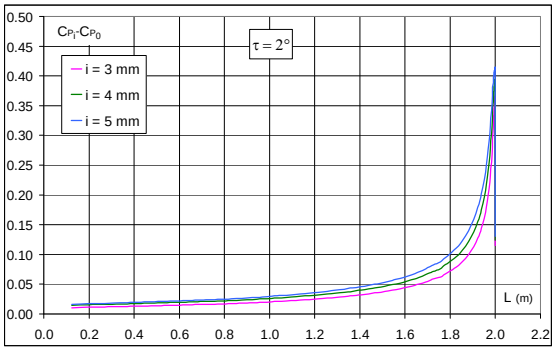

Figure 8 – (C_{P_i} – C_P) behaviour on a flat plate from De Luca et al [18].

The chart in Figure 7 shows the curve of the pressure coefficient of the flat plate with an incidence different from zero and the pressure coefficients when the device is set. In the Figure 7, D is the dimension of the interceptor and the abscissa representing the flat plate is given by the a-dimensional ratio x/Lk, where Lk is the length of the flat plate. The curves start to differ from each other with values of x/Lk equal to 0.5 Figure 8 shows the pressure coefficients with the device installed deducted of the pressure coefficient of the plate without device. In this figure the dimension of the interceptor is expressed in mm and with letter *i*, while the length of the plate is expressed in mm and with letter L.

The charts show that the effects of the device are extended for a good percentage upstream the device, thus causing not only trim variations, but also a non-negligible general increase in dynamic pressures.

Therefore, the positive effects of the interceptors are linked not only to the variations of the trim and a consequent reduction of induced resistance (which up to date is the most widespread reason in naval sector justifying the effectiveness of interceptor) but also to the dynamic lift of the hull and the consequent reduction of immersed volumes.

The work carried out presents different laboratory experiences confirming the hypothesis proposed in this section and specifically the role of interceptor as high lift device. Then, applying the described principles, two new geometries of interceptor are introduced, justifying the same features of the device.

The first non-conventional geometry is called Split Interceptor, SI. It differs from standard geometry because it has an opening at the bottom of the device. The inspiring principle is that of creating a limited water flow avoiding the generation of a closed vortex and allowing a reduction of the curvature radius of the water flow, thus strengthening the field of inertial forces with a consequent increase in local pressures. The loss of the closed vortex clearly causes a reduction of the pressure surge, that is, an unexpected effect. The experimental test will show that it is possible to calculate the dimensions of the openings that assures an overall advantage in terms of hull resistance.

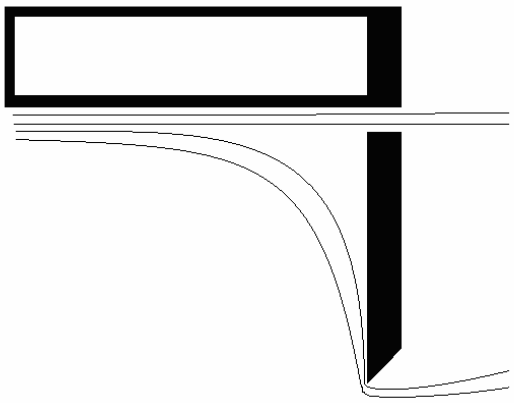

Figure 9 – Flow around a split interceptor.

The setting of interceptor (of whatever kind) leads, at high speeds, to a shift of the centre of pressures initiated on the bottom of the hull towards the stern, thus involving a considerable reduction of the trims at higher speeds and excessive growth of the wetted surface and of the

related viscous component of resistance, while the reduction of the induced resistance component (W×tgτ) brings some advantages.

With a view to exploiting the positive effects of the device, seen in terms of high lift device, a second interceptor has been added to the bow, thus introducing the second solution, defined as Double Interceptor System (DIS). The bow interceptor performs the function of increasing the pressures around the bow, generating a trimming by the stern and a lift rise. The trimming by the stern of the bow interceptor will be coupled to a trimming by the head of the stern interceptor alongside with a further lift rise.

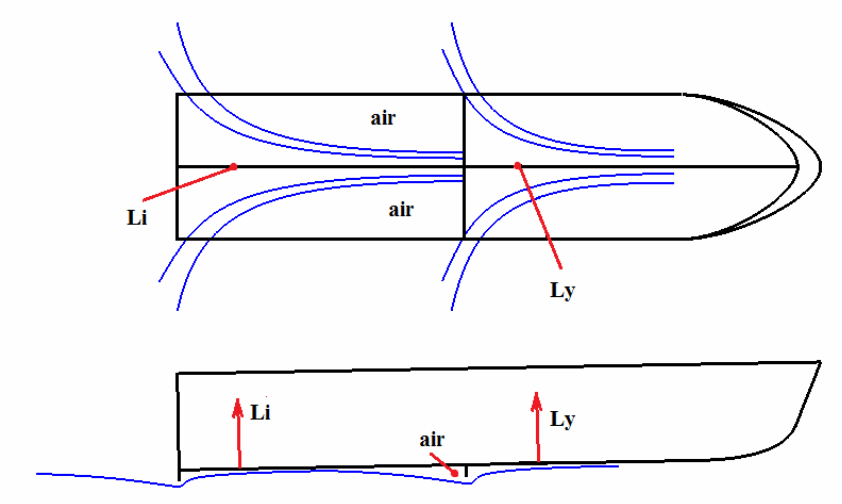

Figure 10 – Scheme of DIS working principles.

Similarly to what happens with steps, downwards the bow interceptor, some low pressure can be generated sucking the hull and contrasting the lift rise generated upwards to the device. In order to avoid the sucking, some pipes have been opened during the tests, so to facilitate a natural air-circulation in the downstream zone.

Furthermore, it has been observed that the air-circulation depends on the trim of the hull, as shown in the following chapters.

The natural air-circulation also leads to a dynamic reduction of the wetted surface and a consequent reduction of the viscous component of resistance.

5. Experimental activities.

The Experimental tests have been performed in the towing tank of the Department of Ingegneria Navale of the University of Naples *"Federico II"*. The towing tank is 136.5 m long, 9 m large and 4.5 m deep, it allows a maximum speed of 10 m/s.

Figure 11 – Towing Tank of DIN.

The towing tests have been performed by using a device called R47. The R47 consists of an arm allowing three degrees of freedom and the measurement of the bare hull resistance, trim variations and vertical displacement. Annex III contains the device fact sheets.

A special attention has been focused on the trims measurements, that have been made simultaneously by using R47, two laser probes and some inertial probes, that is accelerometers having the gravitational field as reference point and considered particularly useful for the repeatability of static trims.

6. The tested models

In this chapter we deal with the problem of the determination of hull geometries where the device can be tested.

Two main procedures have been chosen:

The first one consists of the identification of a relevant hull referring to a database of adequately selected units.

The database refers to the units on which interceptors have been first set. The patrol boat SAR and Pilot boat have been examined in detail, even if over the last years the use of this device has been widespread in the field of leisure boating. The reference data bank is reported in Annex II.

The latter procedure followed is that of experimenting the device on simple geometries being systematically interconnected with each other, in order to provide data that can be generalized and referred to steady geometry variations.

The first model tested, called C954, is characterized by a warped hull, having features, as already mentioned above, which show values being relevant for the data bank taken under consideration. The hull features are summarized in Table 1 as for central displacement. In Figure 12 two perspectives of the line drawings of the model are shown.

Table 1 – Main characteristics of the hull C954

L_{WL}	2,404	m	C_P	0,72	
B_{WL}	0,729	m	β_T	13,2	deg
Δ	121,0	kg	$\beta_{0.5}$	23,3	deg
L_{CG}/L_{WL}	0,40		$\beta_{0.7}$	32,9	deg
A_T/A_X	0,96		i_E	32,0	deg

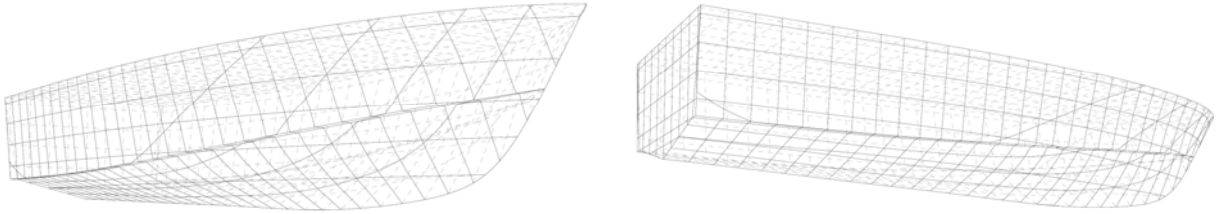

Figure 12 – Model C954.

Figure 13 – Model C954 Displ 103.5 kg Vel 5.326 m/s.

The model object of experiment has been tested as regards displacements ranging between 103,5 and 140 kg, in order to have a complete overview of the bare hull behaviour, according to significant values of the length displacement ratio, $L/\nabla^{1/3}$, with reference to the data bank.

The geometric characteristics of the hull are reported below, according to displacement changes.

Table 2 – Features of the hull C954

Δ F.O. [kg] =	140,00	133,50	121,00	103,50	92,00
L_{WL} [m] =	2,416	2,412	2,404	2,390	2,383
T_{AV} [m] =	0,194	0,185	0,176	0,163	136
T_{AD} [m] =	0,194	0,185	0,176	0,163	136
S [m^2] =	1,677	1,644	1,580	1,488	1,427
$L/\nabla^{1/3}$	4.66	4.72	4.86	5.09	5.28

In order to evaluate the effects of the device according to the variations of deadrise angle, alongside with C954, three prismatic models having deadrise angles of 10, 20 and 30 degrees, have been tested. The models are 2,5 m long and 0,6 m large.

Tests have been carried out with a displacement of 102,8 kg, corresponding to a coefficient value $L/\nabla^{1/3}$ equal to 5,09.

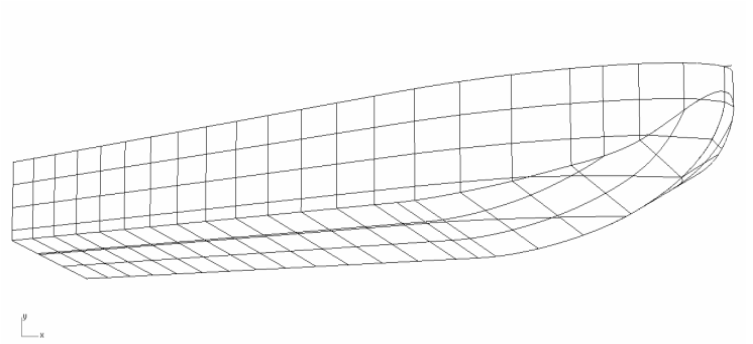

Figure 14 – Model C0301: $\beta = 20$ deg.

In Table 3 the main features of the three models are summarized with reference to zero trim condition at rest.

Table 3 – Features of prismatic hulls

Hull		C 9707	C 0201	C 0301
β	(deg)	10	20	30
L_{WL}	(m)	2,375	2,387	2,385
B_{WL}	(m)	0,600	0,600	0,600
L/B		3,958	3,978	3,975
Δ	(kg)	102,8	102,8	102,8
Lcg/Lwl		0,44	0,44	0,44
τ_S	(deg)	0,0	0,0	0,0
A_T/A_X		1,0	1,0	1,0

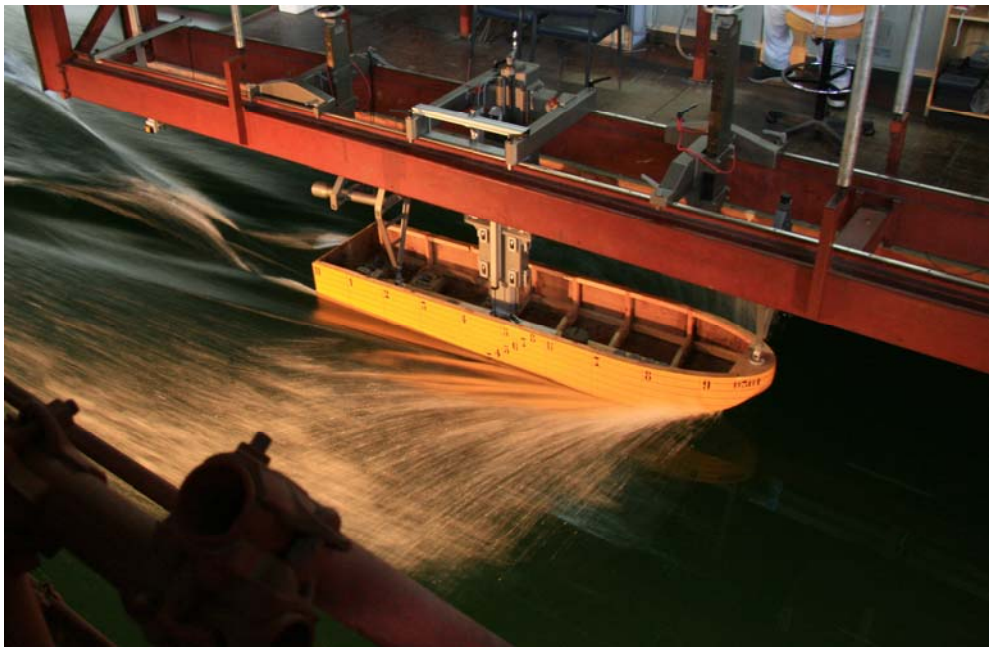

Figure 15 – Model C0301.

6.1 Data correlation

The data reported in the following chapters refer to model scale. Tests have been carried out within a field of temperatures ranging between 11 and 24 centigrade degrees. Quantities have been then reset to the standard temperature of 15°C. For the estimation of density and viscosity

rates the formulas and values suggested by ITTC 7.5-02-01-03 procedure have been taken under consideration, the same formulas and values had already been recommended for the correlations tank-sea concerning the procedure ITTC '78.

The formulas and values being used are reported as follows:

2 viscosity of fresh water in relation to temperature:

$\nu_0 = ((0{,}585\times10^{-3}(T - 12{,}0) - 0{,}03361).(T - 12{,}0) + 1{,}2350).10^{-6}$ m²/s

3 density of fresh water in relation to temperature:

$\rho_0 = 0{,}5\times10^{-6}\ T^4 + 0{,}03\times10^{-3}T^3 - 8{,}1\times10^{-3}T^2 + 999{,}784$ kg/m³

4 Viscosity and density of sea water at 15°:

$\nu_s = 1{,}187\times10^{-6}$ m²/s $\quad \rho_s = 1025{,}87$ kg/m³

To carry out data correlation a resolution of the resistance similar to that suggested by the ITTC'57 for the correlation has been used, it is reported below in terms of adimensional coefficients:

5 Resolution of the total resistance coefficient:

$C_T\ (Fn, Rn) = C_R\ (Fn) + C_F\ (Rn)$

In this approach hull resistance is resolved in only two aliquots: one is due only to gravitational phenomena and one to viscous phenomena, being considered independently from each other. Specifically, C_F is the friction coefficient of an equivalent flat plate having a wetted surface and length equal to that of the model or the ship, increased of 12%, in order to take into account the three-dimensionality of water motion, while the term C_R is the residual resistance coefficient and includes both the resultant of the pressure action over the hull and the three-dimensional effect of viscous resistance not comprised in the already considered 12%. Data correlation

has been carried out by adjusting the value of C_F concerning the standard temperature, as reported in report **6**:

6 Data correlation:

$C_{T_{15°}}(Fn, Rn) = C_{T_M}(Fn, Rn) - C_F(Rn_T) + C_F(Rn_{15°})$

Con $Rn_{15°} = L_{WL}\ V_M\ \nu_s^{-1}$ e $Rn_T = L_{WL}\ V_M\ \nu_0^{-1}$

A similar procedure is suggested by the ITTC 7.5-02-02-02, where a quantification of the shape factor is also provided, even if its calculation would be quite useless as regards the hulls being under consideration.
Friction resistance coefficient has been calculated by using the formula suggested into the ITTC '57 reported in report 7.

7 Friction line according to ITTC'57:

$$C_F = \frac{0.075}{\left(LOG_{10}\frac{VL}{\nu} - 2\right)^2}$$

Hull surfaces and buoyancy lengths refer to static floatation.

6.2 Static correlation vs dynamic correlation.

When reporting data reference has been made to static quantities at rest, but we have also dealt with the problem of correlating data, in order to assess the necessity of measuring the running length and wetted surface. To such an end we have referred to the systematic series USCG [10] having geometric features being very similar to the hull C954, as regards the values of load-displacement ratio being $L/\nabla^{1/3} = 5,09$

Table 4 – Comparison of the geometric features of the hulls C954 e 5628

Hull	C954	5628
$L/\nabla^{1/3}$	5,090	5,090
L/B	3,29	3,24
B/T	5,08	5,08
A_T/A_X	0,86	1,0
β_T	14,5	16,61
$\beta_{0.5}$	21,8	22,81
i_E	27,6	19,5
C_P	0,704	0,696
L_{CG}/L_{WL}	0,40	0,42

The USCG provides data that allow us to carry out both a static and a dynamic correlation, therefore we have estimated resistance by using the two procedures with a varying Froude's volumetric number and the speed range of the provided tests (1.1 ÷ 2.8) and according to a scale factor equal to 6, which is likely to be the actual one for the geometries in object. Since the differences reported were lower than 1%, we decided not to survey the running surface nor the wetted lengths, also considering the possible subjective errors resulting from such a measurement procedure.

7. Conventional interceptors

In this chapter the data concerning the interceptor standard configurations are shown.

On the hull C954 five interceptor sizes have been tested for three different displacements, after an accurate examination of the bare hull behaviour.

On the prismatic models, the effect of the device in five different positions for two different values of the ratio L_{CG}/L_{WL}, at a fixed value of $L/\nabla^{1/3}$ = 5,09 has been evaluated.

7.1 Hull C954: behaviour of the bare hull

In order to provide a useful reference set to compare the performances of the hull with the device applied, a wide range of resistance tests have been carried out on the hull without devices.

Five displacements for $L/\nabla^{1/3}$ ranging between 4,66 and 5,28 have been tested, within a field of $F_{N\nabla}$ ranging between 1,1 and 2,9.

The following figures show resistances, trims and draughts for each displacement.

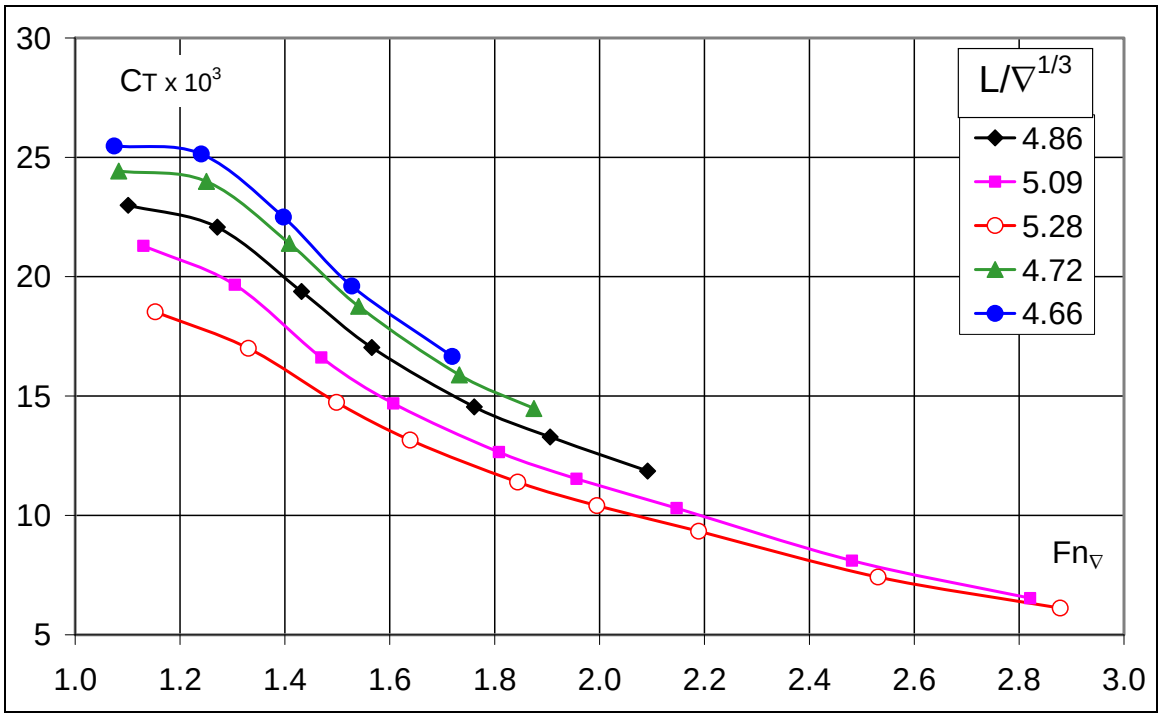

Figure 16 – Total resistance coefficient of the hull C954 without device.

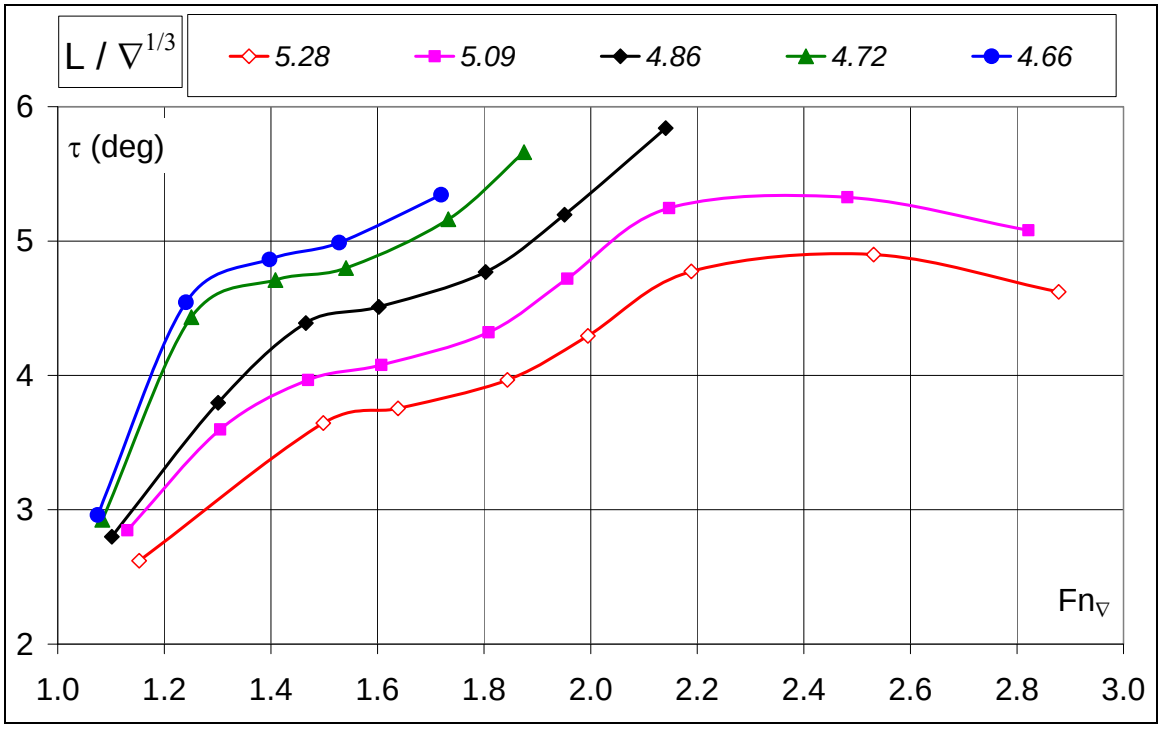

Figure 17 – Trims of the hull C954 without device.

The performances shown above can be considered as a reference for the following data expressed in relative and adimensional terms.

It is worth pointing out that relative speeds, $F_{N\nabla}$, and the reported load coefficients, $L/\nabla^{1/3}$, refer to buoyancy lengths and hull volumes pertaining to the different displacements; for this reason, in the figures shown, according to different displacements, with the same $F_{N\nabla}$, different absolute speeds are reported.

7.2 Hull C954: behaviour of the bare hull according to changes in the Lcg/LWL ratio.

In order to have a complete outline of functioning of the hull C954, towing tests have been carried out by systematically changing the static trim. The tested trims range between -1,10 and 1,51 degrees, and have been obtained by changing the center of mass Lcg according to values of the Lcg/LWL ratio ranging between 0,43 and 0,36.

We decided to carry out tests with a displacement of 103,5 kg corresponding to a value of the ratio $L/\nabla^{1/3}$ equal to 5,09, because it allows us to cover a wider range of car speeds.

Table 5 - τ_S - Lcg/LWL corresponding values.

τ_S	Lcg/LWL
-1,1	0,43
0,0	0,40
1,0	0,37
1,5	0,36

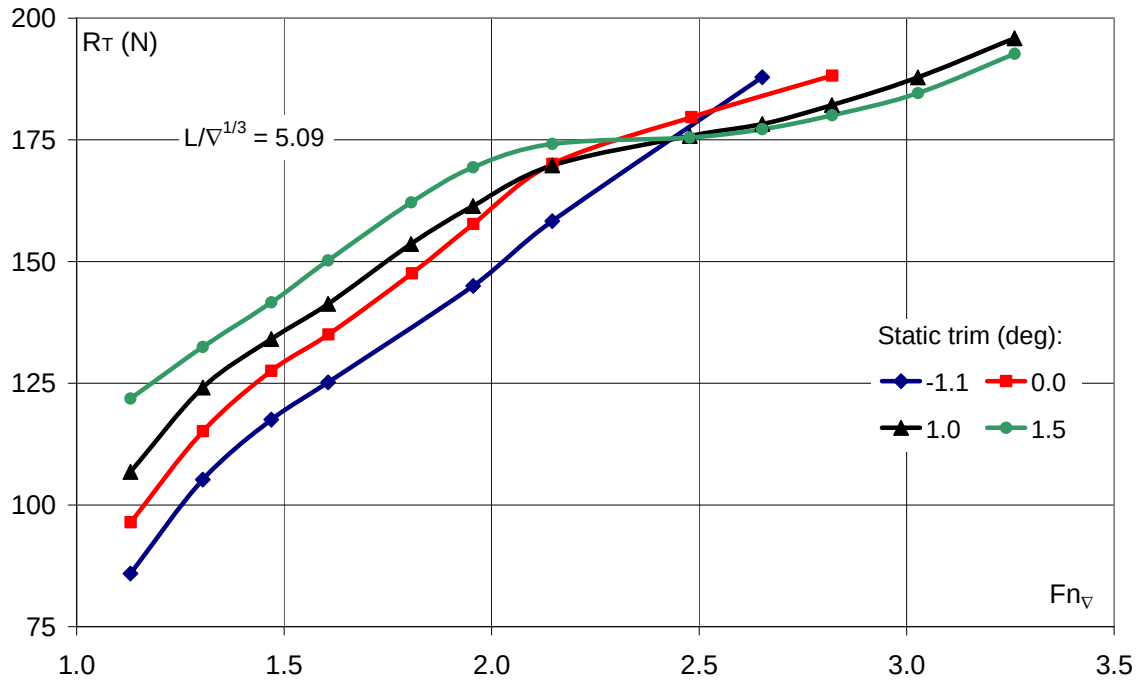

Figure 18 – Model C954: bare hull resistance vs static trim.

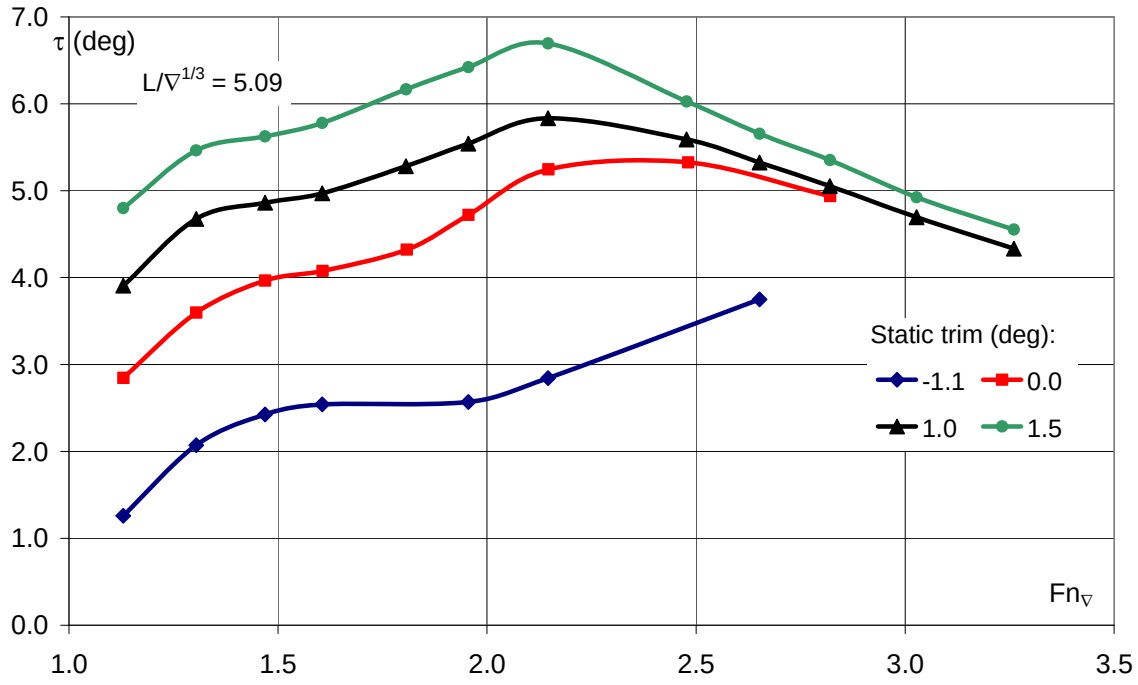

Figure 19 – Model C954: bare hull dynamic trim vs. static trim.

Charts in Figure 18 and Figure 19 show the resistance and the trim during the test of the model. It has been observed that in case of speeds with a

Fn_∇ lower than 2,48, it is more useful to shift the centre of mass towards the bow, as regards hull resistance, this allows to control the trims and consequently to significantly reduce the resistance caused by them. This is the main cause of hump resistance which consists of a relative maximum along the resistance curve, typical at intermediate speeds, corresponding to an absolute maximum along the trim curve and consequently to a peak of resistance caused by them. The charts above clearly show the hump resistance with the hull trimmed by the stern (curves marked in green). With Fn_∇ = 2,0 both the relative maximum along the resistance curve and the absolute maximum in the trims are clearly shown. By taking the centre of gravity, CG, closer and closer toward the bow, the effects which are clearly evident along the green curve, become less and less evident up to fading away completely along the blue curve, which corresponds to a negative static trim of the hull (trim by the head).

At higher speeds the natural dynamic reduction of trims induces an increase of wetted surfaces with a consequent big increase in the resistance connected with it. Therefore with Fn_∇ higher than 2,48, there is a progressive reversal of the behaviour: as the speeds increases the optimum value of the CG gets closer and closer to the stern. By comparing the last two curves, it can be observed that by decreasing the value of the Lcg/LWL ratio below the value of 0,37, only little advantages can be obtained at higher speeds as well as a big increase in hump resistance.

7.3 Hull C954: comparison of performances with the systematic series USCG

As further described in the next chapters, the effectiveness of interceptors, under different load and trim conditions, becomes really high.

In order to avoid that the big advantages obtained can be ascribed to the poor quality of the tested hull rather than to the intrinsic qualities of the device, we have compared the resistance curves of the C954 with the hull 5628 of the systematic series, whose features are reported in Table 4.

In the chart of Figure 20 it can be noticed that the performances of the hull 5628 result to be slightly better than the performances of the hull C954 at lower speeds; with $F_{N\nabla}$ ranging between 1,6 and 2,1 performances are quite comparable; with $F_{N\nabla}$ higher than 2,1 the hull C954 provides better and better resistances.

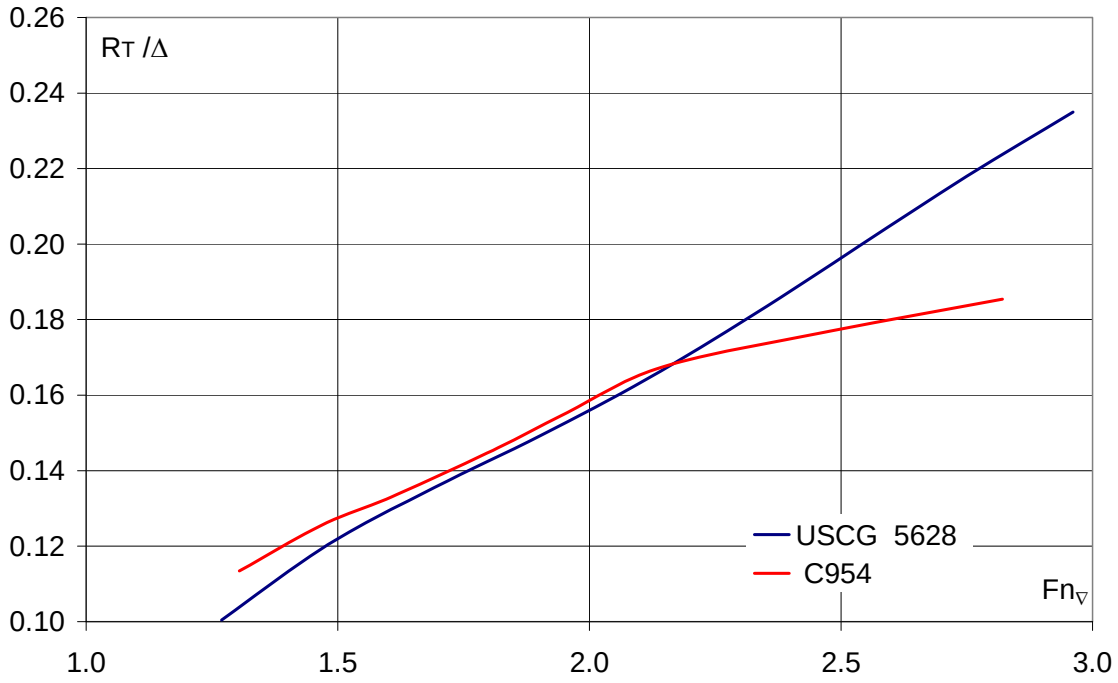

Figure 20 – Comparison of the performances of the hulls C954 and 5628.

7.4 Test on Hull C954 with interceptors.

The hull C954 has been tested with the interceptor applied in five different positions, summarized in table 6. The size of the device has been given in adimensional terms as for the buoyancy length referred to a displacement of the model of 121 kg.

Table 6 – Test size of the interceptor in the hull C954.

Position	*i* (mm)	i/L_{WL}
0	0,0	0,0
A	1,0	0,4 × 10-3
B	2,0	0,8 × 10-3
c	2,5	1,0 × 10-3
d	3,5	1,5 × 10-3
e	4,2	1,8 × 10-3

In this paragraph the results obtained from the three central displacements tested are reported. The hull has been tested with no trim initial condition.

Charts in Figure 21 Figure 24 Figure 27 report the values of the device effectiveness according to speed variation, expressed in terms of Fn_{∇} and according to the variation of the device size.

The effectiveness is expressed as ratio between towing resistance of the hull with interceptor, and the same resistance of the bare hull.

Charts in Figure 22, Figure 25 and Figure 28 report the respective running trims, expressed in absolute terms, and in relative terms in Figure 23, Figure 26 and Figure 29.

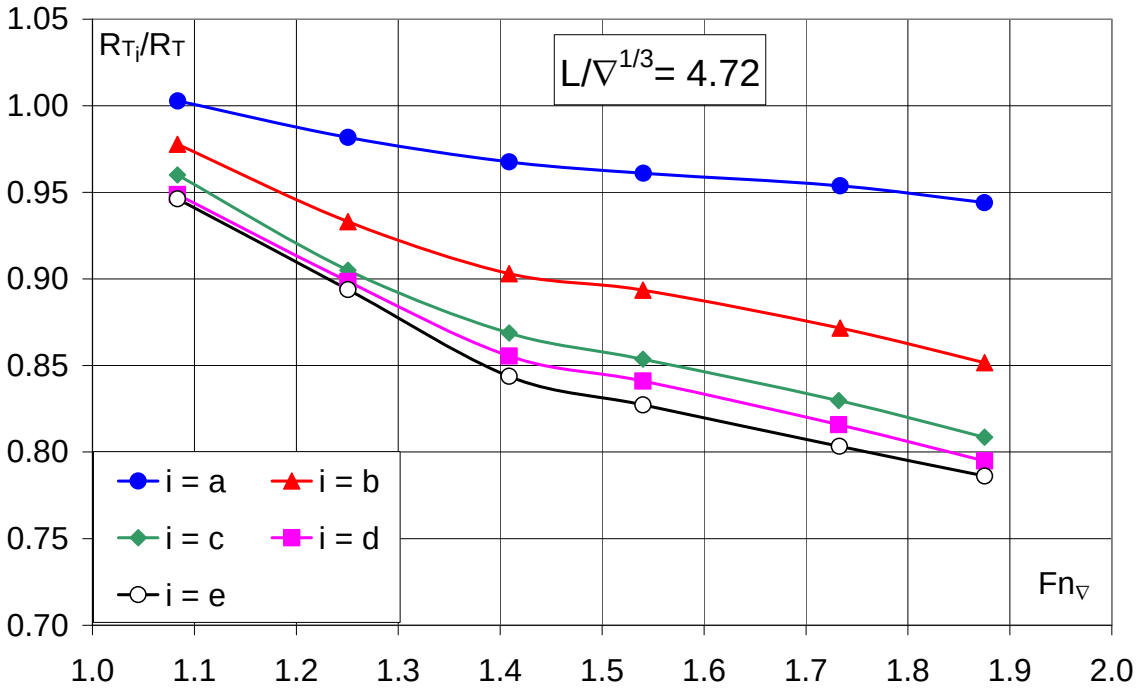

Figure 21 – Effectiveness at different *i*.

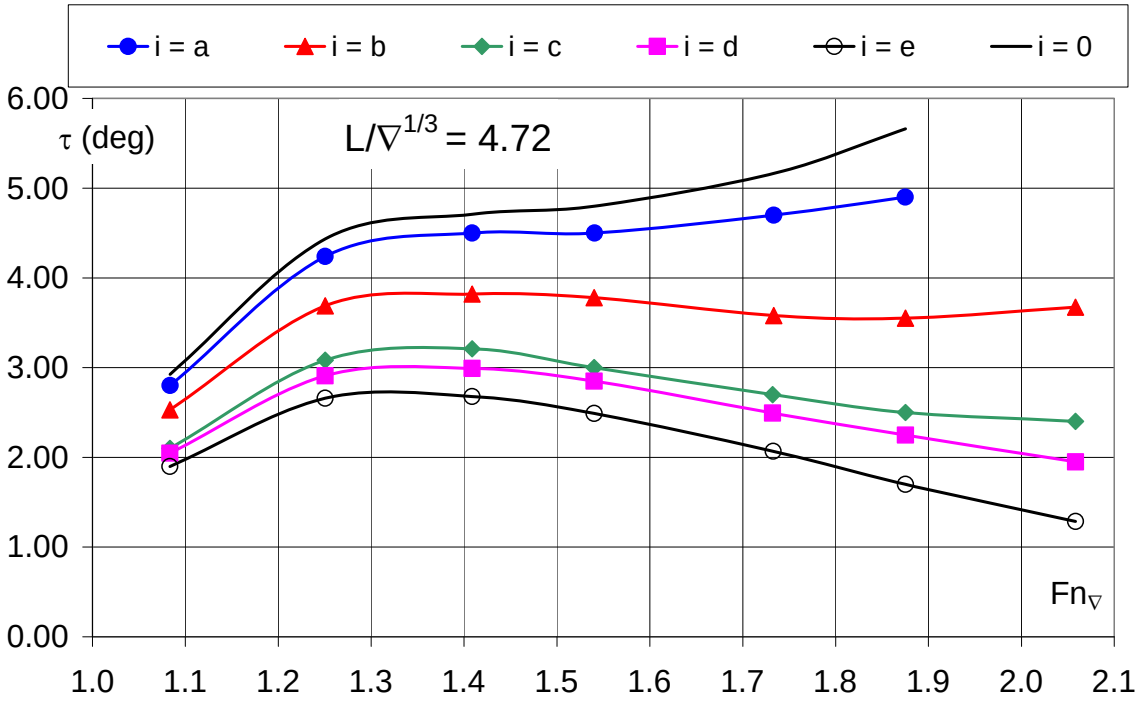

Figure 22 – Dynamic trim at different *i*.

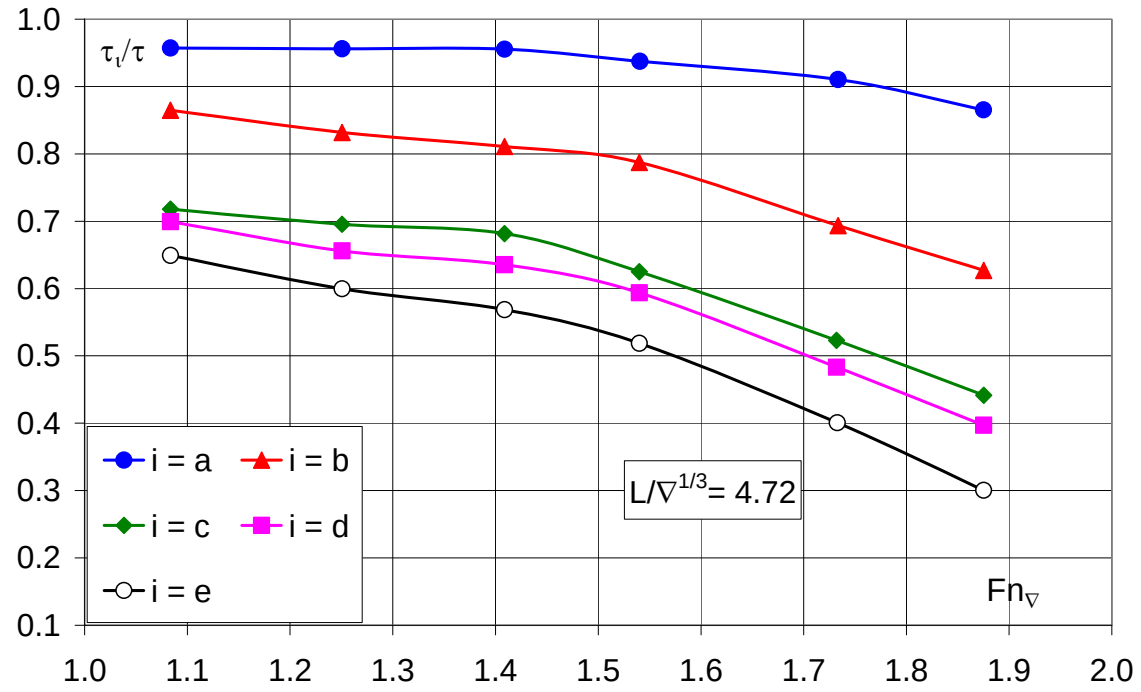

Figure 23 – Dynamic trim ratio for each different *i*.

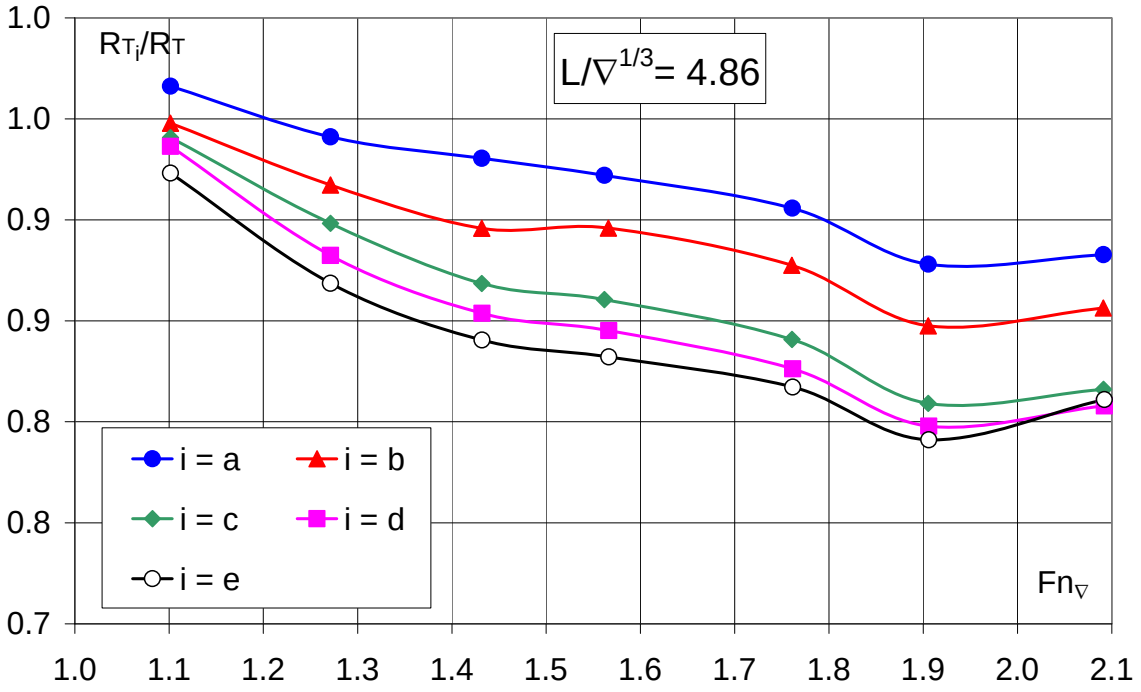

Figure 24 – Effectiveness at different *i*.

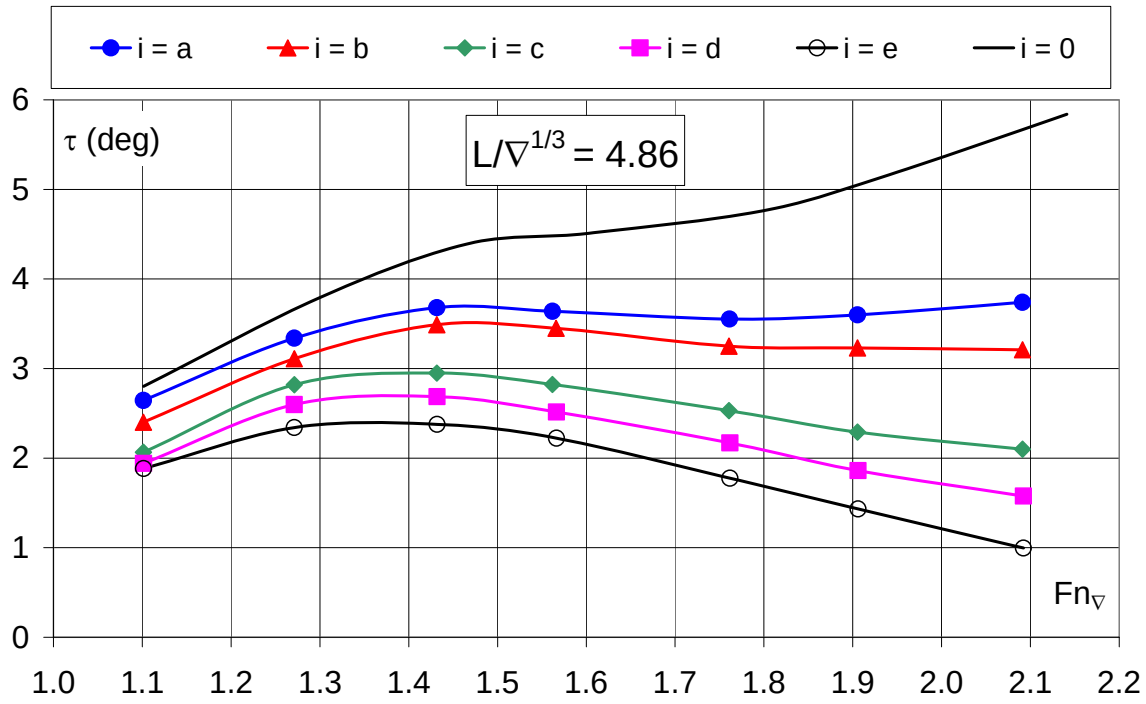

Figure 25 – Dynamic trim at different *i*.

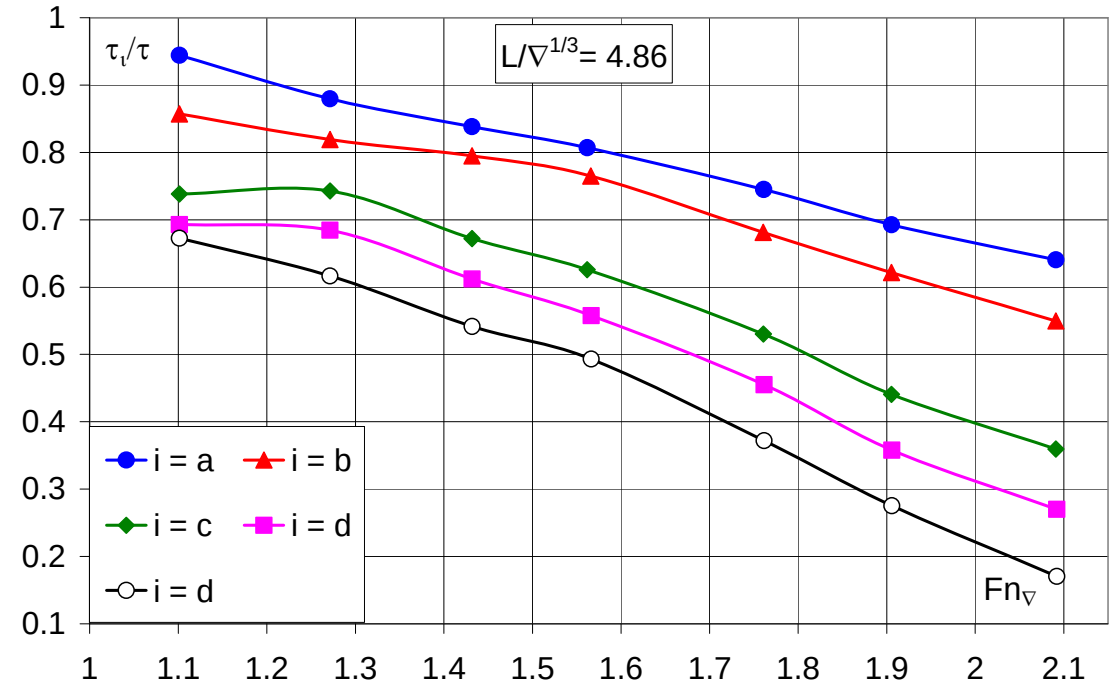

Figure 26 – Dynamic trim ratio at different *i*.

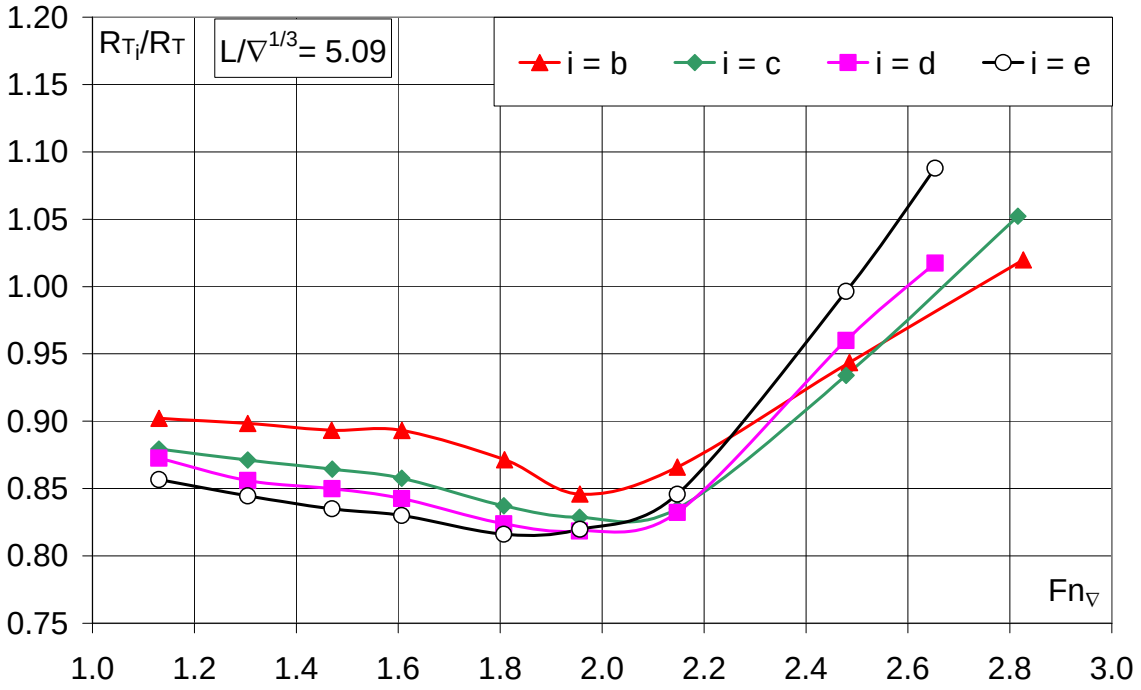

Figure 27 – Effectiveness at different *i*.

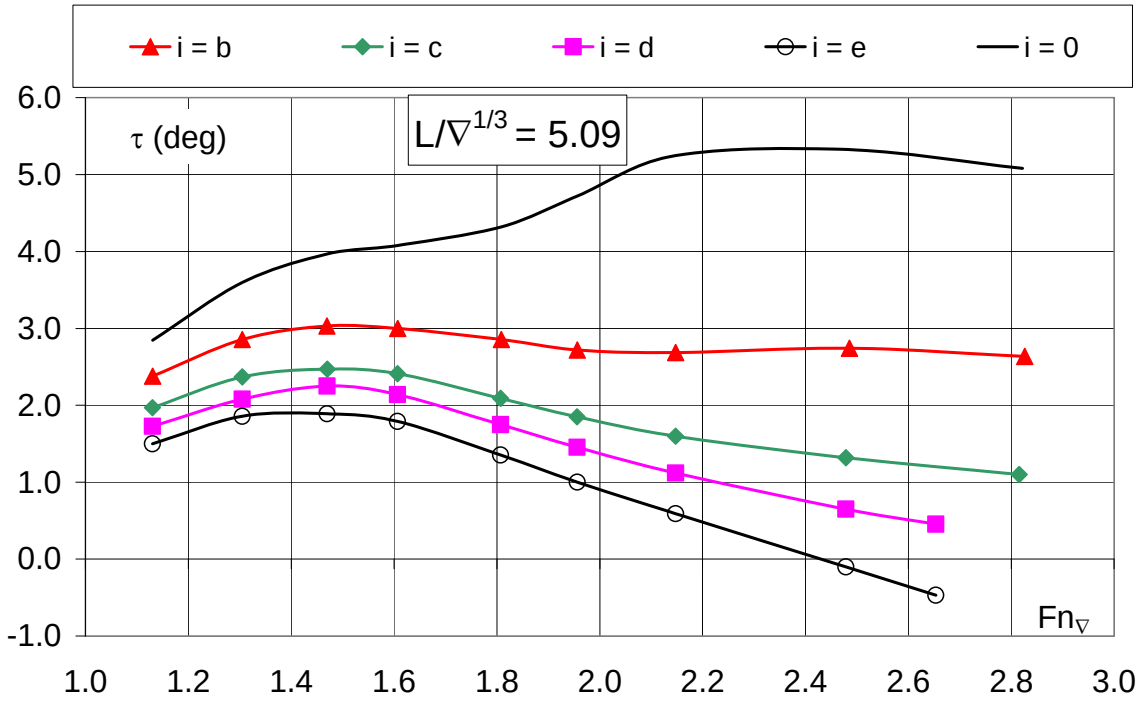

Figure 28 – Dynamic trim at different *i*.

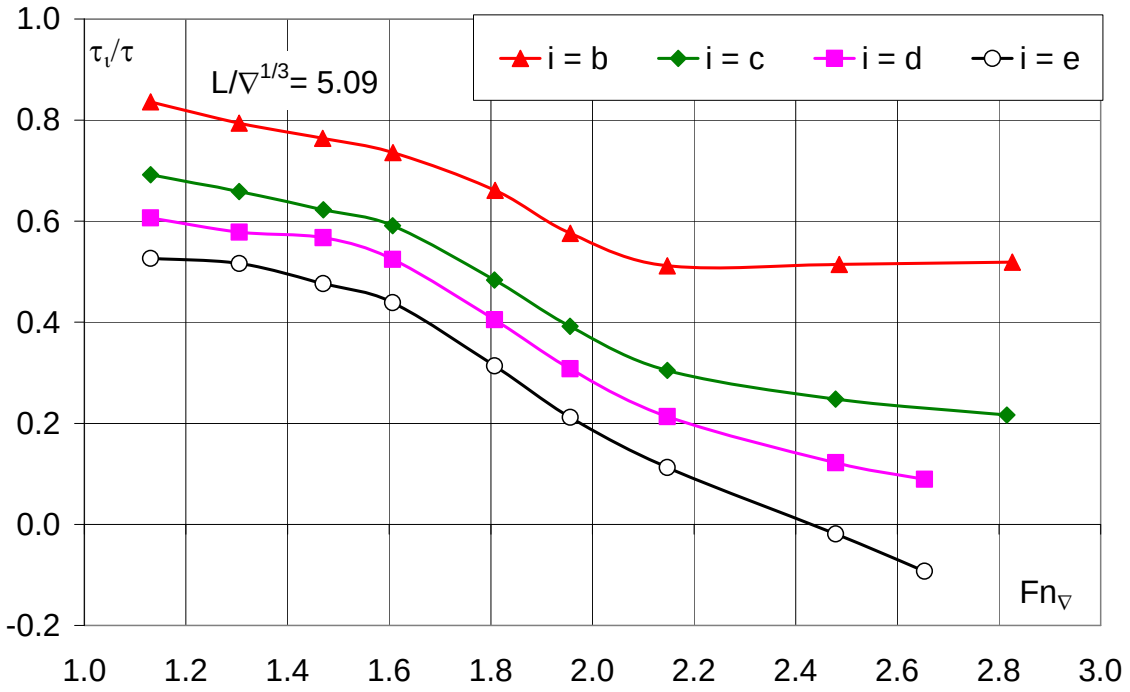

Figure 29 – Dynamic trim ratio at different *i*.

The highest effectiveness values have been found with heavier displacements.

By heavier displacement a reduction of the resistance by 21% has been obtained through, but though the best performance has not been attained. The diagram trend lets expecting that, at higher speeds, the device allows better performances but the limits imposed by the instruments available for the displacement under discussion, have not allowed us to investigate further possibilities at higher speeds.

By intermediate displacement the highest performance of 21% at a volumetric Froude number of 1,92 has been reached, over which effectiveness decreases.

By a lighter displacement and lower speeds, a direct proportionality between the interceptor size and resistance decrease is to be noticed, up to a resistance decrease of 18% at Fn_{∇} = 1,85. By increasing speeds, effectiveness decreases and consequently the optimum size of the

interceptor is also reduced. This is due to an excessive trim correction induced by the device, as shown by chart in Figure 28.

It is therefore interesting to observe that under some testing conditions, sizes show a new aspect. By a light displacement ($L/\nabla^{1/3}$ = 5,09) and *i* = d, with Fn_∇ = 2,48, a really big trim reduction (0,65 deg) is reported, while, in spite of this, resistance results to be lower compared to the bare hull. It is clear that advantages are not to be ascribed to trim corrections but to the lift rise induced by the device.

Consequently performances can be surely improved by shifting the centre of the mass closer to the stern.

Then, we have tried to find the best trim at the same speed and for the same extension of the interceptor

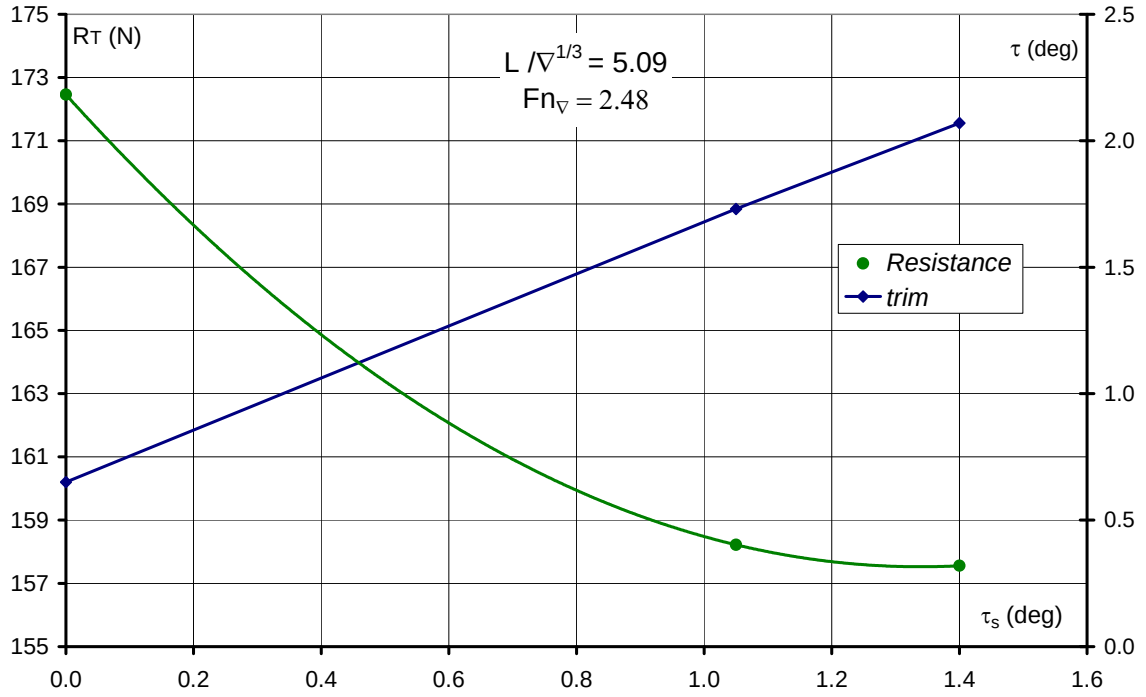

Figure 30 – Search of the best trim configuration *i* = d.

As shown in the chart, by shifting the canter of mass towards the stern, performances are further improved, up to a further reduction of R_{Ts} by 9%. It is clear that the values of Lcg, involving lower resistances, decrease when the device is applied.

What observed so far, suggests us to carry out a more accurate examination of the influence of the interceptor on the CG optimum longitudinal position.

7.5 Influence of the interceptor on the CG optimum longitudinal position

A variety of tests have been carried out on the hull C954, with varying longitudinal position of the CG, and with different interceptor sizes, in order to find the configuration involving the lowest resistance.

Charts in Figure 31 and Figure 32 are reported in terms of total resistance and static trim for two different displacements.

They refer to the speed of the model with Fn_{∇} = 2,09 for a 121 kg and 103,5 kg displacement on model scale that in adimensional terms correspond to load coefficients being respectively 4,86 and 5,09.

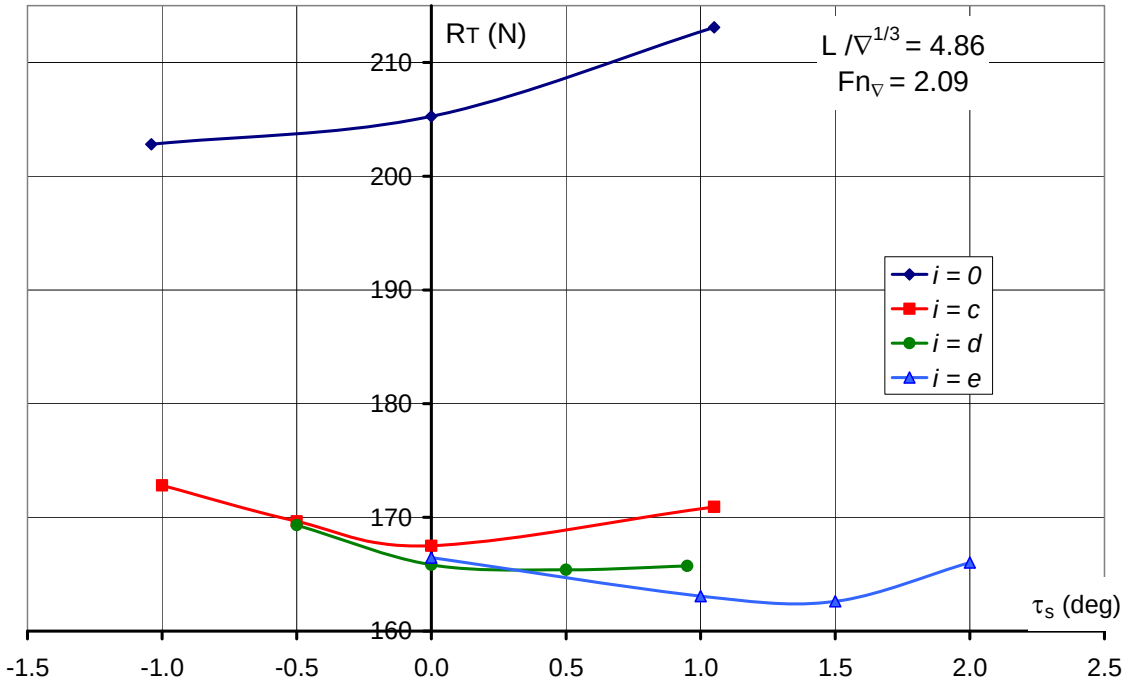

Figure 31 – Rresistance vs trim (to positive trims down by-the stern model corresponds).

In chart in Figure 31 it can be noticed that the hull behaviour is clearly different when the device is applied to it:

- Resistance variation, according to trim variation, in the bare hull results to be higher, compared to that of the hull with the device applied.
- The bare hull shows a lower resistance when shifting the CG towards the bow. When equipped with the device, the hull behaviour is reversed and trimming by the stern seems to be more beneficial.

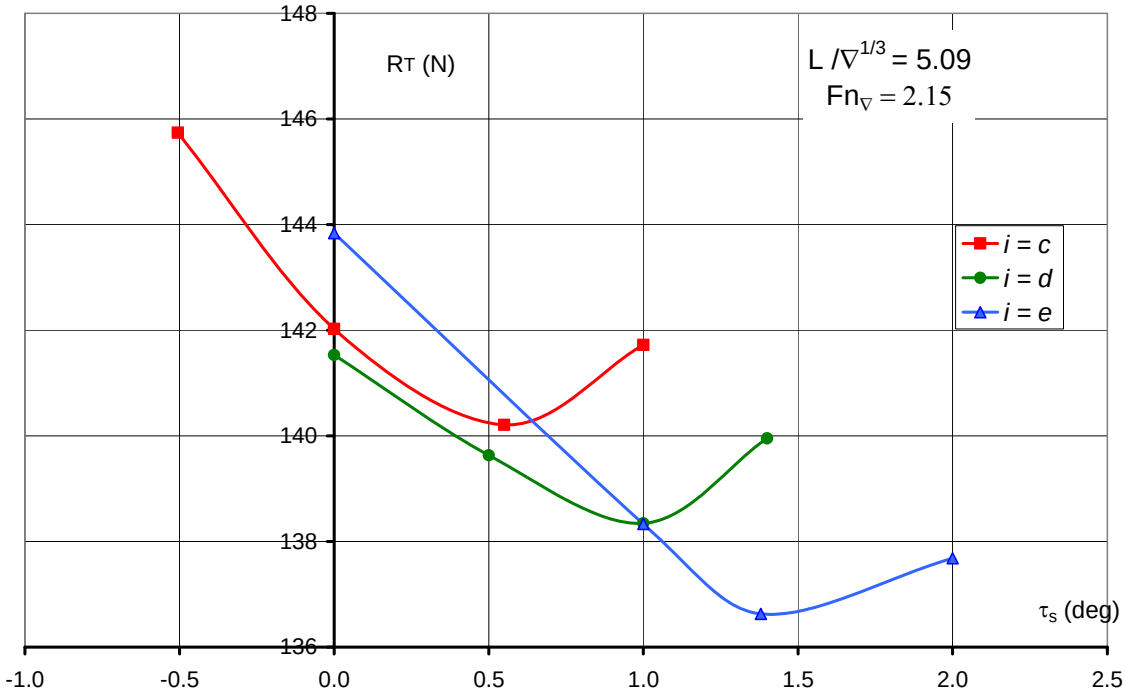

Figure 32 – Rresistance vs trim (to positive trims the down by-the stern model corresponds).

In chart in Figure 32 resistance trends are reported with varying mass barycentre and by focusing on three different positions of the interceptor for the lightest displacement.

From the figure it is even clearer that as the device size increases it is better to shift the CG towards the stern, thus contrasting the effects of the dynamic trim reduction of the interceptor.

It should also be observed that the biggest size interceptor on zero static trim conditions does not imply the highest effectiveness of performance; the behaviour changes when the CG is shifted towards the stern: with more static 1 deg trims, the direct proportionality between the interceptor size and resistance decrease is restored.

The configuration showing the best performance in terms of resistance, is the one providing the biggest size interceptor and a static trim of 1,4 deg.

It is evident that a contrast between static trim correction and the interceptor effects engenders a virtuous cycle which allows an improvement of hull performances.

Furthermore, it is clear that the positive effects due to the presence of the device are not only to be ascribed to dynamic trim variations, but also to its clear effects on the dynamic lift that, at these speeds, helps achieving a hull resistance reduction.

Finally, it is worth pointing out that the conclusions here reported, essentially refer to the investigated speeds ($Fn\nabla$ = 2,15). What described further in the next chapters, will lead us to deduce that the substantially negative relationship between *i* and Lcg is typical of the upper area of the speed field, while at lower speeds the behaviour is less clear.

In order to evaluate the behaviour of the phenomenon observed as regards displacement variations, the charts in Figure 33 and Figure 34 have been drawn up.

For each of them the interceptor position has been fixed and, at the same absolute speed being considered in the previous charts, the performance trends have been compared according to the static trim following the displacement variation.

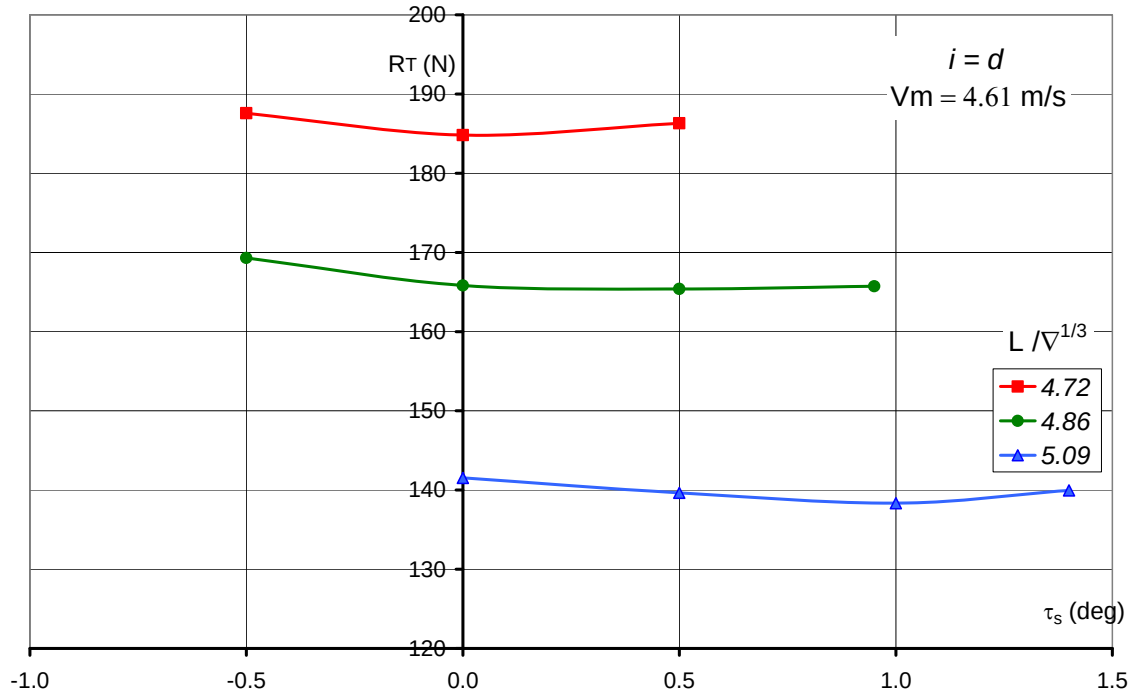

Figure 33 – Rresistance vs trim.

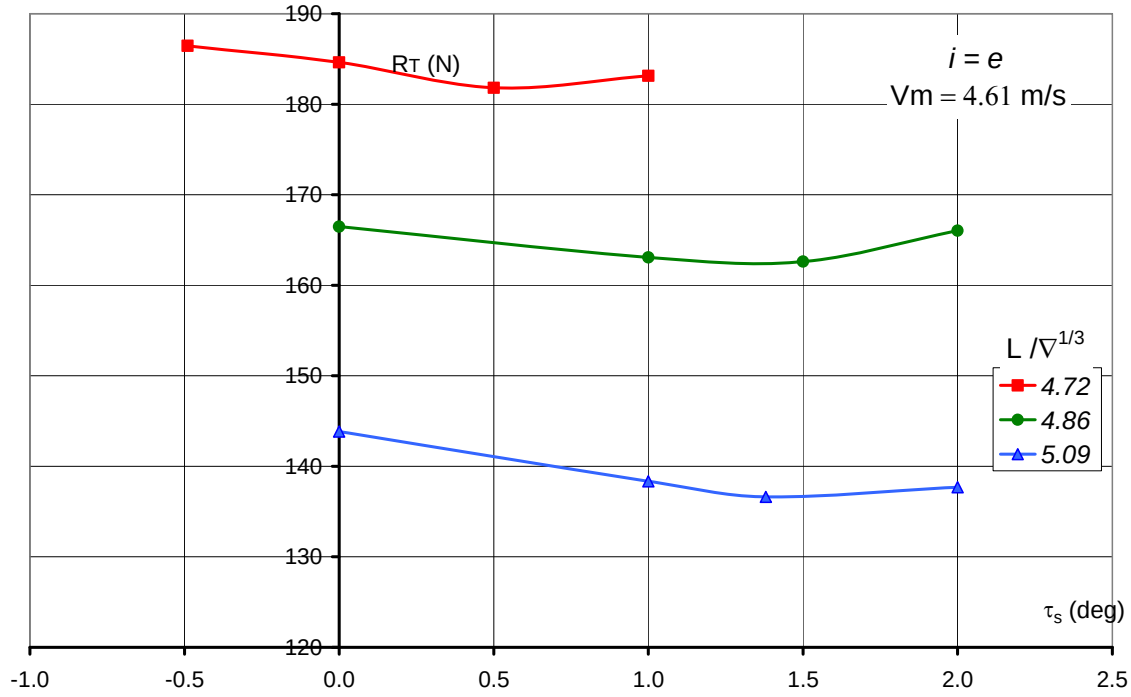

Figure 34 – Rresistance vs trim.

From the two above reported charts it can be observed that the previously described phenomenon is inversely proportional to displacement: the lighter

is the craft the more convenient is to shift the barycentre towards the stern and to increase the device size.

This behaviour is consistent with what happens in the phenomena linked to dynamic lift for intermediate speeds. It is to underline that as regards the speeds being under consideration, the less is the displacement the more important the effects of dynamic lift are in terms of reduction of hull resistance. It is also to observe that by reducing displacement induced resistance is also reduced and then the craft offers less resistance.

7.6 Hull C954: Effects of the interceptor with respect of displacement variations.

In this paragraph the effectiveness of the interceptor is evaluated according to displacement variations on the warped hull C954.

The charts reported below show the relationship between resistance and displacement, on each chart the interceptor size is fixed and the values of the R_T/Δ ratio, according to Froude number, are compared.

The R_T/Δ ratio can be interpreted as an index of the effectiveness of the hull: at equal speed, the hull that at equal resistance succeeds in having a bigger displacement or at equal displacement succeeds in providing lower resistances, will be as much better.

As it can be observed in Figure 35 the ratio R_T/Δ as it usually happens, increases at the increase of displacement with i = 0. The chart shows that the ratio R_T/Δ increases in the same way with speeds corresponding to Fn > 0,60.

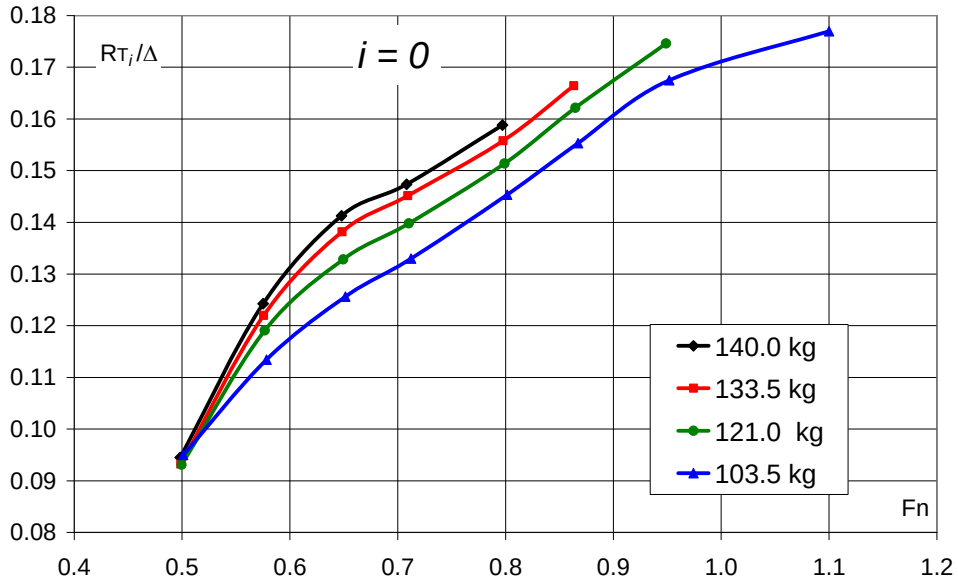

Figure 35 – C954 bare hull performances.

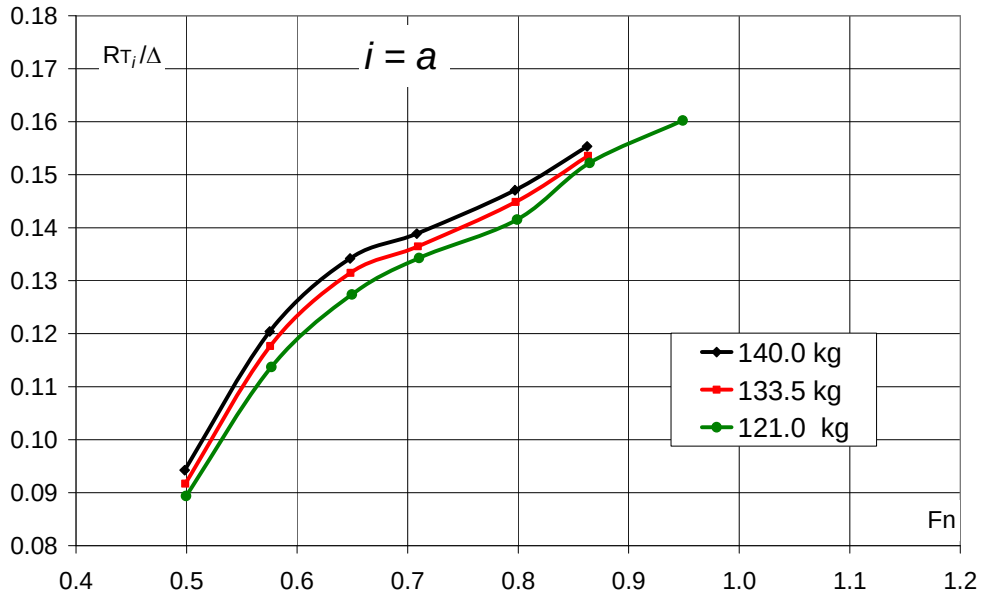

Figure 36 – C954 *i* = a performances.

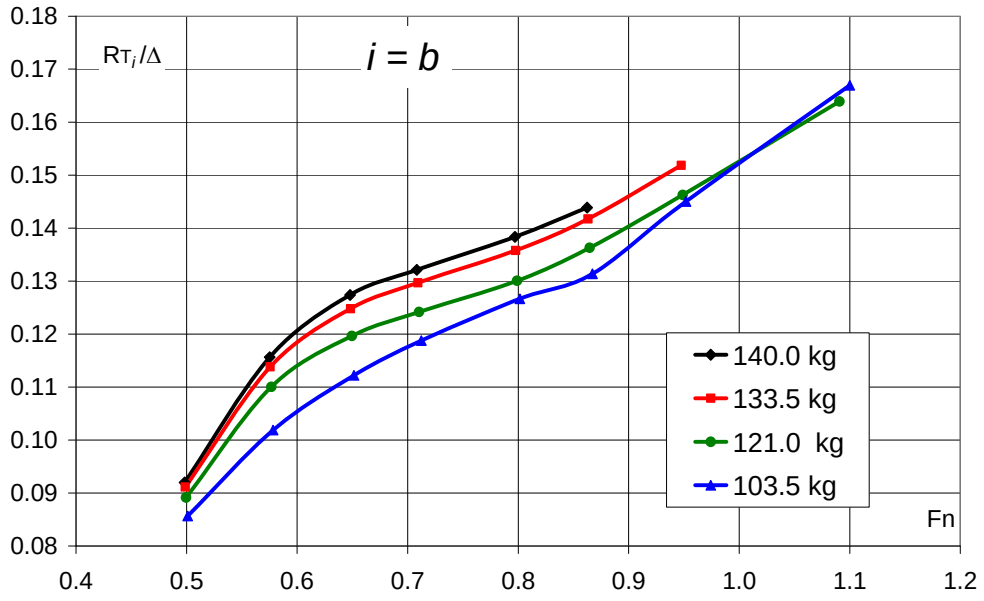

Figure 37 – C954 *i* = b performances.

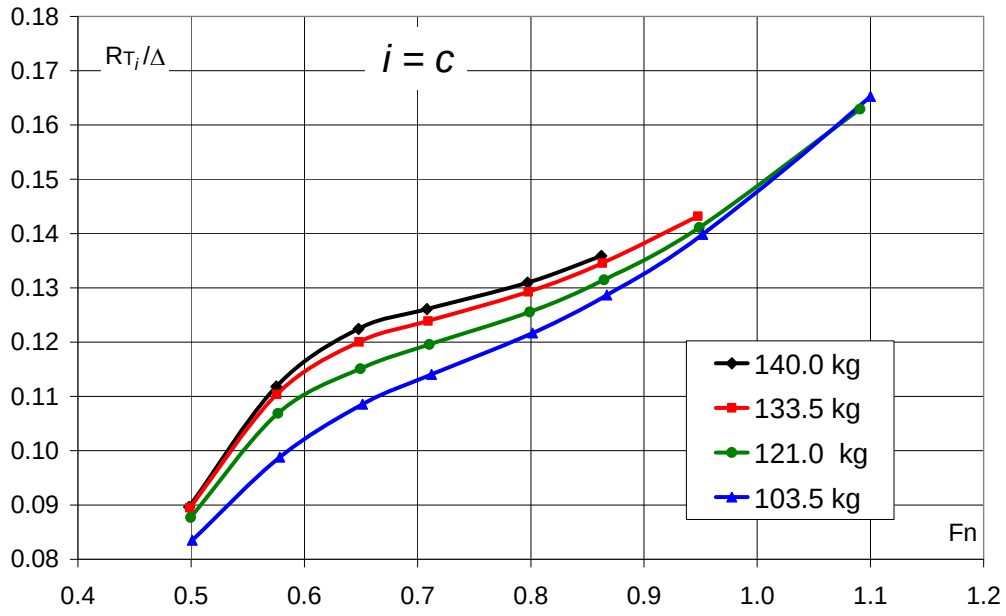

Figure 38 – C954 *i* = c performances.

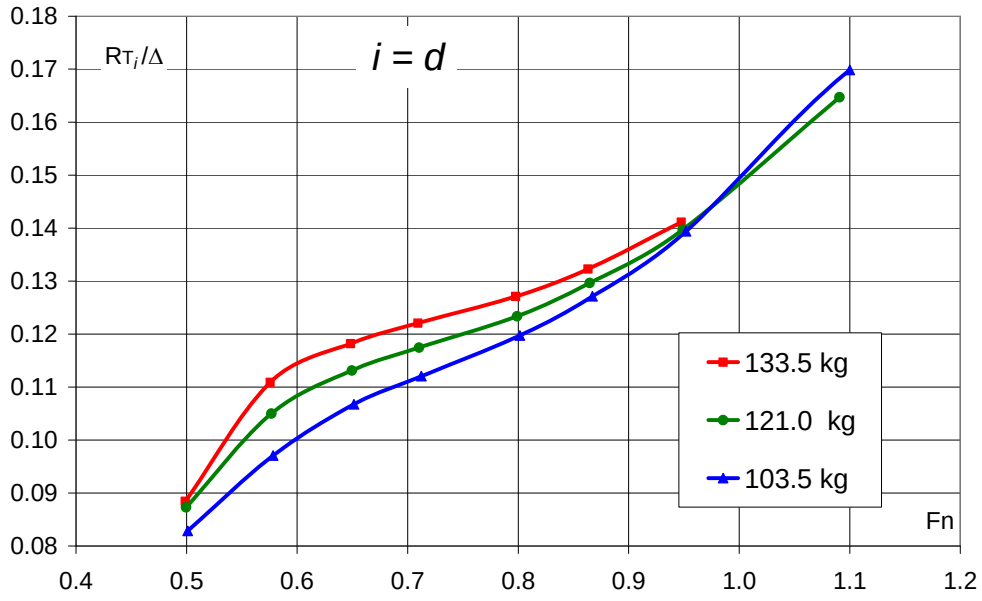

Figure 39 – C954 *i* = d performances.

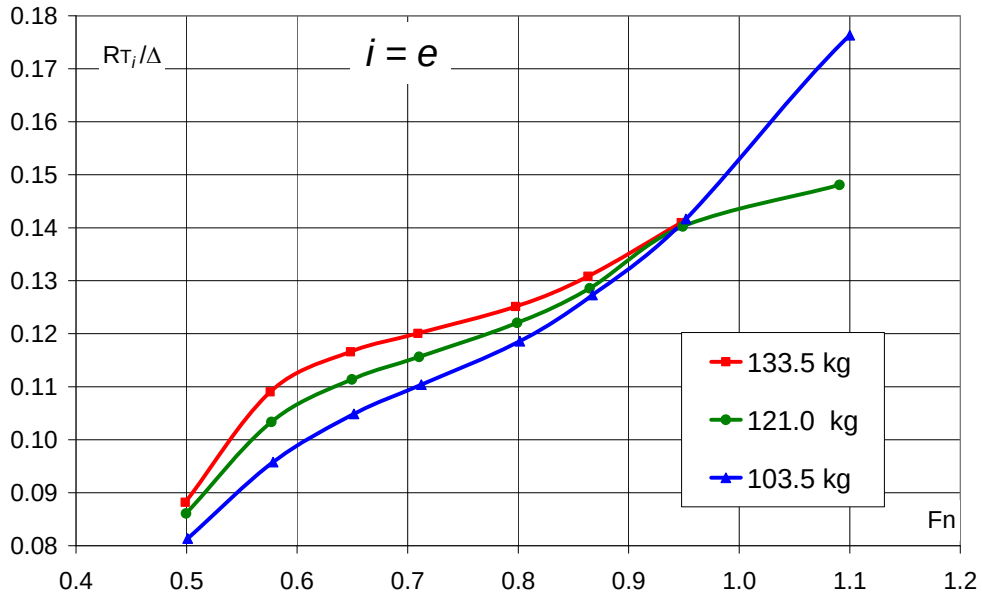

Figure 40 – *i* = e C954 performances

With increasing values of i, it can be observed that the values of RT/Δ converge with increasing speeds and increasing displacement. This shows that the interceptor by heavy displacement, at higher speeds, improves hull effectiveness.

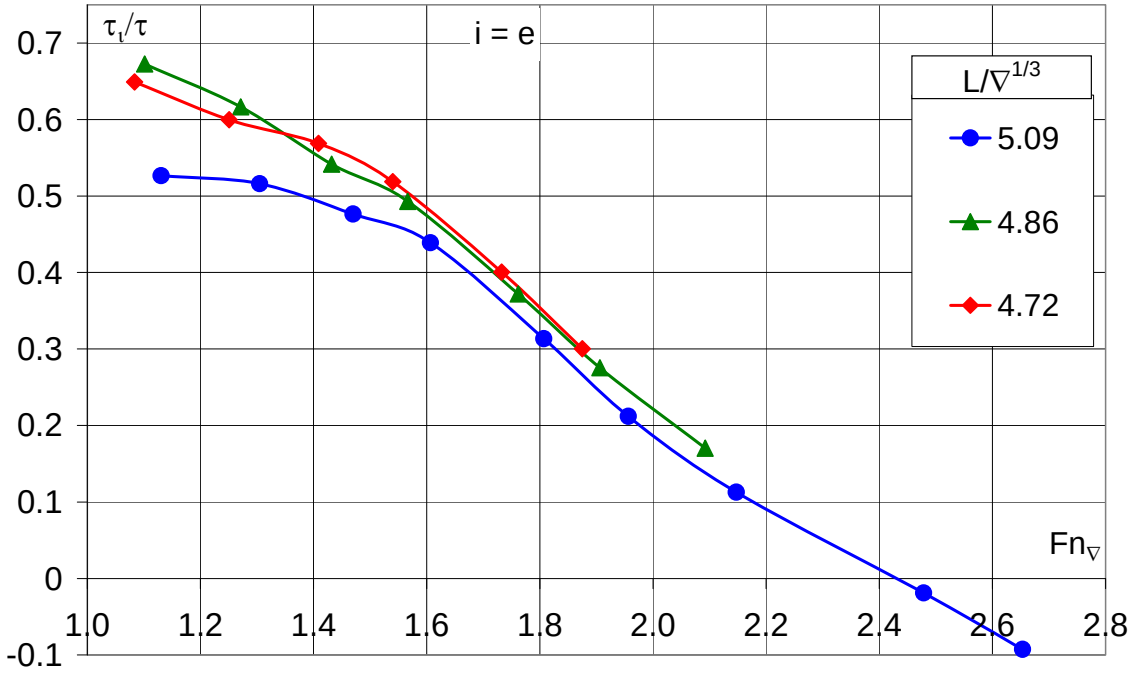

Figure 41 – Dynamic trim ratio

The chart in Figure 41 shows the trim variations induced by the device with varying displacement and with the biggest extension of the tested device. No big behaviour variations are reported, except for the lightest displacement when, at lower speeds, trim corrections result to be higher compared to heavier displacements.

7.7 Comparison of the hull C954 performances flap – interceptor.

The hull C954 has been tested with flaps arranged along a 6° incidence angle and a 0,5 degrees static trim with trim by the stern.

The results obtained have been then compared with the results presented in the foregoing paragraph.

It is to observe that the tests with the interceptor refer to the zero trim at rest, therefore the behaviour differences of the two arrangements are

not to be ascribed only to a different device, but also to the different position of the barycentre.

The comparison has been carried out with $L/\nabla^{1/3}$ = 4,86 (corresponding to a 121 kg displacement of model scale)

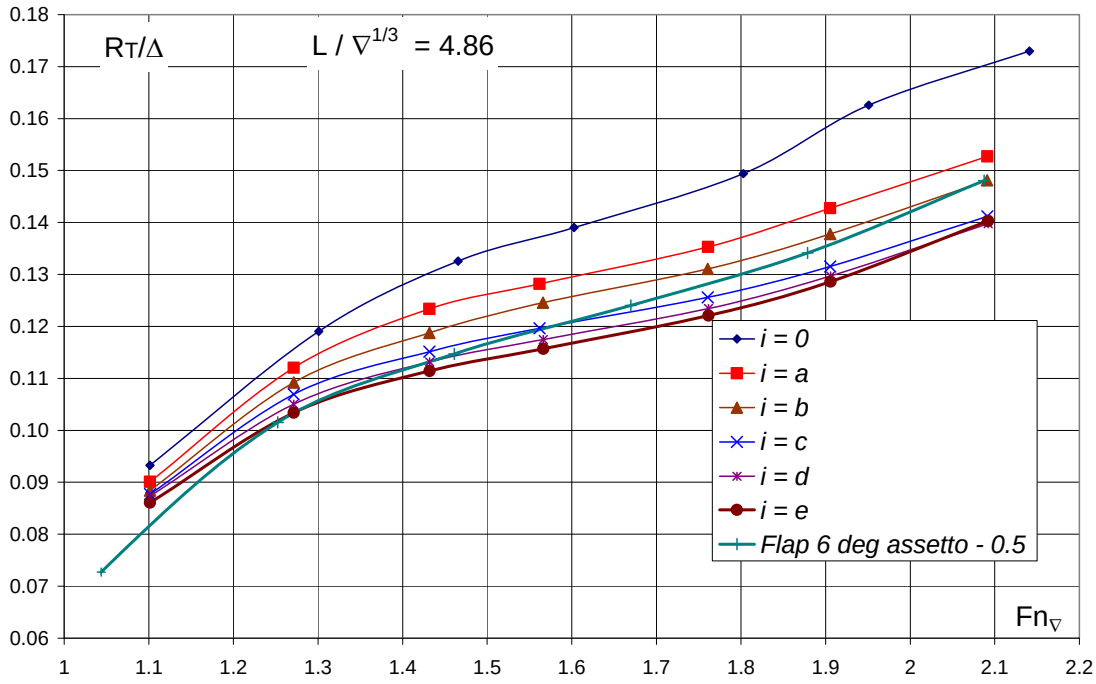

Figure 42 – Flap – interceptor comparison

The chart shows, as it is well known in literature, that as the speed increases, the interceptor becomes more and more effective.

On the contrary, at lower speeds, the tested configurations show a higher effectiveness of the use of flaps.

This seems to be contrasting with what is shown in the following chapters, as regards displacing hulls, but differences in the behaviours are likely to be ascribed to the different geometries taken under consideration and to the working conditions of different types of hull.

The results obtained confirm the different behaviours between flap and interceptor, also obtained in [5] from which a comparison chart is reported below.

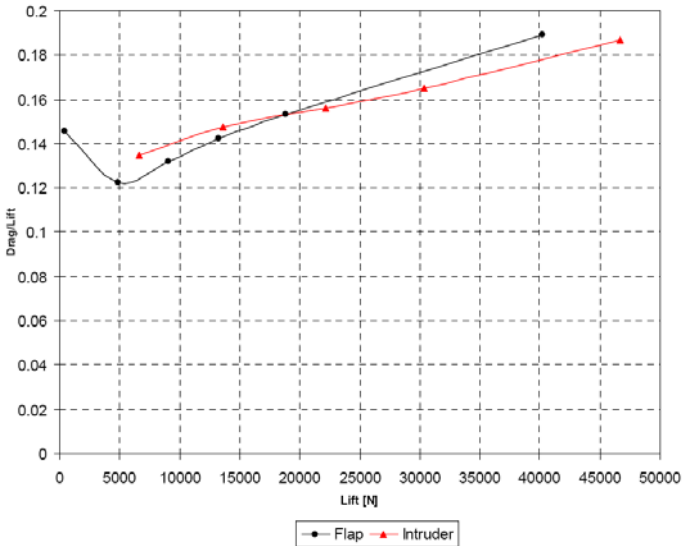

Figure 43 – Flap interceptor (intruder) comparison from Brizzolara, Villa [5]

The chart in Figure 43 shows that as the forces exerted on the device increase, the interceptor results to provide a higher and higher effectiveness.

7.8 Tests on prismatic models.

At first, tests on prismatic models C0201 C9707 C0301 (with deadrise angles of 10, 20 and 30 deg respectively) without interceptors have been carried out; we have chosen to test hulls with small values of the ratio LCG/L_{WL} = 0,332 and 0,368, in order to avoid that the shapes of the bow could influence resistance assessment.

Figure 44 – model C0301.

In Figure 45 and in Figure 46 the towing resistance trends of the three models are reported for the two different positions of the barycentre.

Tests have been carried out for a value of load coefficient $L/\nabla^{1/3}$ = 5,09 and a speed field ranging between 1,3 and 2,8 Fn_∇.

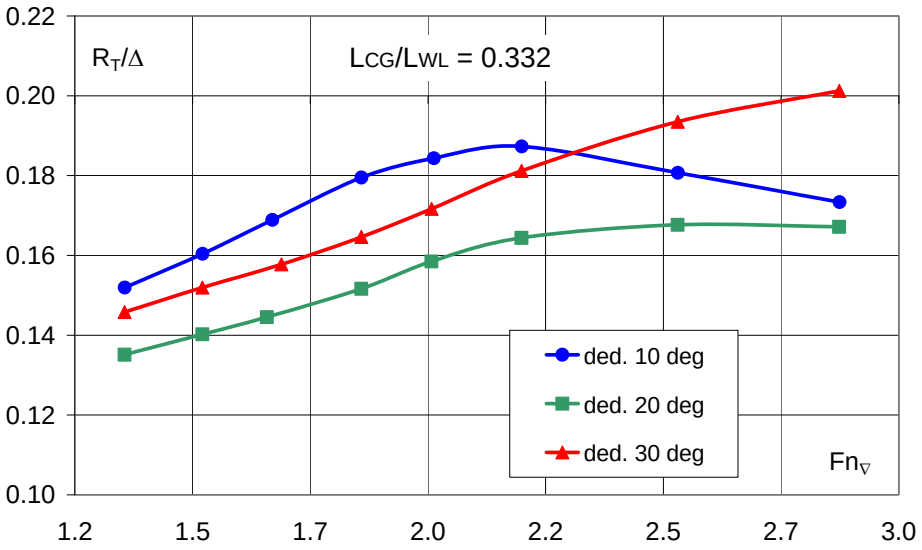

Figure 45 – Prismatic models performances

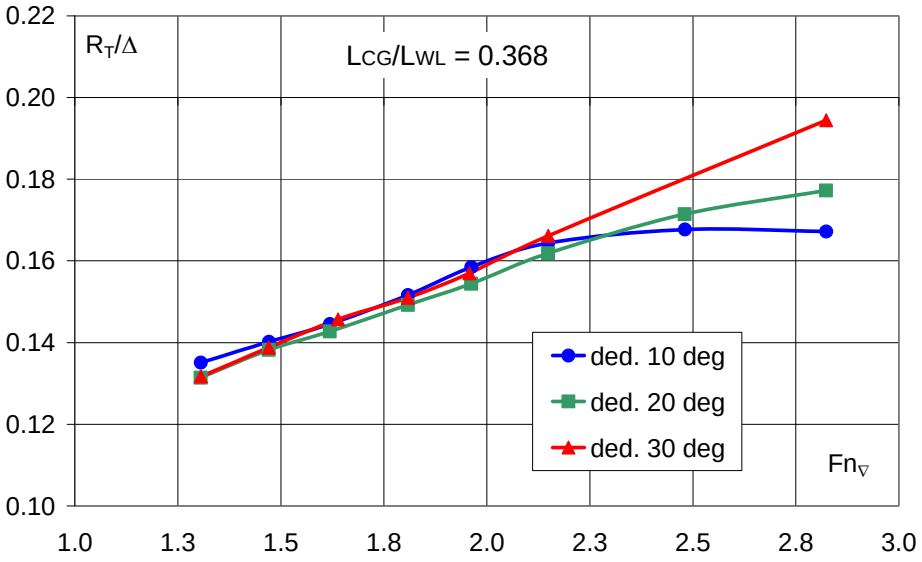

Figure 46 – Prismatic models performances

The reported charts can be considered as reference for the values that will be shown in the next pages.

However, models have been tested with zero trim at rest for β = 10 and 20, as well.

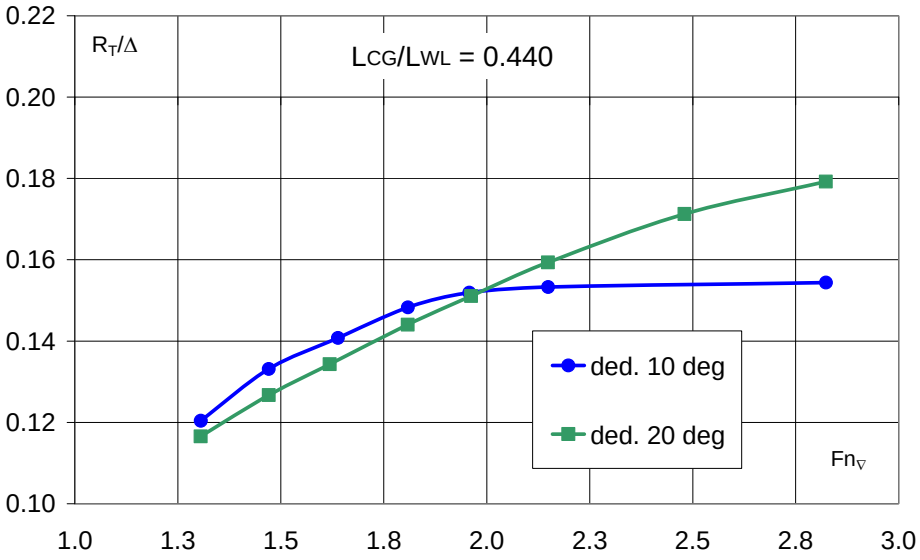

Figure 47 – Prismatic models performances

It is clear that the settled by the stern trim (that has been chosen in order to avoid that resistances and trims of the hull could be influenced by bow geometries) can imply performances differing from the best possible ones at any speed. Therefore, as regards the model with a 20 deg deadrise angle an envelope curve of optimum resistances has been created (BPE Best Performance Envelope) in function of the static trim: it represents the best possible performance achievable at any speed in the testing field, as regards the hull without device. This curve, even if it is not referred to a real condition of the hull, represents a strict comparison term in the assessment of the model performances with devices applied (conventional and non conventional ones)

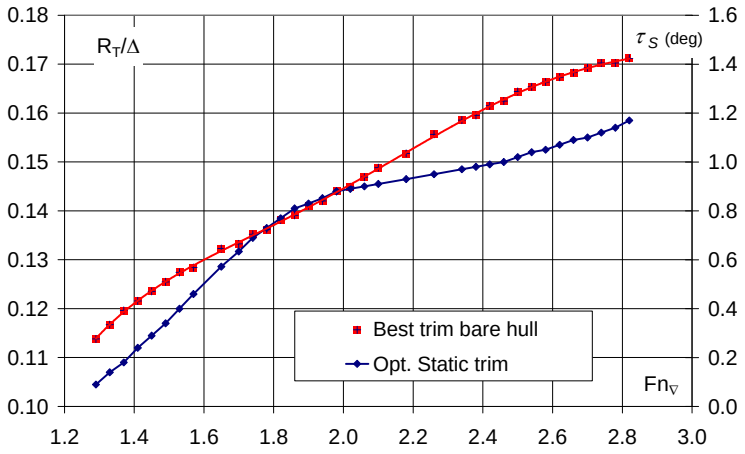

Figure 48 – BPE curve and with respect of the static trim angle

The comparison procedure carried out by using BPE is particularly strict because the comparison term is not a condition that can really take place but instead, a condition that dynamically pursues an optimum condition by varying the longitudinal position of the gravity centre according to speed variation.

The charts comparing the C0301 hull resistance tested for the two gravity centre positions being under examination and the BPE are reported below.

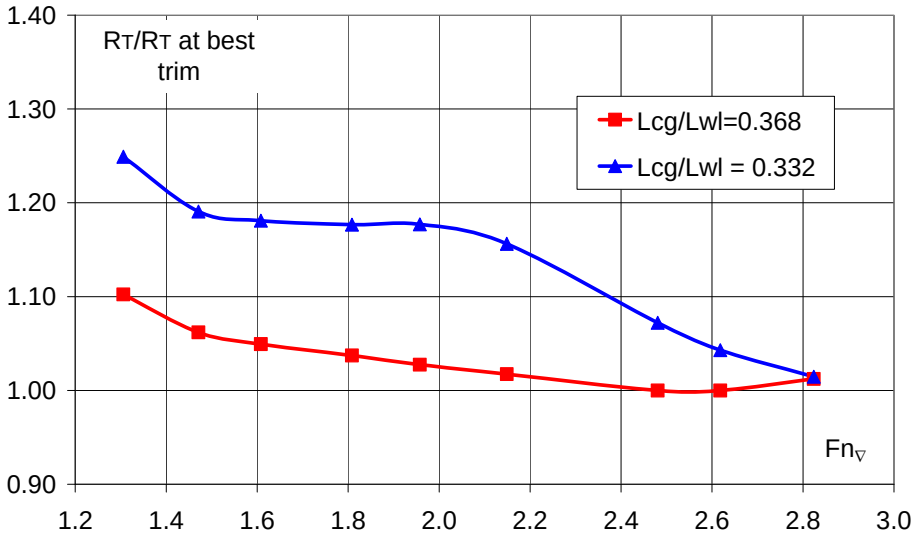

Figure 49 – Resistance of C0301 with respect of BPE.

The curves here shown highlight that, as already well known, with increasing speeds, it is better to put the hull down by the stern, this is due to the fact that as speeds increase, pressure centres shift towards

the stern, thus inducing, over a certain speed, a lesser and lesser dynamic trim and a consequent increase in wetted surfaces.

Finally experimental data have been compared with the results achieved by using the method suggested by Savitsky with a value of Lcg/Lwl = 0,338.

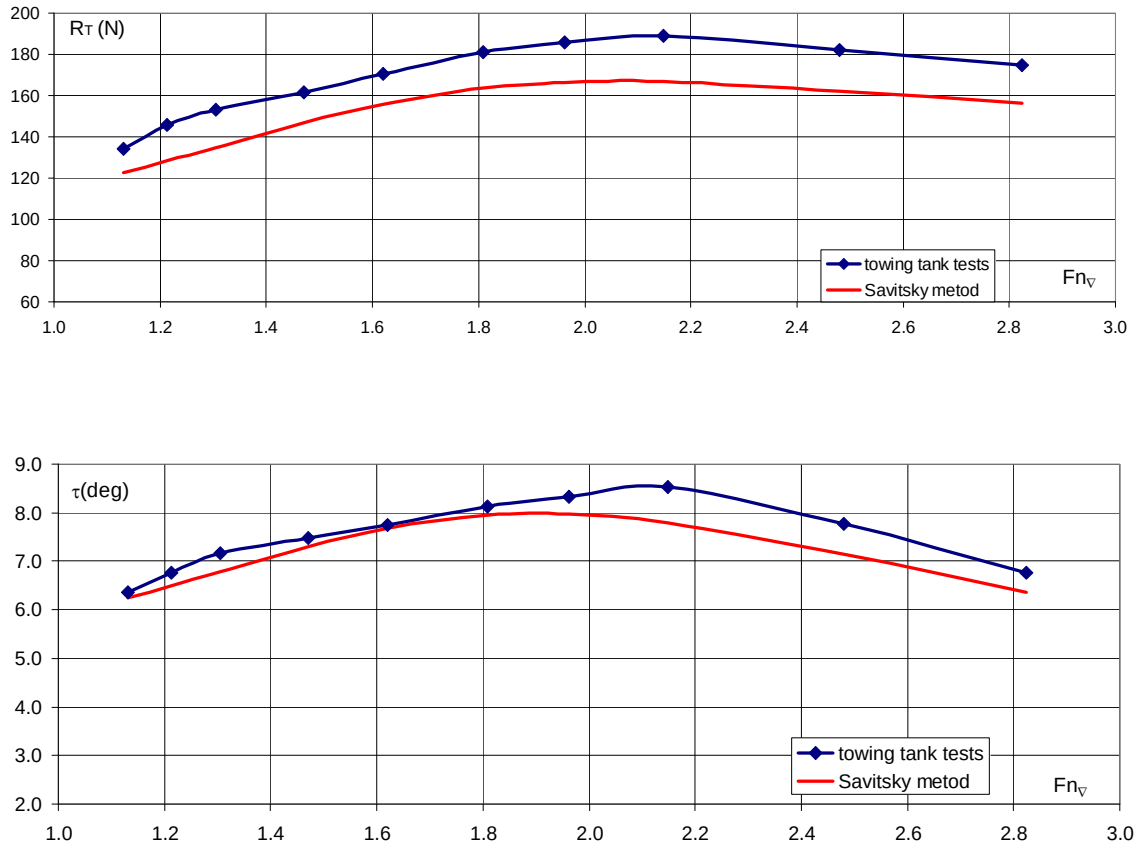

Figure 50 – C9707 β = 10 deg.

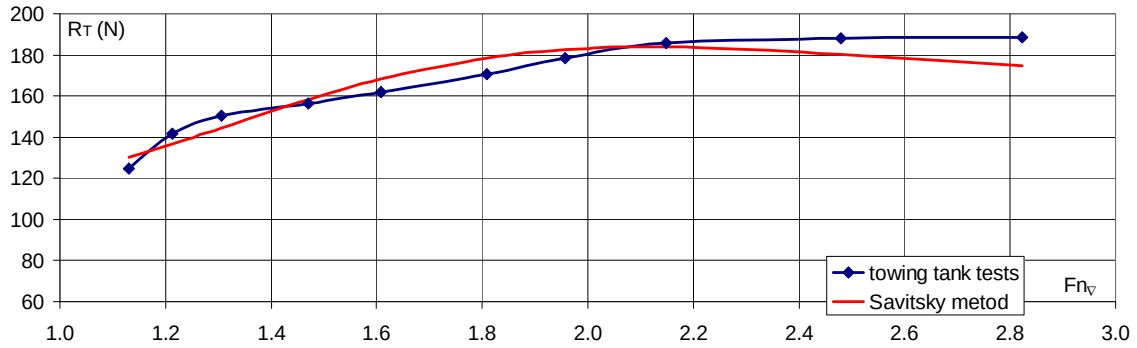

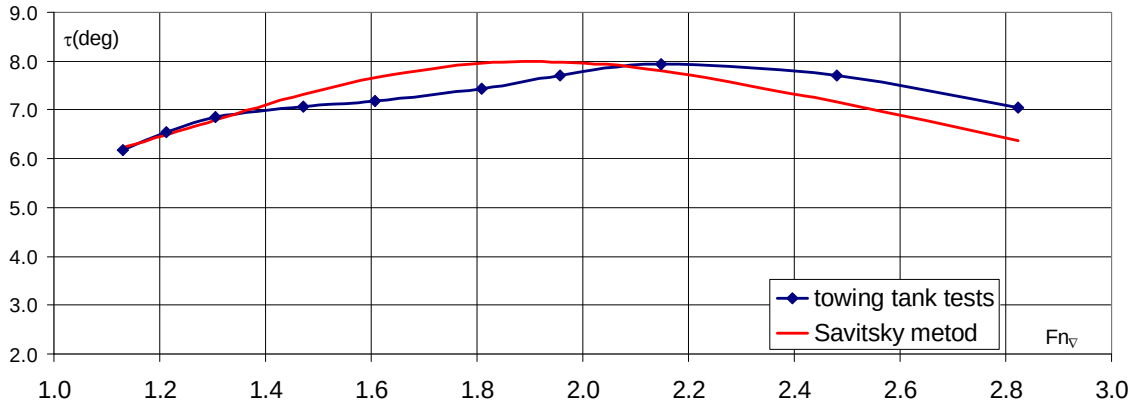

Figure 51 – C0301 β = 20 deg.

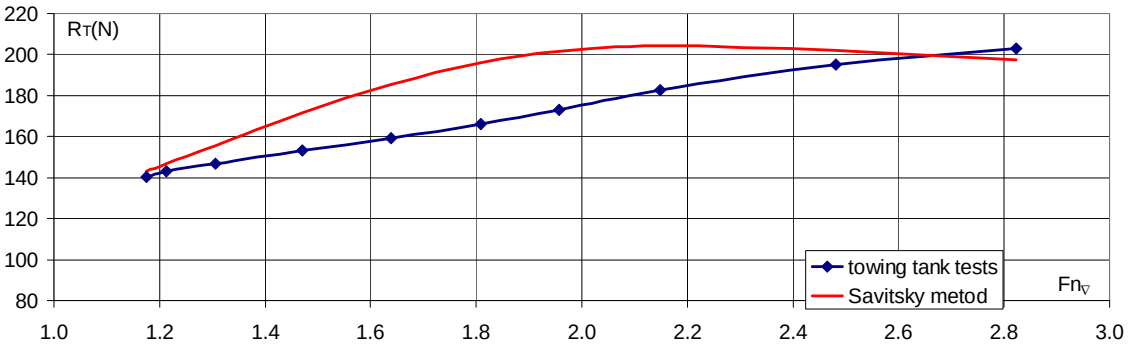

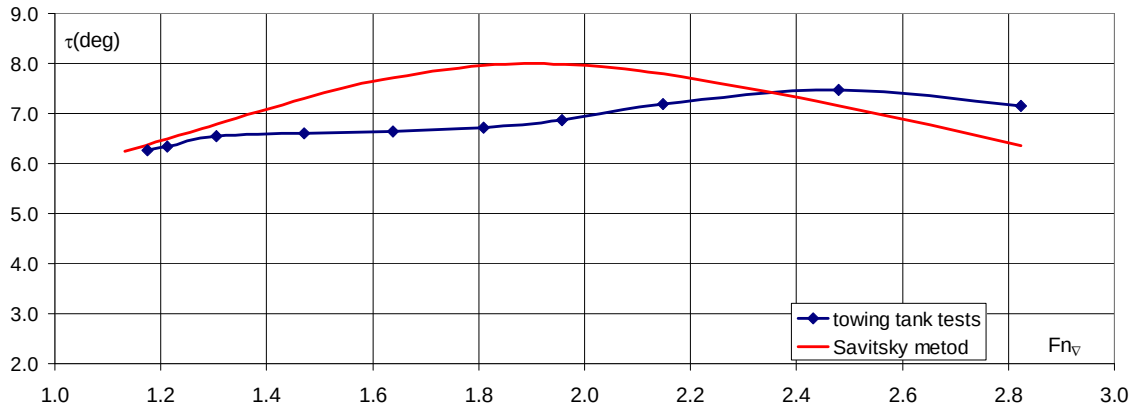

Figure 52 – C0201 β = 20 deg.

Charts show that the most evident differences concern hump resistance both as regards the trim and the resistance. The biggest differences can be found when testing the model with the biggest deadrise angle, for which

the effects of dynamic lift are considered less relevant because of a lesser capacity of controlling overpressures.

7.9 Tests of prismatic models with interceptors.

The conventional interceptors have been tested for different dimensions of devices and different positions of centre of gravity.

Table 7 - Dmenions tested

Lcg/ L_{WL} =	0.440	0.368	0.332
i/L_{WL} = 0 (bare hull)	10 deg 20 deg	10 deg 20 deg 30 deg	10 deg 20 deg 30 deg
i/L_{WL} = 4.19×10^{-4}		10 deg 20 deg	10 deg 20 deg 30 deg
i/L_{WL} = 8.38×10^{-4}		10 deg 20 deg	10 deg 20 deg 30 deg
i/L_{WL} = 1.26×10^{-3}		10 deg 20 deg	10 deg 20 deg 30 deg
i/L_{WL} = 1.68×10^{-3}		10 deg 20 deg	10 deg 30 deg
i/L_{WL} = 2.09×10^{-3}		10 deg 20 deg	10 deg 20 deg 30 deg

This paragraph describes the results obtained by carrying out the program shown in Table 7.

The results are reported as fraction of resistance of the corresponding bare hull.

The dynamic trims are evaluated from zero trim condition (Lcg/L_{WL} = 0.440 $\Rightarrow \tau_S$ = 0)

The speed range considered is Fn_∇ = 1.3 ÷ 2.8

Model 10 deg diagrams:

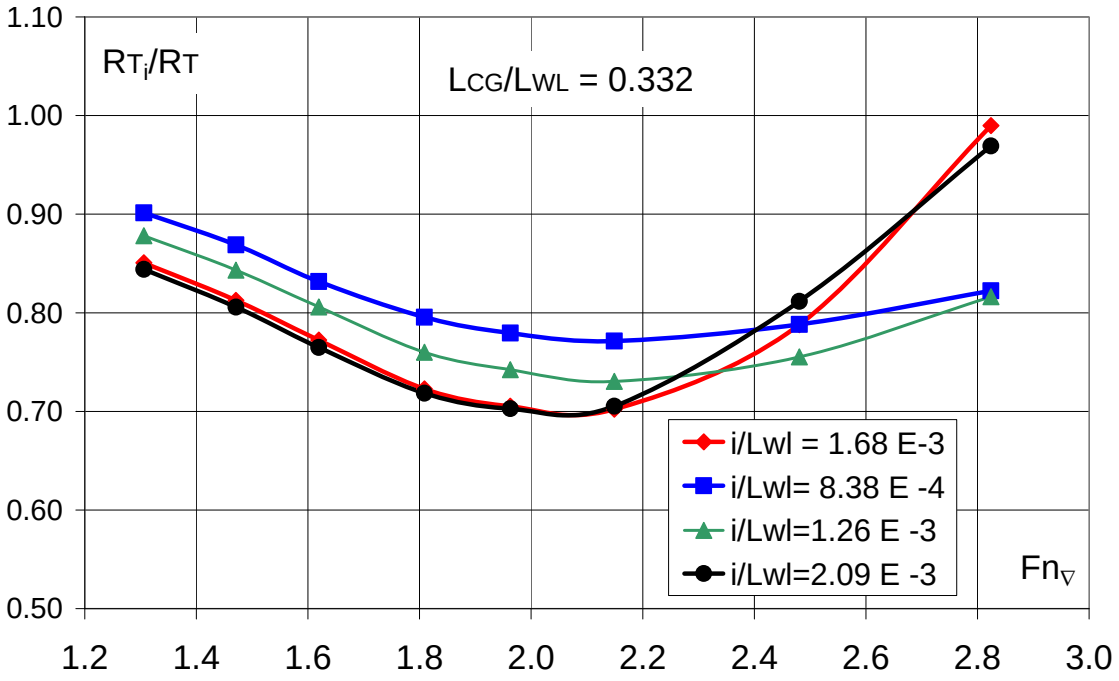

Figure 53 – Effectiveness for each different *i/LWL (β = 10 deg)*

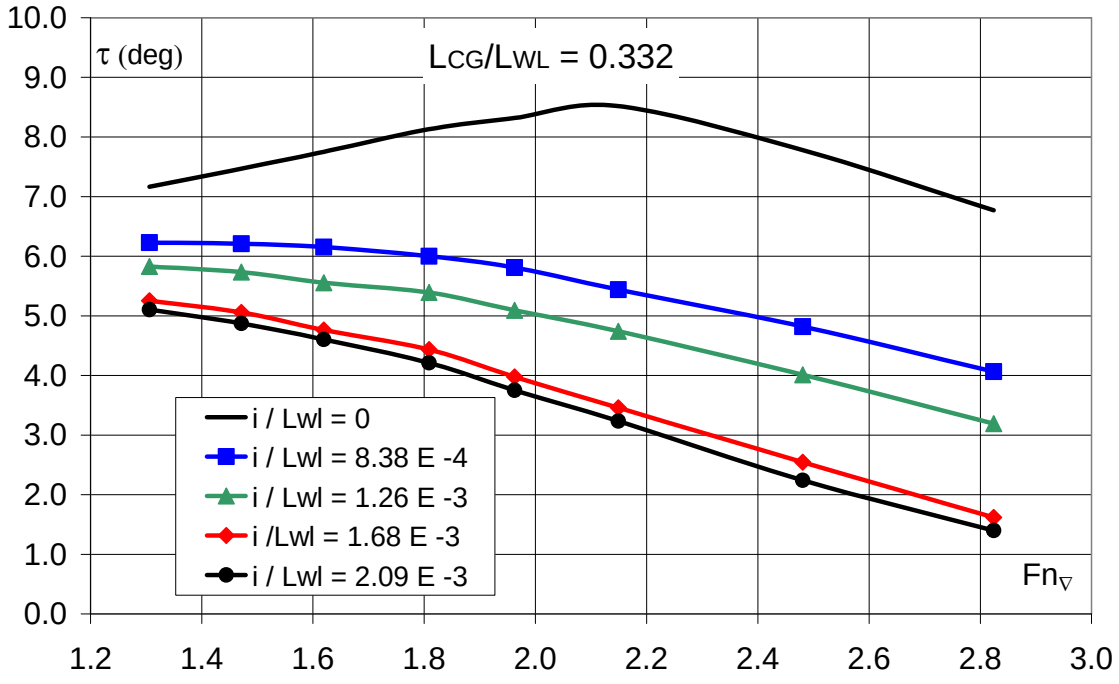

Figure 54 – Dynamic trim at different *i/LWL (β = 10 deg)*

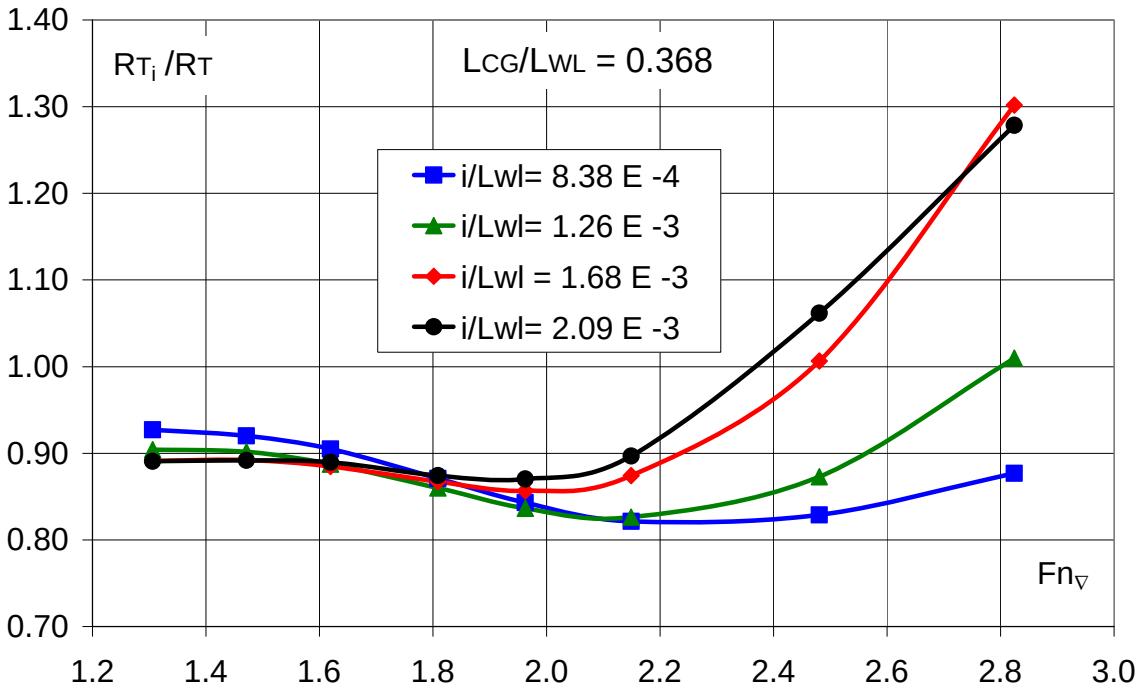

Figure 55 – Effectiveness for each different *i/LWL (β = 10 deg)*

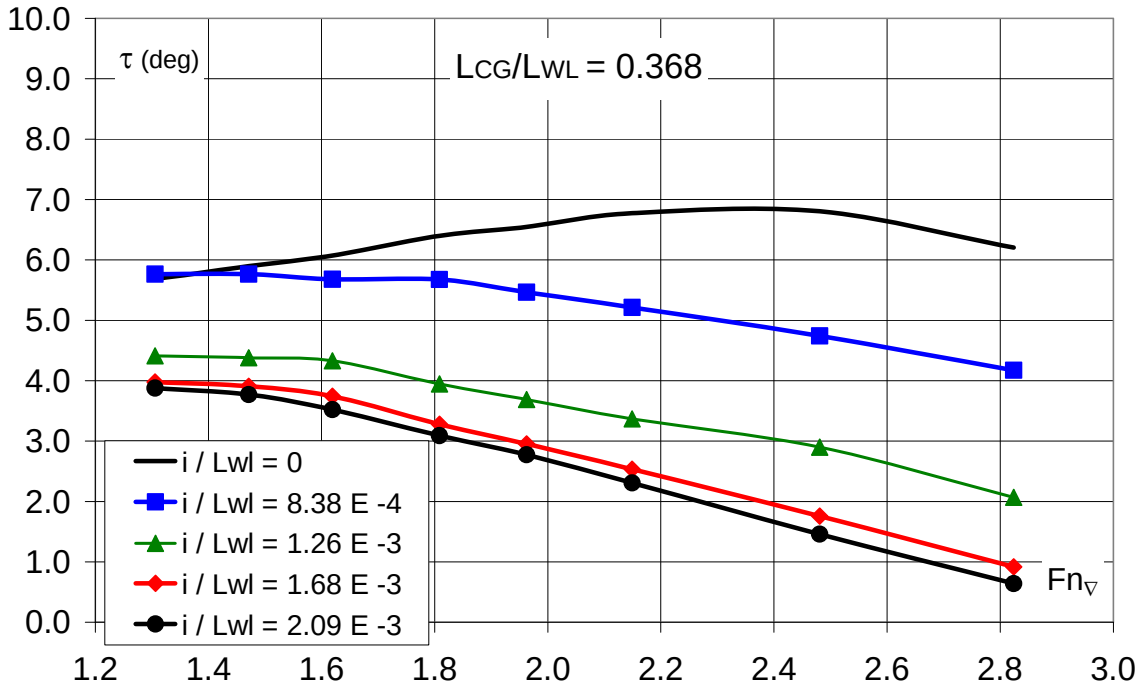

Figure 56 – Dynamic trim for each different *i/LWL (β = 10 deg)*

Model 20 degrees diagrams:

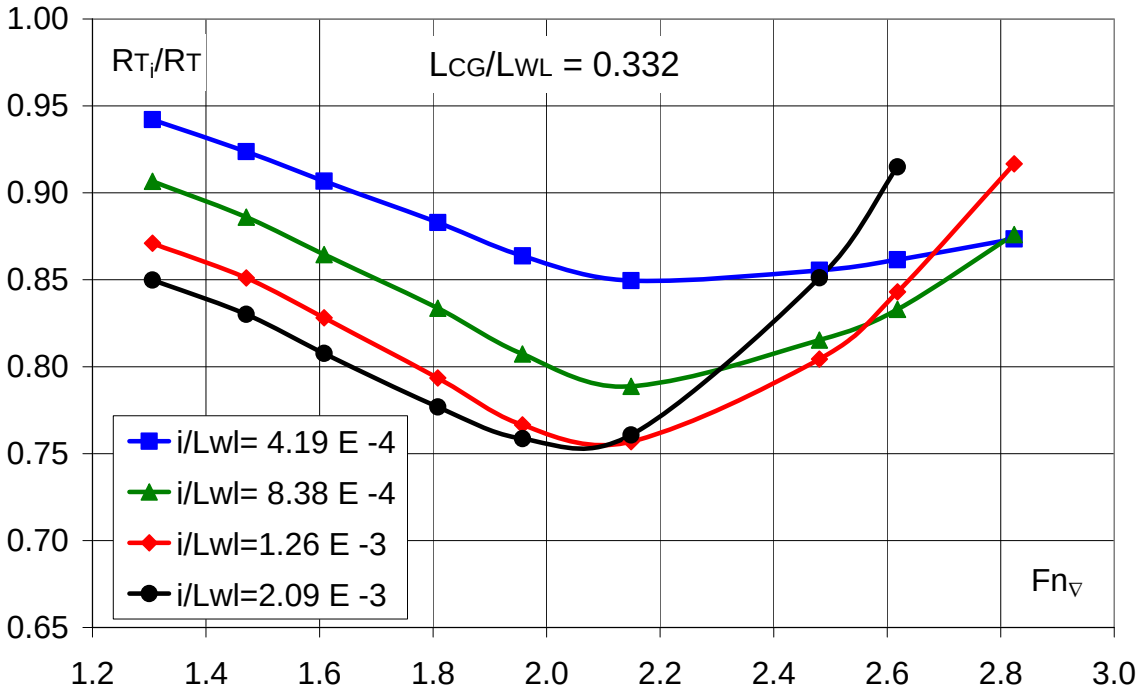

Figure 57 – Effectiveness for each different *i/LWL (β = 20 deg)*

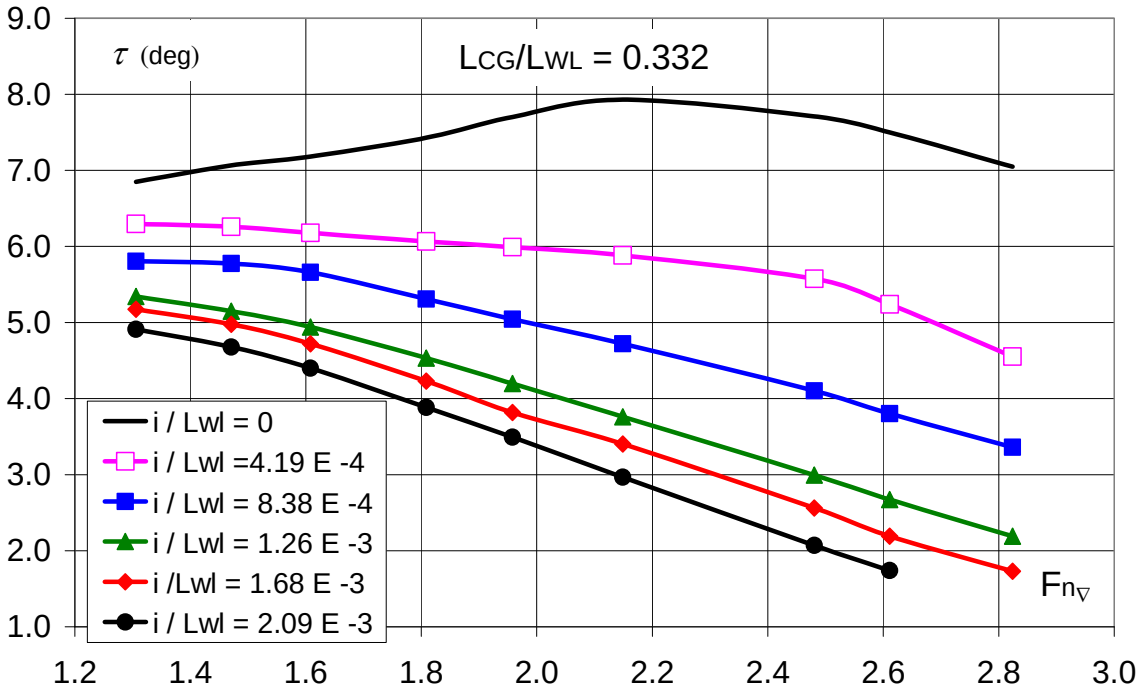

Figure 58 – Dynamic trim for each different *i/LWL (β = 20 deg)*

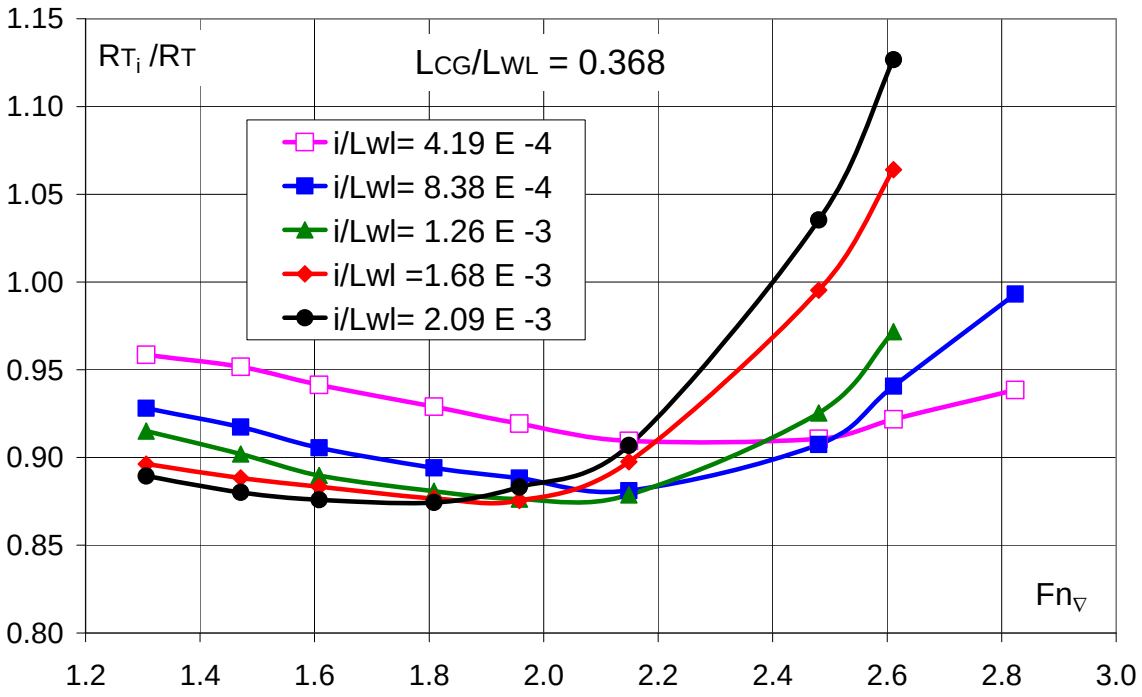

Figure 59 – Effectiveness for each different *i/LWL (β = 20 deg)*

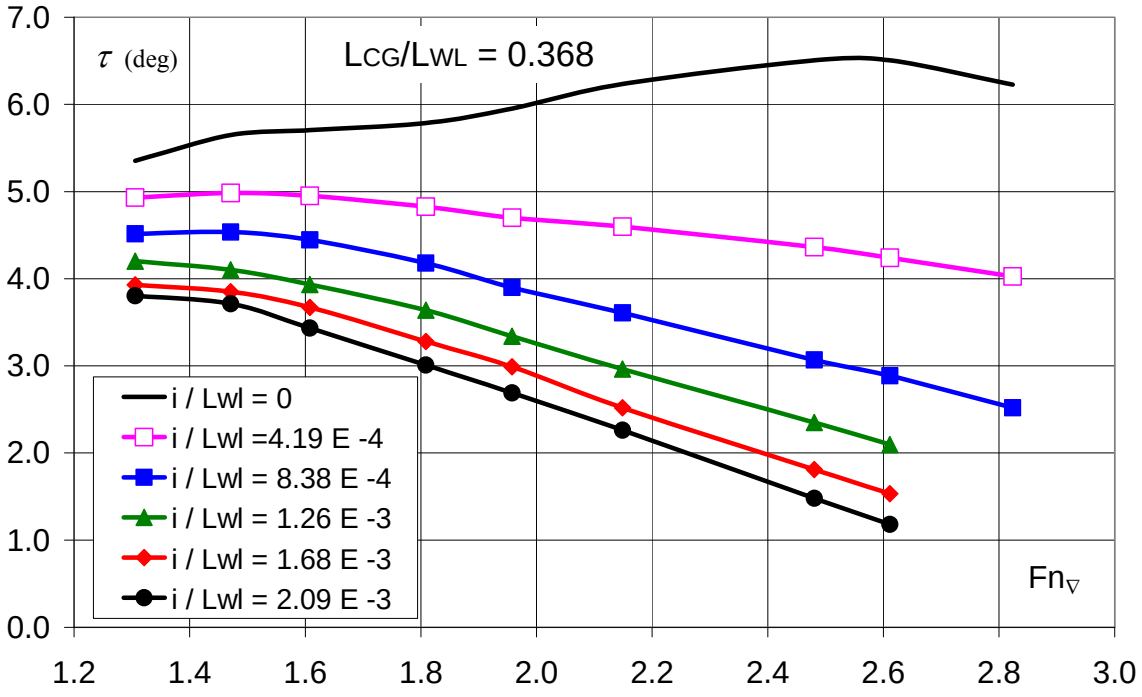

Figure 60 – Dynamic trim for each different *i/LWL (β = 20 deg)*

Model 30 degrees diagrams:

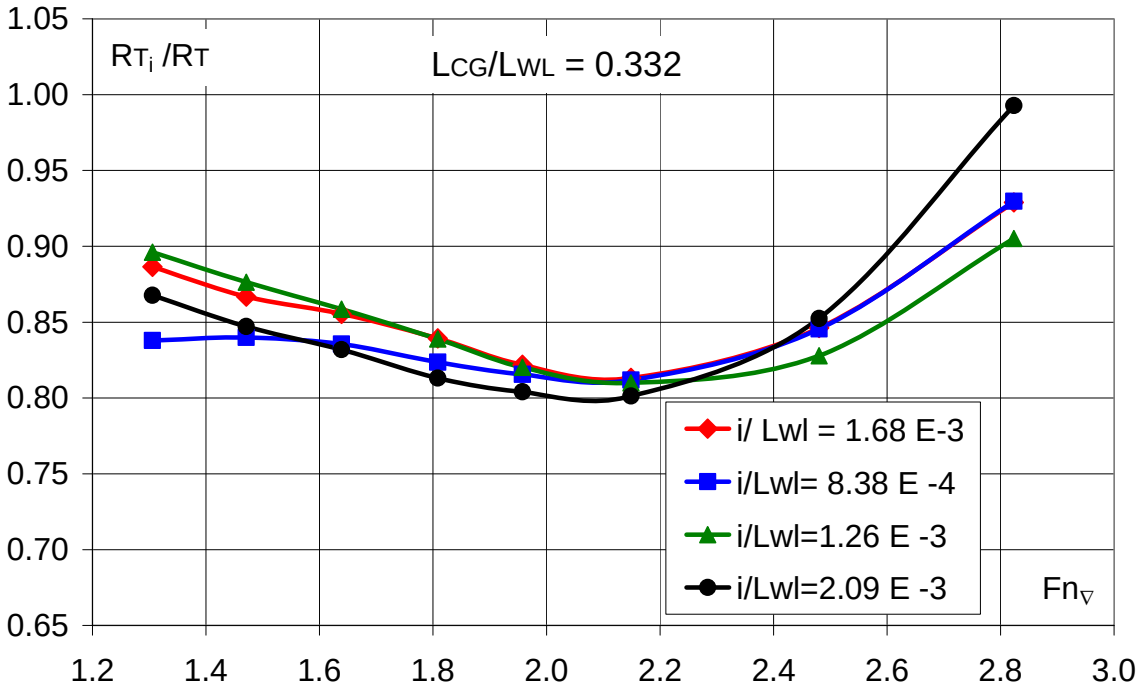

Figure 61 – Effectiveness for each different *i/LWL (β = 30 deg)*

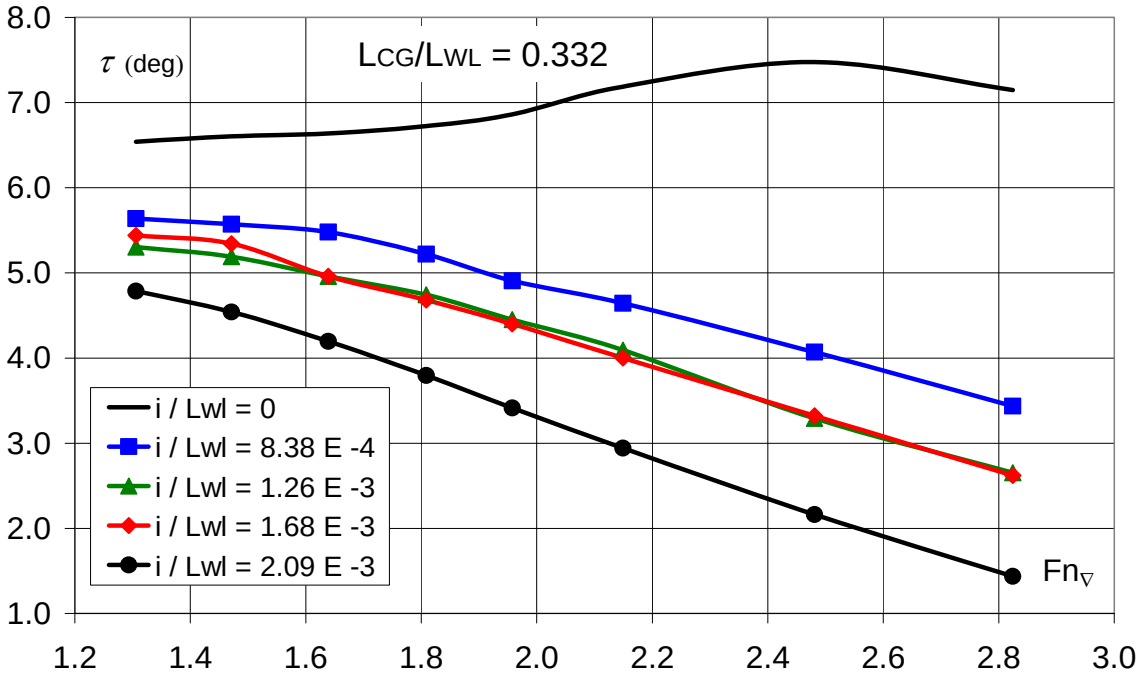

Figure 62 – Dynamic trim for each different *i/LWL (β = 30 deg)*

The previous figures highlight that:

- the best performances are obtained within a speed range of Fn_{∇} = 2.0÷2.2;
- the resistance reductions are inversely proportional to the deadrise angle; this is probably related to a greater transversal flow at a greater β that is associated to a lower effectiveness of the bottom in pressure keeping;
- the performances, of all the models, at the highest speeds, underline extreme trim corrections; coherently, the interceptor's dimensions have to be smaller for higher speeds.

8. Non conventional interceptors

In this chapter two non conventional geometries of interceptors are presented:

- The DIS (Double Interceptor System)
- The SI (Split Interceptor).

The two geometries, already described in the two foregoing chapters, are the result of the observation of the hull behaviour with the standard device applied.

8.1 Double Interceptor System

The study of the physical model and of the interceptor working principle have led us to work out the Double Interceptor System (DIS). The principle behind it is that of enhancing the effects of the overpressures induced by the device, by matching the typical interceptor on the stern, with another interceptor set at 0,524 LWL. In this way, both is possible:

- To increase overpressures.
- To compensate the trimming by the head, caused by the stern interceptor by exploiting the bow device action

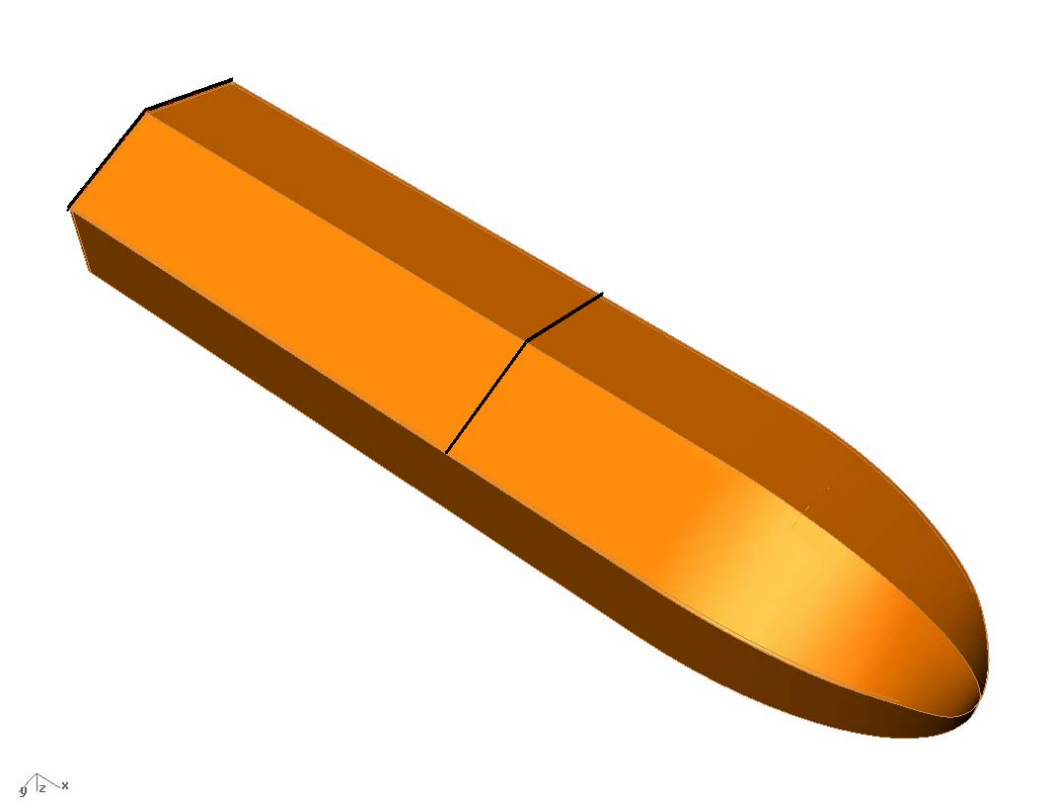

Figure 63 – Double Interceptor System (DIS).

The longitudinal position of the bow device has been chosen by observing the hulls during the test with and without the conventional device; the criterion adopted has been that of setting the device as closer to the head as possible, and letting an area wide enough, be immersed where the increase in pressure induced by the bow device could have be exerted. Then the head interceptor has been set at 0,524 LWL.

Figure 64 – Model C0301 running with DIS applied

We have also chosen to set it parallel to the stern interceptor at the first experimentation stage. Future developments will certainly be achieved by testing other lying positions.

Three different settings have been tested, obtained from the combination of two different sizes of the device, that is 3 and 5 mm.

The chart in Figure 65 shows the DIS performances. On the same chart the performances of the classical configurations illustrated in the previous chapters are also reported.

A comparison of the curves clearly shows that the DIS can provide performances undoubtedly higher than those achieved with the classical interceptor.

Table 8 – DIS testing size on the hull C0301

After Interceptor	*Forward interceptor*
i (mm)	*y* (mm)
3	3
5	3
5	5

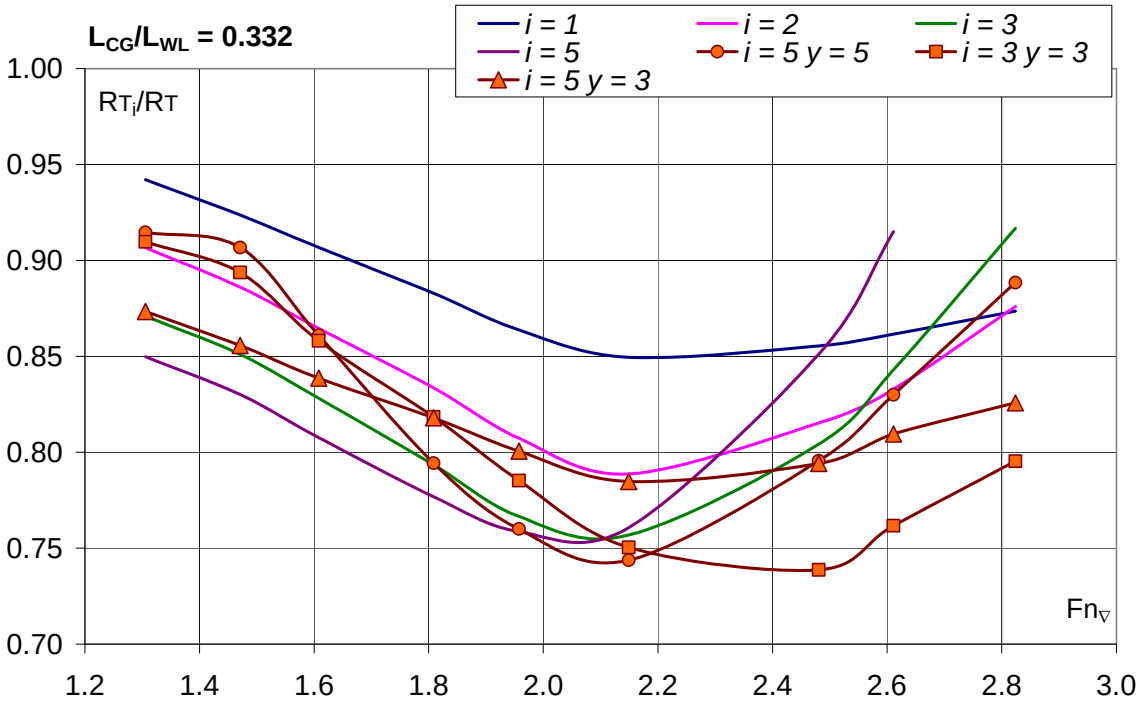

Figure 65 – DIS effectiveness.

As above said, the purpose of using this device is that of increasing the hydrodynamic lift of the hull and of reducing the negative effects of an excessive trim reduction.

As Figure 66 shows, the trim of the hull provided with the DIS decreases in the hump resistance area, while it shows a minimum hump resistance with a volumetric Froude number value of 2,1 and it remains quite constant at higher speeds.

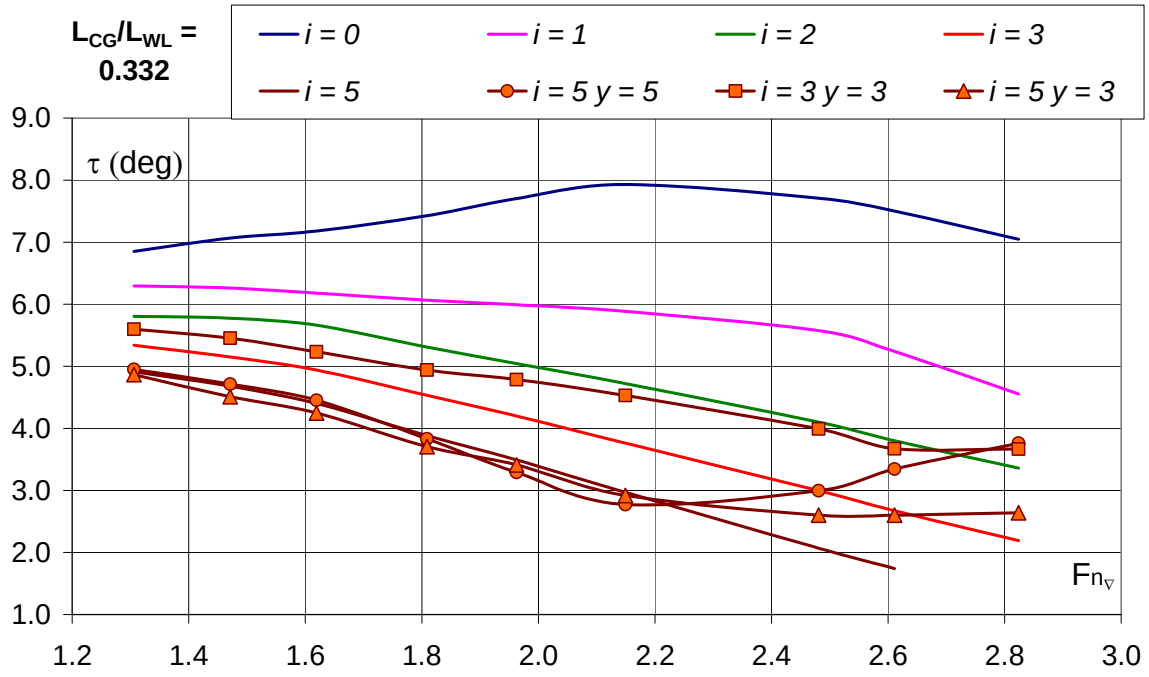

Figure 66 – Dynamic trim with DIS applied.

Downstream the forward interceptor some pressures can be caused that suck the hull downwards.

They, opposing the lift rise caused upstream the device, counteract its effect.

We have been then forced to set some air ducts letting the air in and avoiding the suction of the hull downwards.

An inappropriate ventilation causes an almost complete counteraction of the beneficial effects of the lift of the bow intruder and a consequent big increase of hull resistance.

Inappropriate ventilation can be observed in Figure 68; it shows the hull C0301 at a 5,3 m/s speed with Lcg/LWL = 0,368 to which the DIS is applied. On the left side of the picture the hull without air ducts is shown; with this configuration, a right ventilation cannot be obtained. On the right side the picture the model in motion is shown, which provides an appropriate ventilation of the area downstream the device.

In the test carried out, without using the air ducts the air could be let in to the area downstream the bow interceptor only through the sides. Without the ducts it has thus been necessary to facilitate the ventilation by trimming the hull by the stern of at least 2,2 deg.

In the chart, resistances measured at two different speeds and obtained by gradually settling the CG by the stern, are shown. A high discontinuity caused by τ_s = 2,2 deg can be observed, where an opening of a side channel is produced that lets the air in the downstream interceptor depressed areas. As mentioned above, this problem is really similar to what happens in the case of steps (redans)

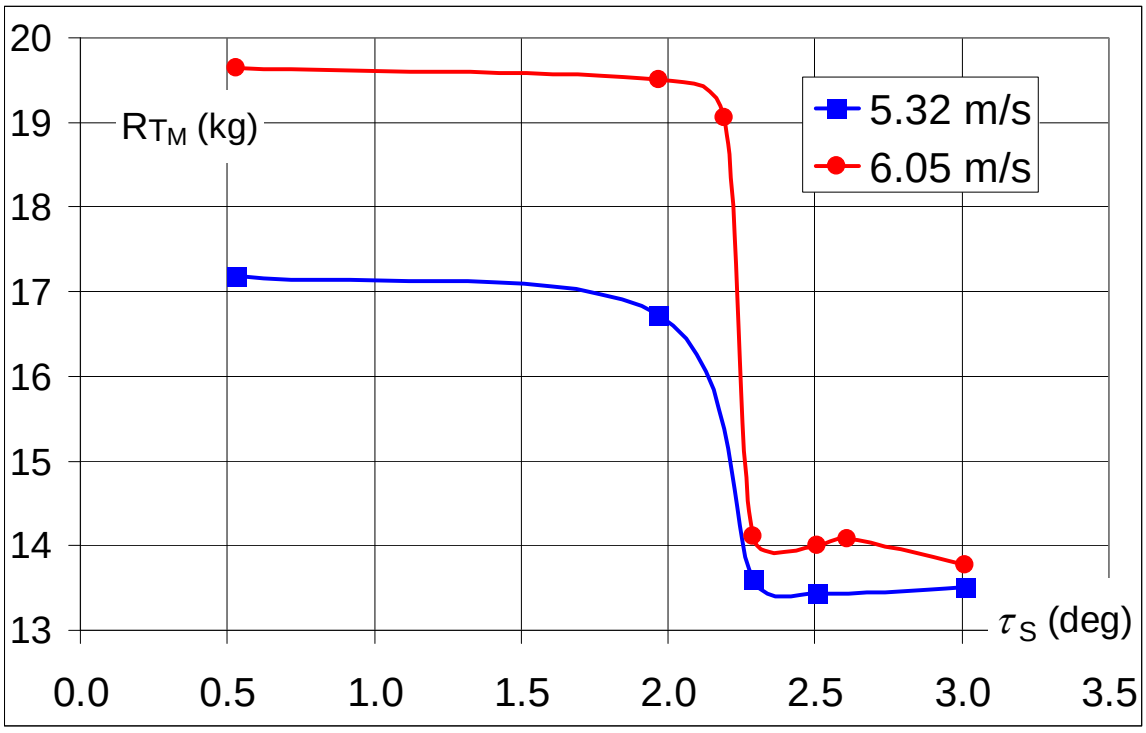

Figure 67 – Ventilation analysis.

Figure 68 – Ventilation analysis

The air ducts the model was provided with, consist of three holes on each side with a 3,5 mm diameter, being homogenously distributed on the bottom of the hull just downstream the device.

Figura 69 – Air ducts

The DIS has been also tested on warped hull. The second device, whose size is represented by letter y, has been set at a distance Ly equal to 0,524 L_{WL}, similarly to what has been done with the other hull. Then, a different position has also been tested, represented by Ly', equal to 0,542

LWL. The hull has been tested with a ratio Lcg/LWL = 0,37 because such position has been found as helping device ventilation.

Also in this case the desired trim trend can be obtained: at speeds lower than the hump resistance the trim correction of the stern interceptor prevails, with a consequent reduction of the hull trims during the test the hump resistance. As the speed increases the pressures upstream the bow interceptor start playing a key role, thus causing a trend reversal and the consequent increase of trims.

Table 9 – Testing sizes of the DIS on the hull C954

After interceptor	*Forward interceptor at Ly*	*Forward interceptor at Ly'*
i (mm)	*y* (mm)	*y'* (mm)
4	4	
4		4

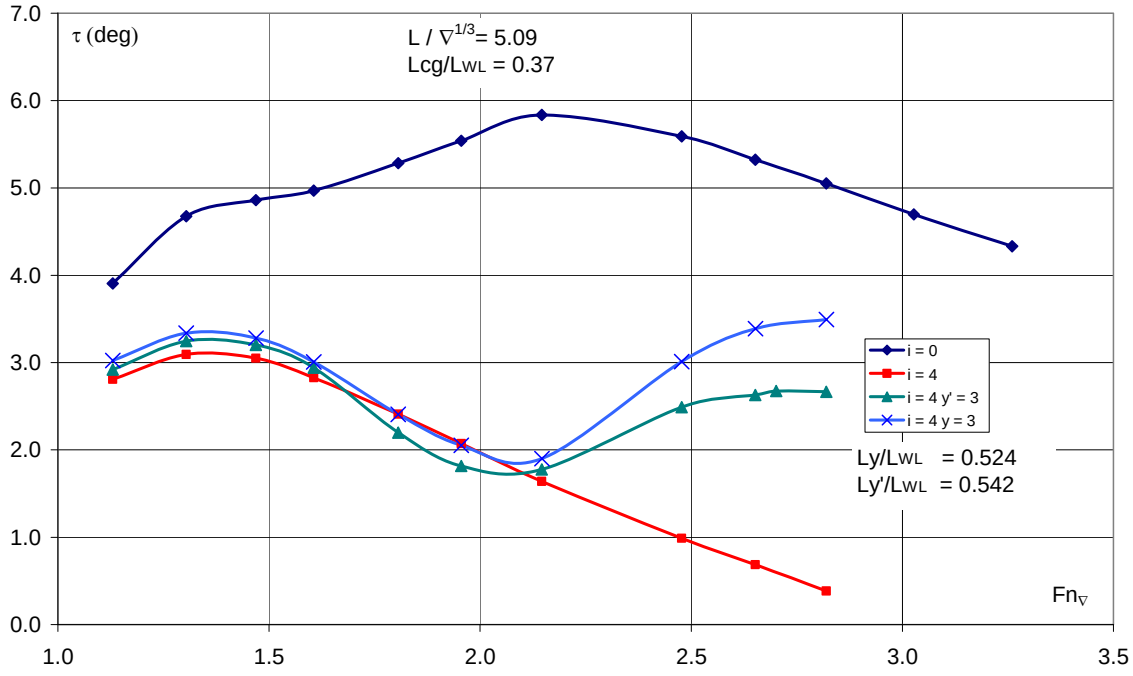

Figure 70 – C954: dynamic trim behavior with DIS

Despite the achievement of the desired trim trend and the big rising of the hull from water, performances are not better than those with the classical configuration, except the case of Fn_{∇} = 2,65.

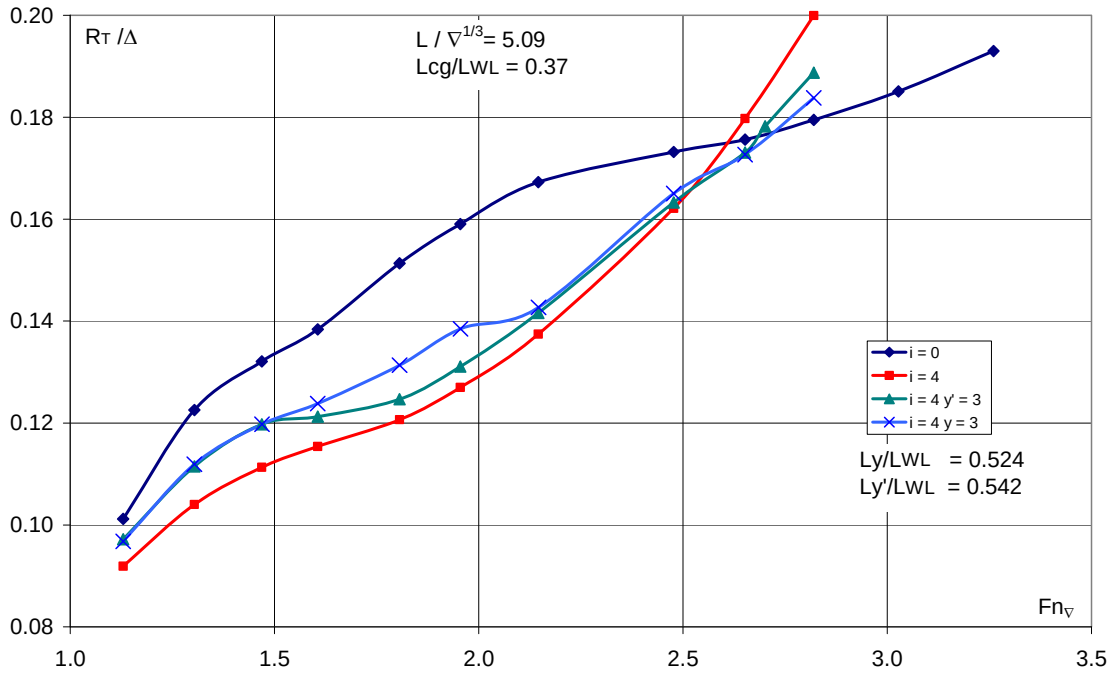

Figure 71 – Performances of C954 with different DIS settings

This is also probably due to the orientation of hull surfaces upstream the device: by increasing pressures in an area where buttocks have an increasing angle, a high horizontal component of pressure integral in that area will be produced.

As a matter of fact, many other factors influence the effectiveness of the DIS, such as the ratio L/B of the hull, the device positioning angle, the variation law of the deadrise angle, and so on. Many derivations remain then unsolved and suggest new developments of this research field.

On the hull C954 provided with the DIS a problem of longitudinal dynamic instability has been found. During the tests carried out, after reaching a 6,055 m/s speed, corresponding to Fn_{∇} = 2,8, a rather uncommon effect has occurred: the model started to periodically change trim, draught and

consequently resistance; the instability tends to occur at higher speeds if the ratio Lcg/Lwl is increased. The following chart describes the behaviour of the model during a run when the phenomenon occurred.

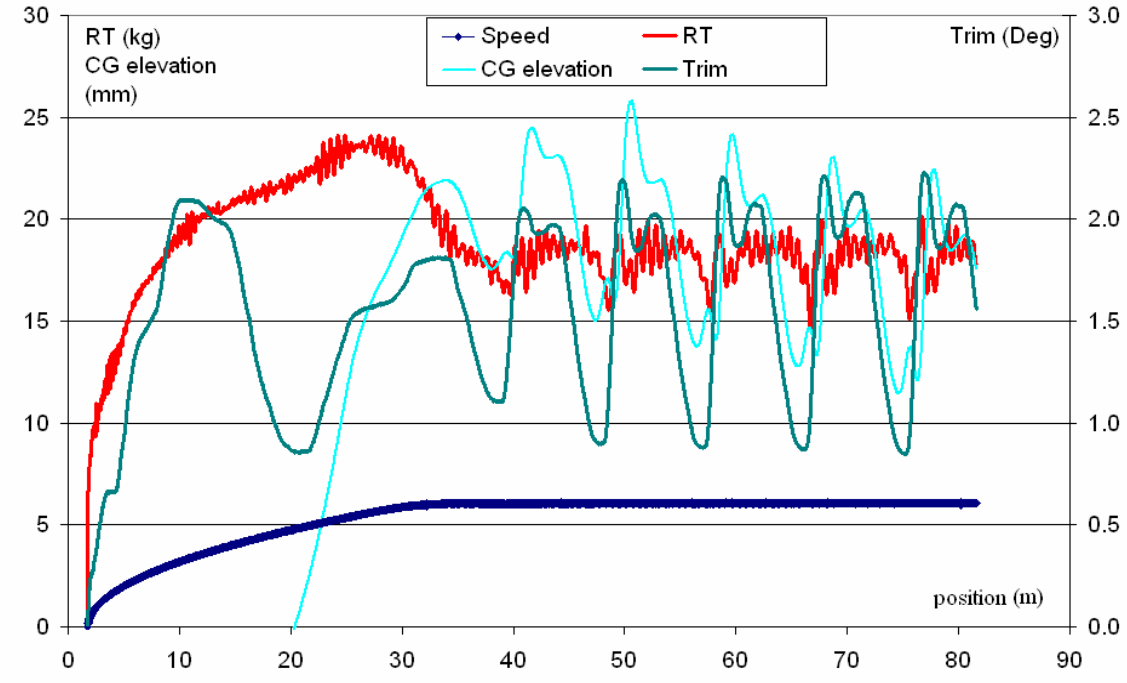

Figure 72 – Dynamic instability

In future developments of this research, it be will thus, of the uttermost importance to investigate the causes, in order to avoid that the phenomenon takes place on sailing crafts.

Instability is probably caused by the head interceptor crossing the stagnation line. This phenomenon is well known in literature, as regards steps. This problem is dealt with in Savitsky, Morabito [15]:

If stagnation line does cross the step, large, high velocity spray sheets originate at these intersection points and impact against the bottom of afterbody. This will result in a large increase in total resistance and possibly initiate longitudinal instability.

It's not simple to represent what observed in the above described phenomenon, therefore the following figure shows the stagnation line of the stern system crossing the stern interceptor. The same phenomenon occurring on the head interceptor is likely to initiate dynamic instability, similarly to that occurring in hulls with steps.

Figure 73 – Stagnation line across the aft. interceptor in DIS configuration.

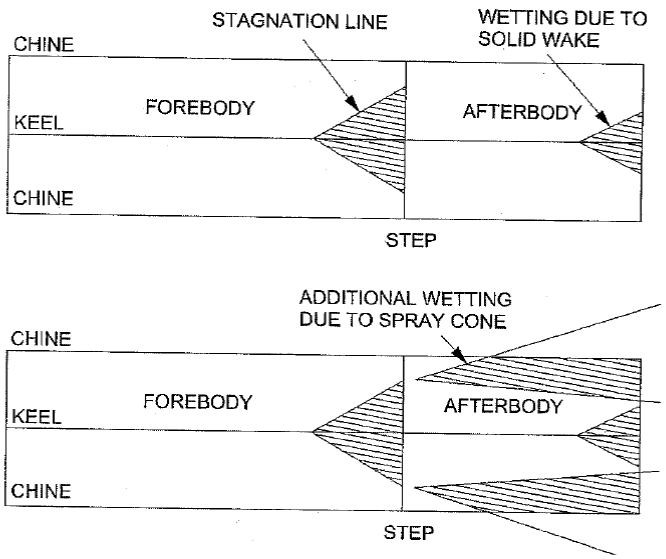

Figure 74 – Stagnation line across the step, from Savitsky Morabito [15]

8.2 Split Interceptor.

The second solution consists in creating an opening on the bottom of the interceptor. The criterion chosen is the one described in the previous chapters and synthesized in the following points:

- Avoiding the generation of closed vortices and the related energy waste
- Reducing the curvature radius of the streamline by increasing the local overpressures

The device shown in the figure below has been tested with an opening of two different sizes (*h* = 0.25 *i* and *h* = 0.08 *i*) and with two different positions of the CG.

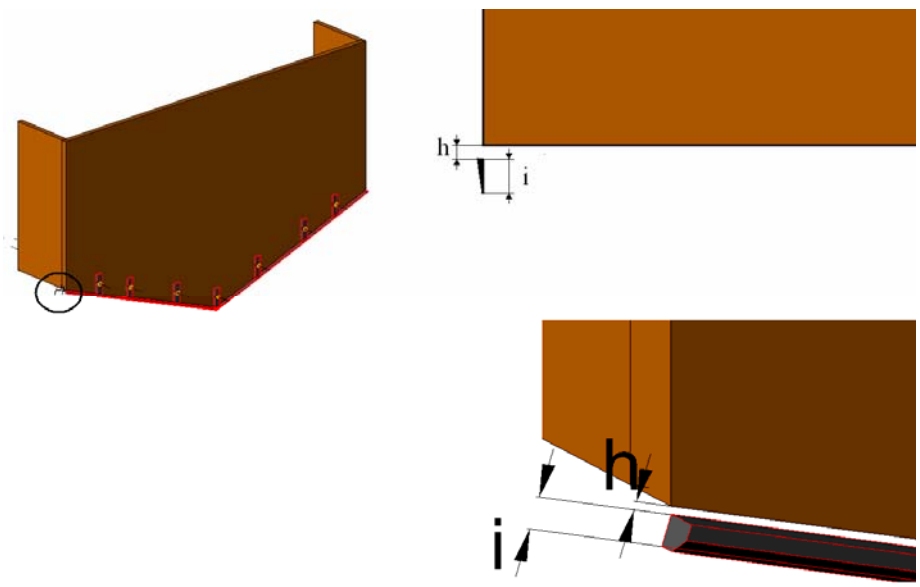

Figure 75 – Split Interceptor (SI)

Below are the charts representing the ratio between resistance and trim, on the background of the same chart again the data related to the

standard configuration in order to have an immediate comparison of the effectiveness of the device.

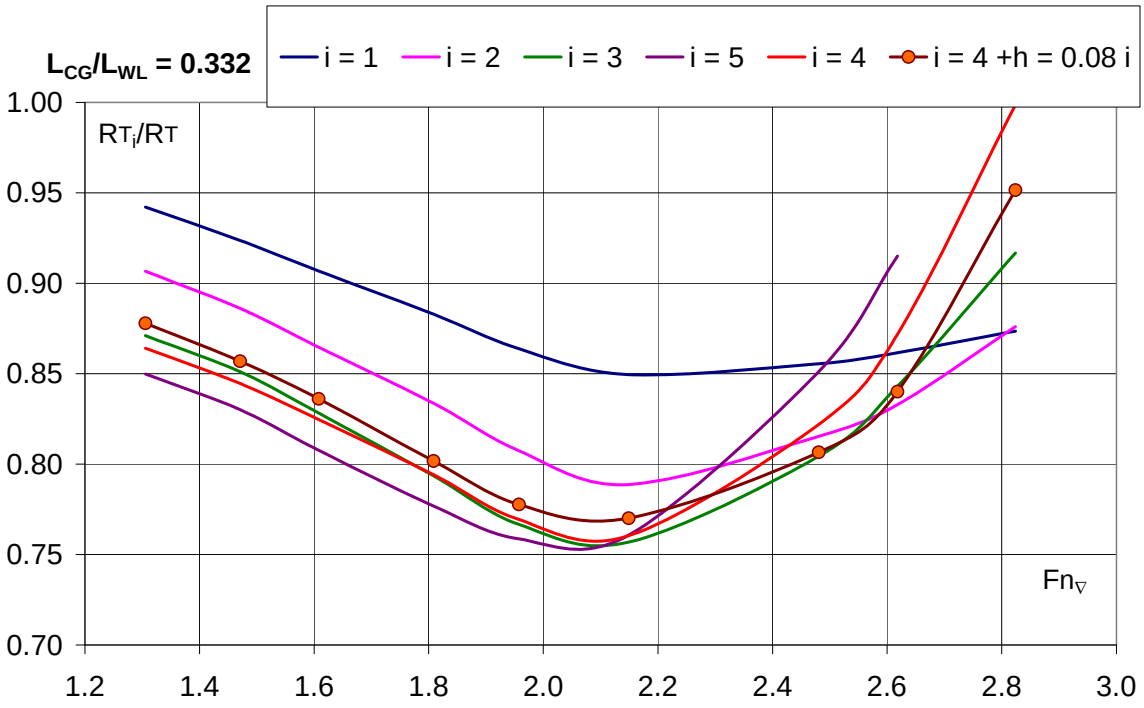

Figure 76 – SI performances

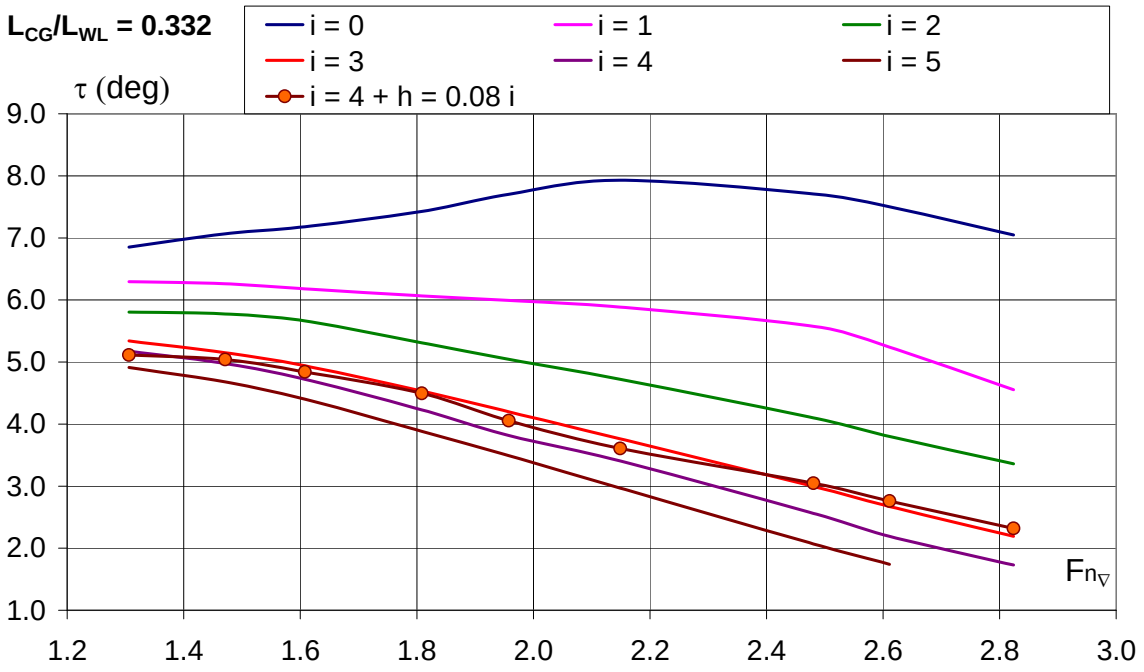

Figure 77 – SI dynamic trim behavior

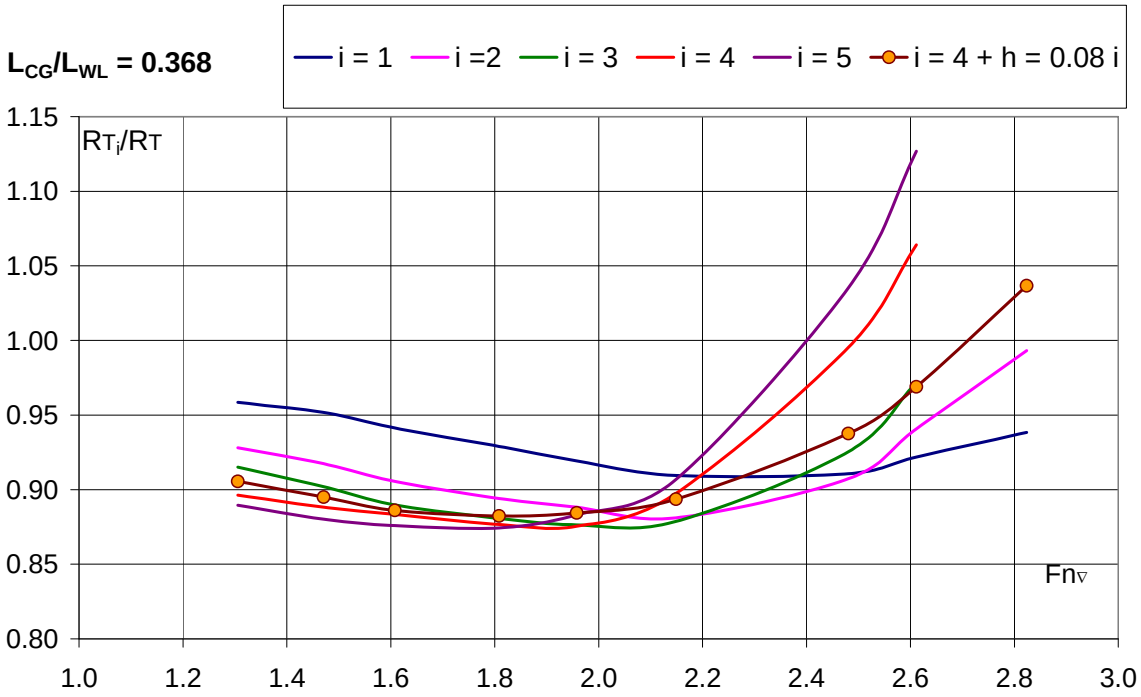

Figure 78 – SI performances

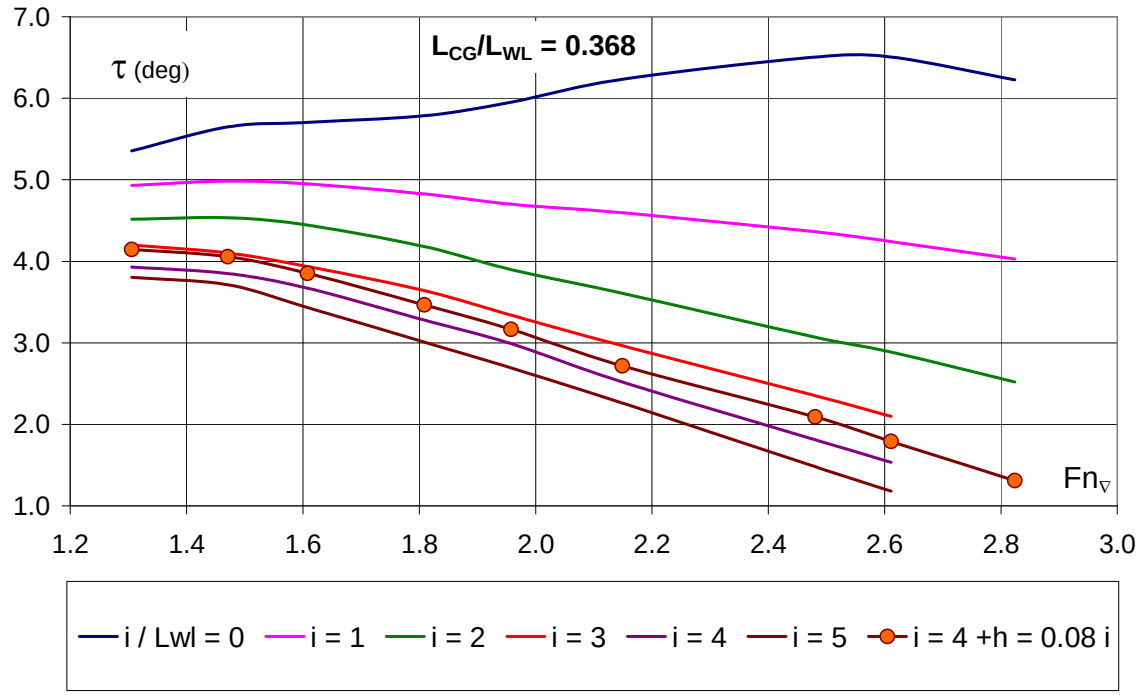

Figure 79 – SI dynamic trim behaviour

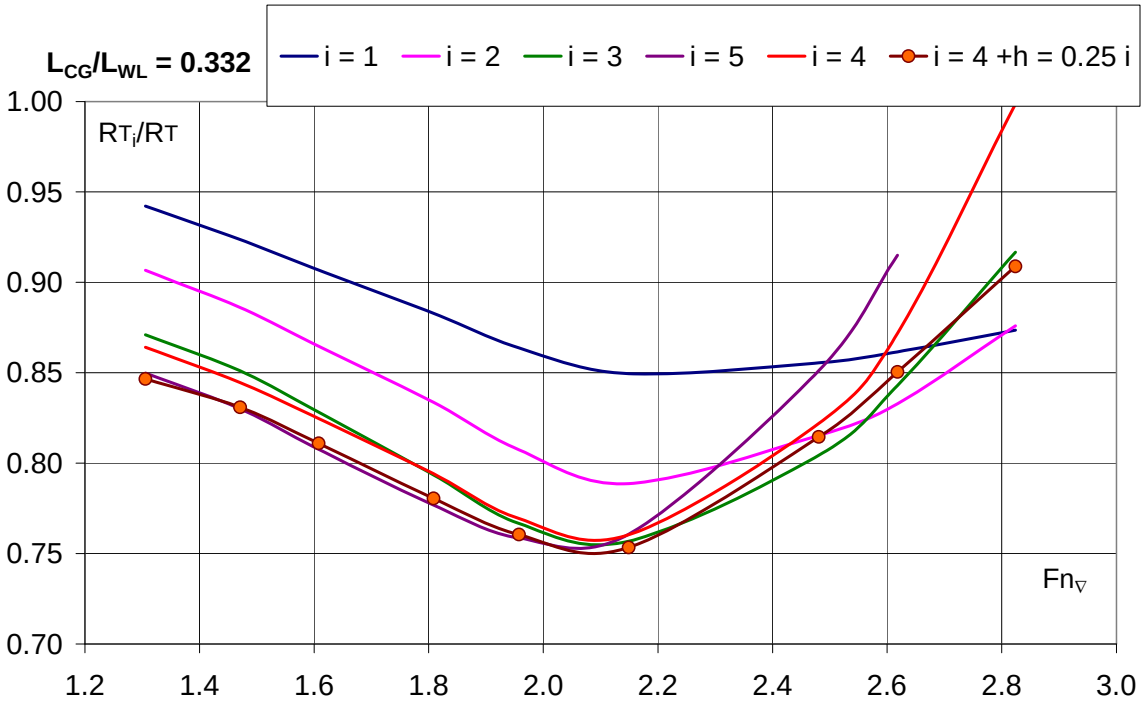

Figure 80 – SI performances

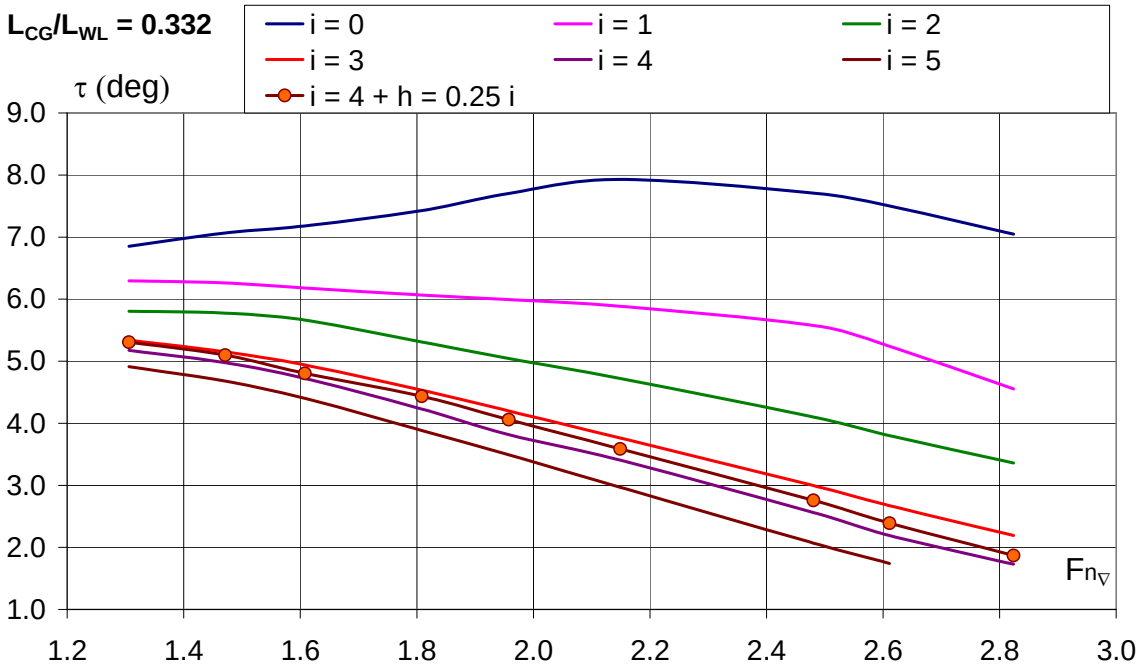

Figure 81 – SI dynamic trim behaviour.

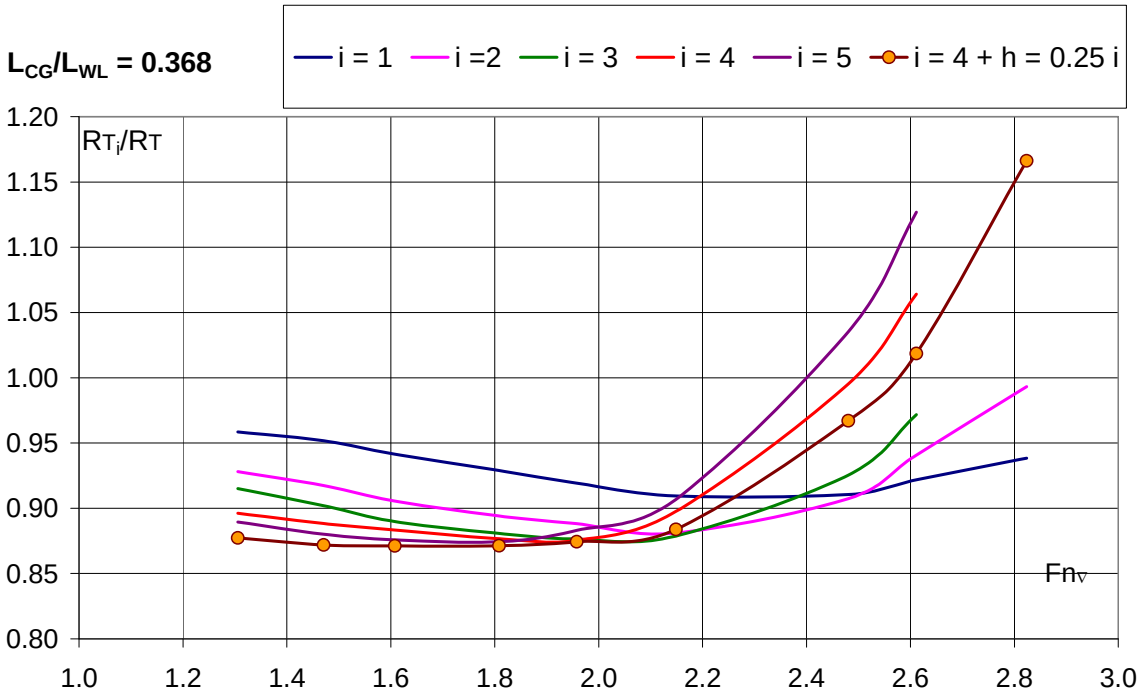

Figure 82 – SI performances

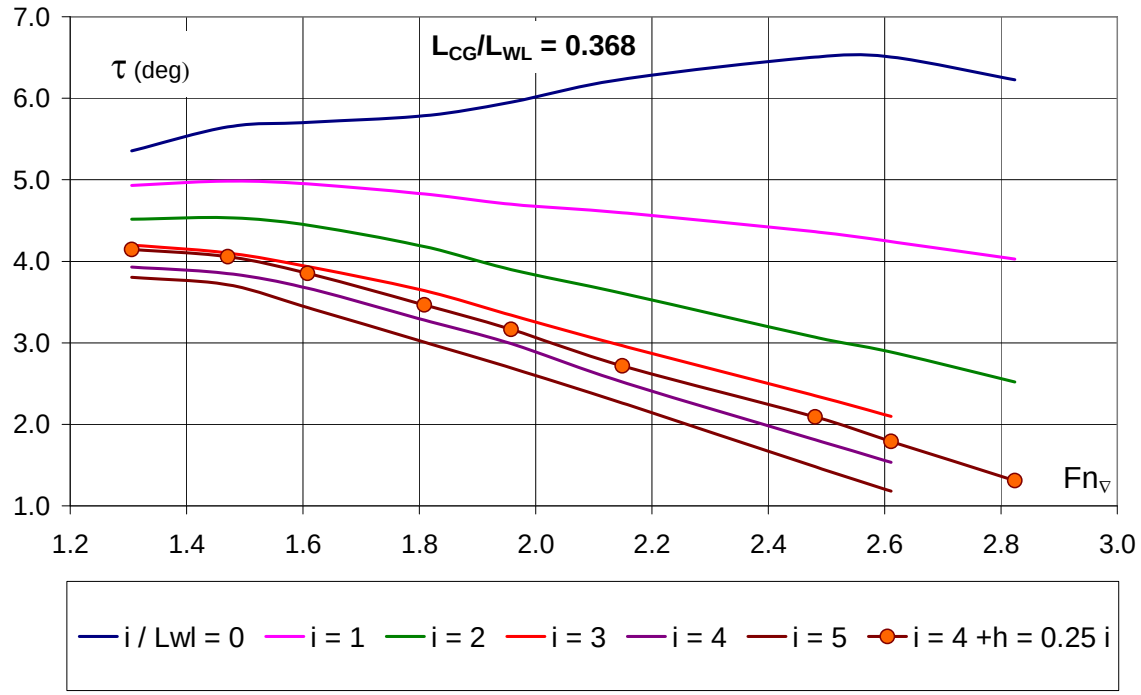

Figure 83 – SI dynamic trim behaviour

The charts show that this device, compared to the standard configuration, has a big potential.

The charts show that:

- The behaviour in terms of trim changes does not differ too much from the one of standard configuration.
- The *h* = 0.08 *i* configuration allows good performances on the overall speed range, approaching an average value of the performances with different dimensions of *i* and at different speeds.
- The *h* = 0.25 *i* configuration allows optimum performances on the overall speed range, approaching the envelope of the best performances obtained with standard devices.

Figure 84 – Model C0301 with SI applied

Clearly, with a movable interceptor at higher speeds, better performances can be achieved.

Nevertheless, the proposed devise is found to be a solution far more cost-effective to choose.

9. A stricter evaluation of effectiveness

In order to avoid the wetted bow effects that make the performances worse at high speed (and very low trim), all the models have been tested down by the stern. As a consequence, the results expressed in terms of resistance fraction of bare hull data, are affected by the non- excellent resistance due to the small Lcg/L_{WL} of the bare hull.

With a view to avoiding an overestimation of the virtues of the arrangements tested, in previous chapters the BPE (Best Performance Envelope) was proposed as fraction terms. It represents R_T for each speed with the best static trim.

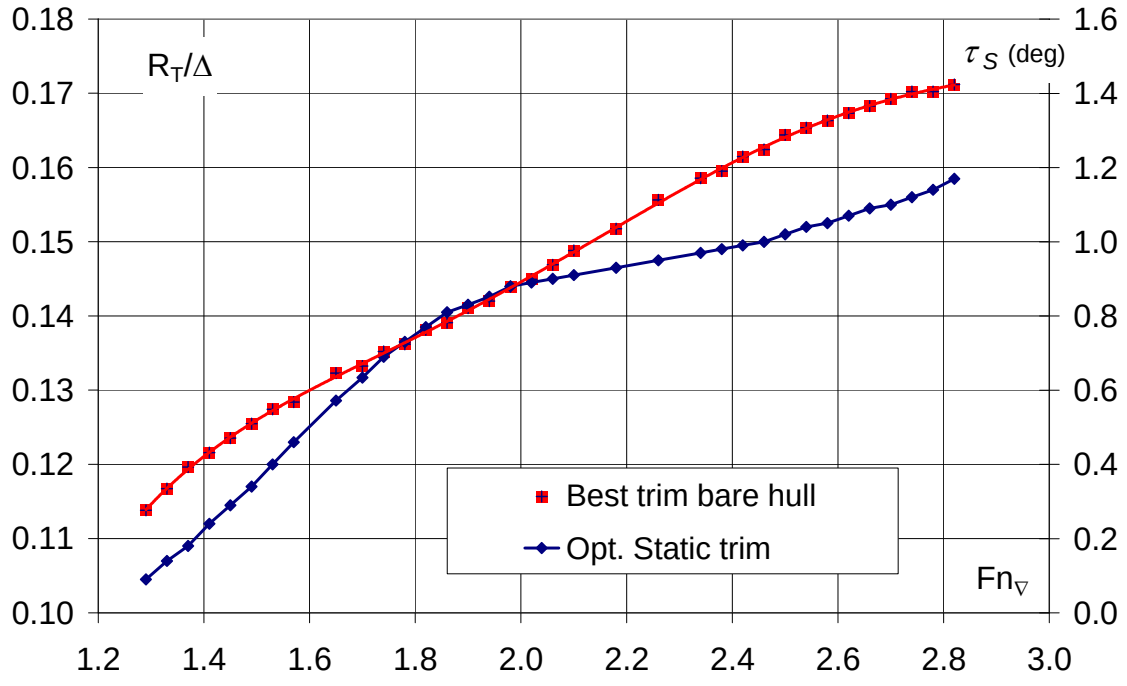

Figure 85 – Best Performance Envelope (BPE)

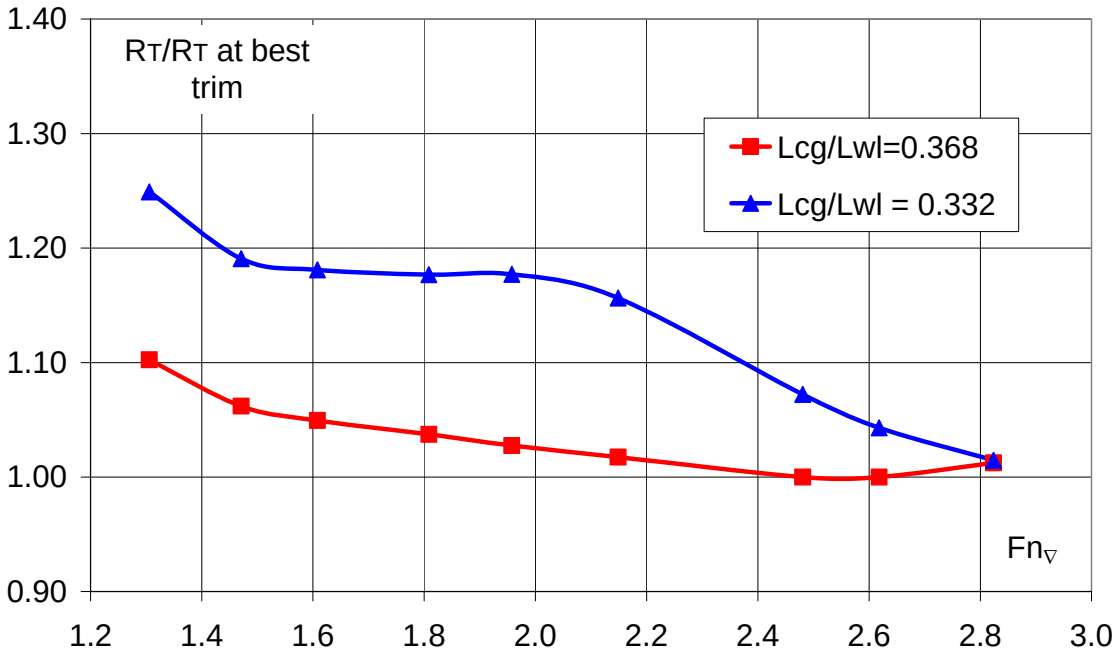

Figure 86 –effectiveness of bare hull C0301 whit respect of BPE

The Figure 86 shows the resistances of the model as fraction of the resistance of the same model sailing with the best position of CG for every single speed.

The Figure 87 and Figure 88 show the comparison between the bare hull (at the best positions of CG for each speed) and the different interceptors arrangements. (conventional and non conventional)

It is important to clarify that the R_{T_i} in figures sown, are related to BPE that represents $R_{T_{best-trim.}}$. BPE is not a resistance curve of a real hull, it represents the performance of the ideal hull that adjusts the CG to the speed. Obviously, such a way to evaluate the effectiveness is strongly precautionary.

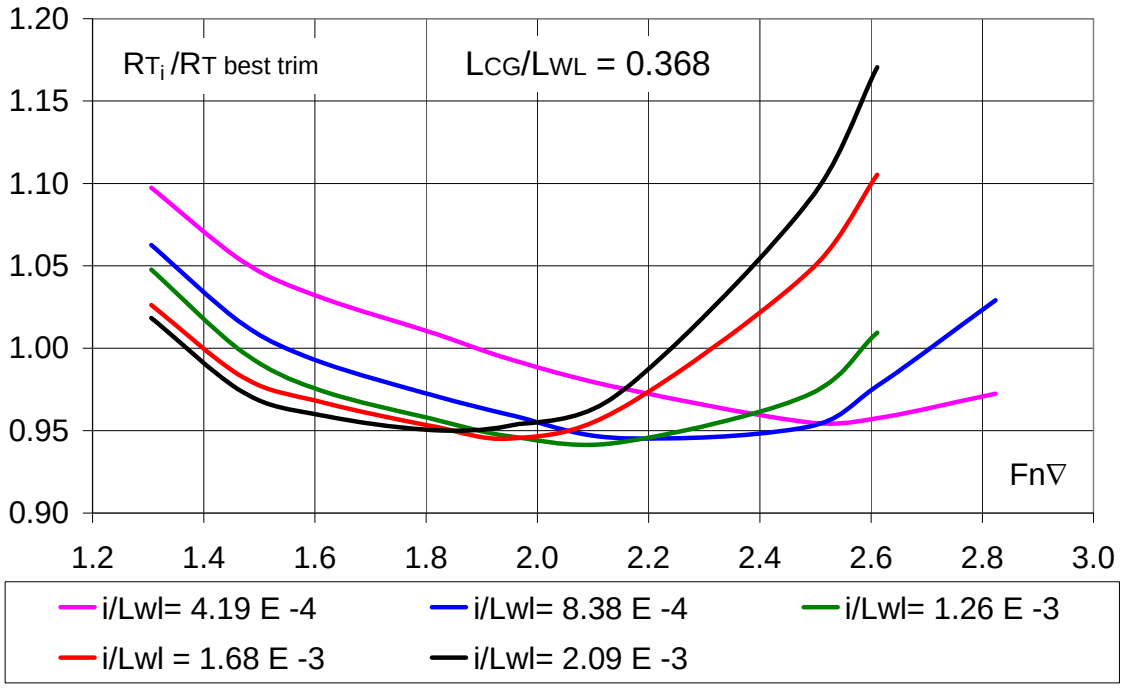

Figure 87 – Effectiveness at differents i/L_{WL} with respect of BPE

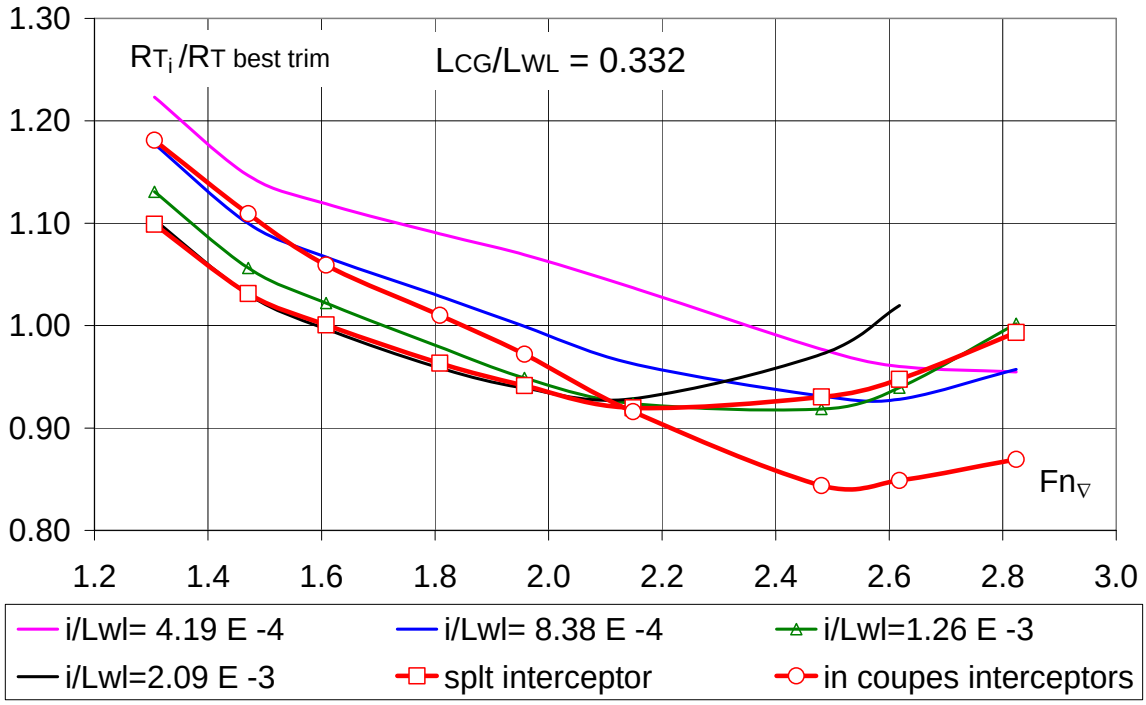

Figure 88 – Effectiveness at differents i/L_{WL} with respect of BPE *(conventional and non conventional in their best configuration)*

The comparison between the performances of the hull with interceptor and those shown with the BPE confirms that the advantages are not only those

linked to the change of the trim, but also to the high lift, otherwise the $R_{Ti}/R_{Tbest\ trim}$ ratio would never be less than 1.

Moreover, the charts above confirm the clear advantages obtained with the reduction of the L_{cg}/L_{WL} ratio, alongside with the increase of the *i* dimension.

10. Constrained trim tests and constrained trim and draught tests

In the previous chapters a frequent distinction has been made, between the effects of interceptor linked to the change of the trim and those linked to the lift of the hull due to an increase in the hydrodynamic lift. This distinction was, so far, only based on an analysis of trims and resistances.

Now, in order to separate the two effects and to have an objective quantification of the single effect on the lift, tests have been carried out by constraining the model trim during the test to some useful positions, with devices of different sizes.

So, during the tests, it has been limited :

- the dynamic trim,
- the speed,

With the interceptor at different positions it has been measured:

- the rising of the hull ΔG
- the hull resistance .

It's worth highlighting that by constraining the trim the advantages obtained can be limited only to the hull rise. I

Table 10 – Constrained test conditions

	i/LWL	Lcg/LWL	τ (deg)	Fn_∇	$L/\nabla^{1/3}$
C 0301	1.26E-3	0.368	3.34	1.96	5.09
C 954	1.75E-3	0.400	1.03	1.91	5.09

The tests with constrained trim have first been performed on C954 and C0301 models, taking into account the trims related to the free-running

conditions shown in Table 10. The speed chosen for the tests is a speed close to the hump resistance $Fn_{\nabla} \cong 2$

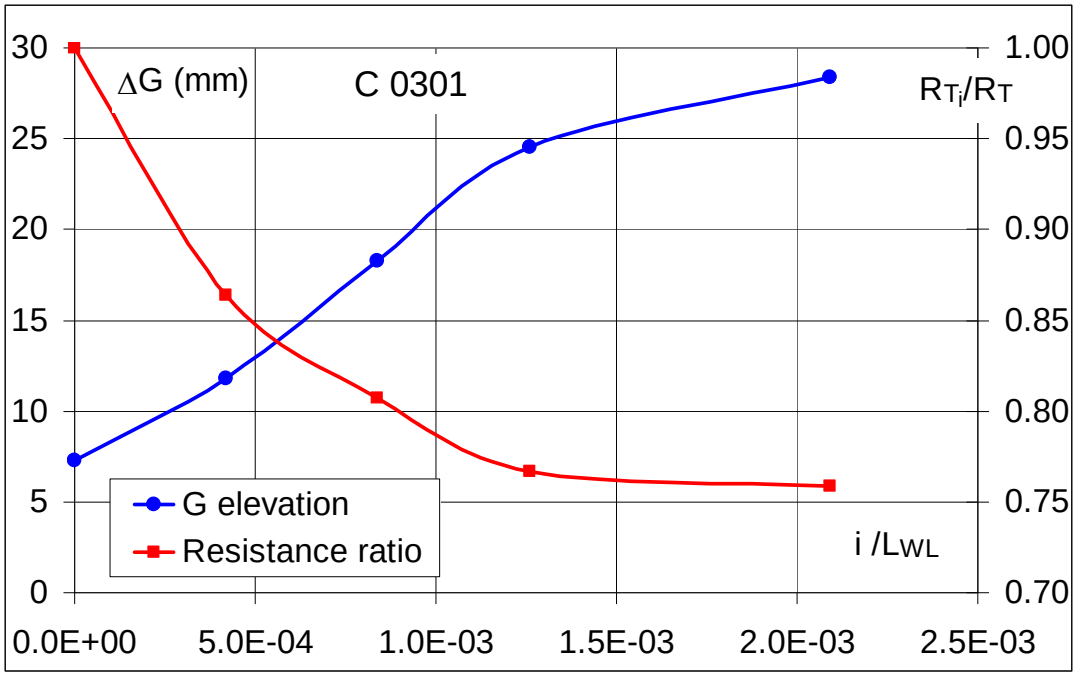

Figure 89 – Fixed trim test.

The chart in Figure 89 refers to the trim during the test (τ = 3.34 deg) measured at Fn_{∇} = 1.96 with the interceptor in a position with *i* = 3 (corresponding to a value of *i*/LWL= 1.26E-3) related to the tests described in previous chapters. This target value was chosen since good performances of the hull during standard tests have been reported with this arrangment. Resistance is expressed in the chart in Figure 89 as the ratio of the hull resistance with *i* = 0 and τ = 3.34 .

The chart shows that an increase in the size of the device corresponds to a significant rising of the hull and, consequently, a reduction of hull resistance. The test has reported that a significant part of the reduction of hull resistance is due to the hydrodynamic rising and not to the change of the trim.

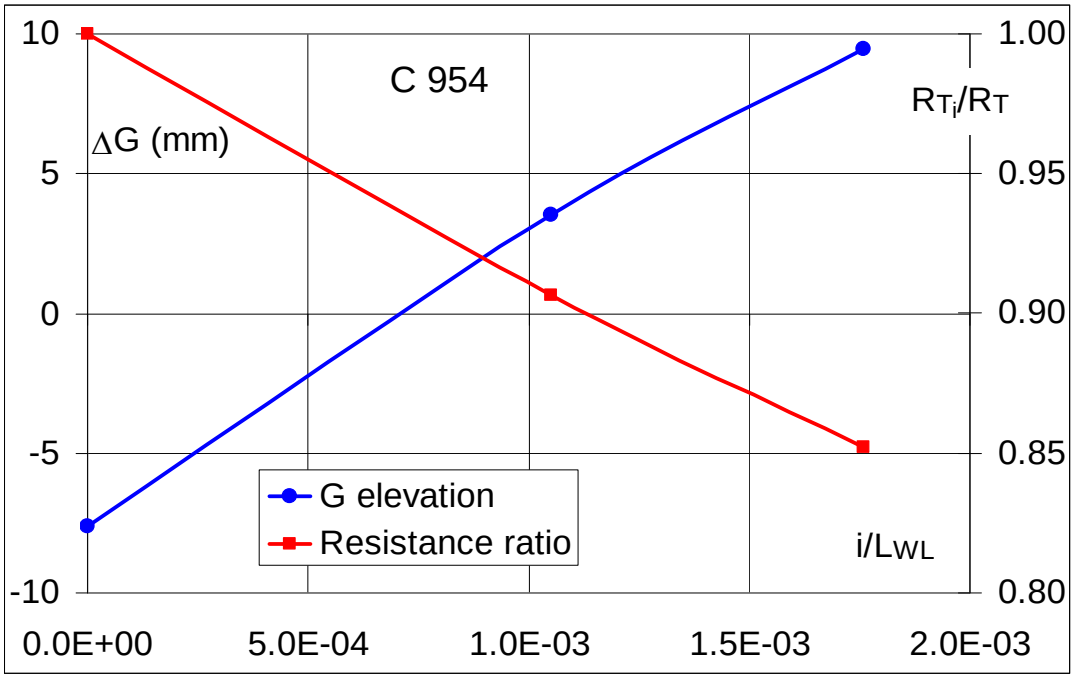

Figure 90 – Fixed trim test

The chart in Figure 90 shows the tests performed on the C954 hull with the same method. Also in this case is possible to observe the strong rising of the hull and a resistance reduction, proportional to the dimension of the device. These are strictly dependent on the high lift effect. It is important to observe that at a constant trim angle the increase of lift implies an increase of induced resistance (lift × tgτ).

At the same time the strong reduction of total resistance and the observed similar wetted area, imply a significant reduction of wave resistance. So, it is inferable that the component of pressure resistance separated from the resistance induced by trim is significantly lower.

In order to estimate the influence of β on this quality, all the three models have been tested at Fn_{∇} = 1.96 keeping constant the value of dynamic trim. In particular, for each model the trim related to the best interceptor performance for L_{CG}/L_{WL} = 0.332 (τ =3.75, 3.49, 3.41 deg respectively for

β = 10, 20, 30 deg) has been chosen. Because of the similar values of τ a direct comparison is significant:

In the chart the rising of centre of gravity of the model is shown and resistances are expressed as fraction of bare hull performances at the same trim condition.

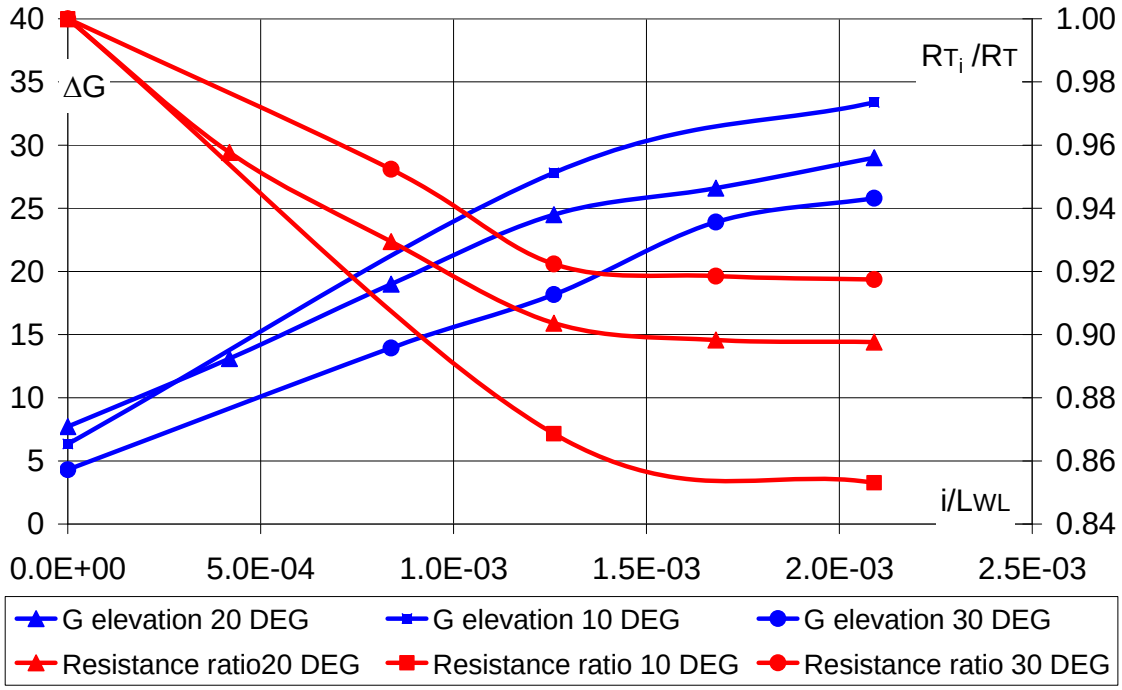

Figure 91 – Fixed trim test

The figure confirms the strong effectiveness of interceptor as high lift device and the dependence of its performances on deadrise angle: as the figure shows, the high lift effects is inversely proportional to the deadrise angle.

A second procedure of constrained tests has been performed, varying the interceptors' dimension, at constant value of trim (like above) and with the same position of the centre of gravity. In other words, the model has been tested in a constrained dynamic position.

The tests have been carried out on 30 deg model (with lower lift effects) at Fn_{∇} = 1.96 and $L/\nabla^{1/3}$ = 5.09

The table below shows the dimensions of the device and the related performances.

Table 11 – Dimensions of Interceptors tested and results.

i (mm)	ΔG (mm)	τ_{din} (deg)	RT (N)	τ_s (deg)	L_{CG}/L_{WL}	Displacement (kg)	Displacement reduction	RT/Δ
5	25.8	3.41	133.0	3	0.332	102.8	0%	0.132
3	25.8	3.41	117.7	2	0.363	90	12%	0.132
0	25.8	3.41	108.2	1	0.396	77	25%	0.138

In Figure 92, the vectors related to the data shown in the table are plotted. The blue and red colours refer to *i* = 5 and *i* = 0 interceptors, respectively. The green vector represents the force to be applied to simulate the interceptor's action.

The relatively forward position of the green vector highlights the great extension of the high lift area and confirms the significant role of the interceptors as high lift devices.

Finally, the extent of the vertical force variation shown in table 3 (25 %) underlines the increase of the induced resistance caused by overpressures.

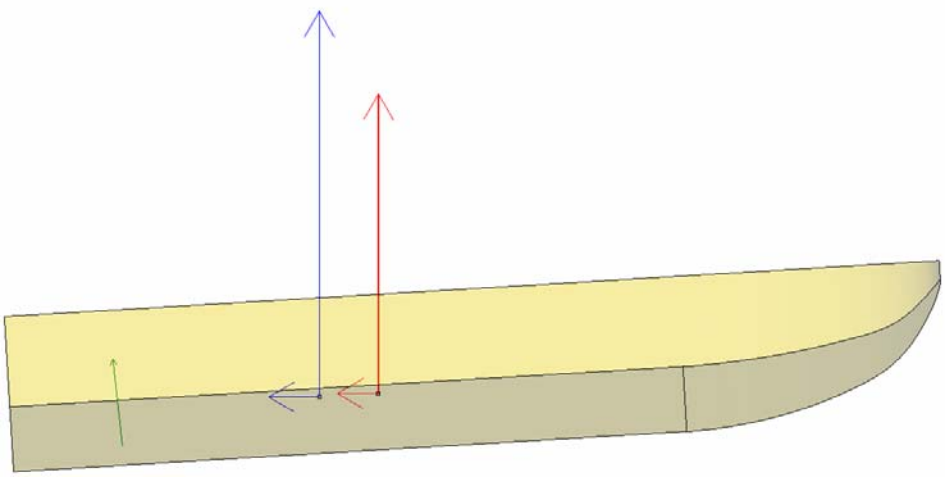

Figure 92 – Fixed test

11. Experimental difficulties

This chapter describes the typical difficulties arising from this kind of experimental tests. First, the main sources of errors for the standard towing tank tests are pointed out. Then, the problem is described focusing on the tests with interceptor (both in terms of reliability of the tests and as for the full scale transfers), up to a final direct evaluation of the reliability of the tests performed.

In this work, as already mentioned above, non totally conventional tests have been chosen: test with constrained trim and with constrained trim and draught. Several are the techniques that can be used in order to perform these tests; this chapter outlines the strategies applied.

11.1 Uncertainty analysys

The precision of a measure is given by the closeness of a mesured magnitude and its actual value. The mistake is given by the difference between the actual value and the one calculated experimentally.

The main sources of errors during the tank tests derive from many variables, such as the precision of the arrangement and construction of the model and the quality of its measurements (speed, resistance and temperature or density etc.).

The total errors are made up of two components: an aleatory one, defined as precision limit and a systemic one, called bias limit.

The ITTC 7.5-02-02-02 procedure recommends a criterion for the estimation of the total error on the resistance coefficient C_T, expressed with the formula 8, and equal to the quadratic sum of the precision limit, formula 11, and the bias limit, formula 9.

8 Total error on the resistance coefficient:

$U_{CT} = (P_{CT}^2 + B_{CT}^2)^{1/2}$

9 Bias Limit:

$$B_{CT}^2 = \left(\frac{\partial C_T}{\partial S} B_S\right)^2 + \left(\frac{\partial C_T}{\partial V} B_V\right)^2 + \left(\frac{\partial C_T}{\partial \rho} B_\rho\right)^2 + \left(\frac{\partial C_T}{\partial R_X} B_{RX}\right)^2$$

with

$$B_\rho = B\rho + \left|\frac{\partial \rho}{\partial T}\right| B_T$$

Below are the explicit partial derivative of the resistance coefficient

10 Partial Derivative of the total resi stance coefficient:

$$\frac{\partial C_T}{\partial S} = \frac{Rx}{0.5\rho V^2}\left(-\frac{1}{S^2}\right) \qquad \frac{\partial C_T}{\partial V} = \frac{Rx}{0.5\rho S}\left(-\frac{2}{SV^3}\right) \qquad \frac{\partial C_T}{\partial Rx} = \frac{1}{0.5\rho S V^2}$$

$$\frac{\partial C_T}{\partial \rho} = \frac{1}{0.5 S V^2}\left(-\frac{1}{\rho^2}\right)$$

11 Precision Limit:

$P_{CT} = k\ sDev/(N)^{0.5}$ with k = 2 and N number of measurements performed.

The aleatory component of the error is strongly linked to the numbers of samples collected during the test and it is inversely proportional to the number of values obtained. The number of samples depends on the frequency of data collect, that is 500 Hz for the towing tank tests performer and by the usable length of the tank. The usable length of the tank depends not only on the speed but also on the acceleration when setting off and braking.

It also depends on the maximum allowable load of the equipments, that is 50 kg during acceleration and 20 kg at a constant speed, with R47.

The acquisition times during the tests ranged from 8 to 35 seconds. Data dispersion (in terms of resistance) mainly depends on the water conditions, that is on the residual disturbance of the water free surface.

Before performing each run, the surface condition of the tank has been assessed, both with a visual check and with an ultrasonic probe. Just as an example Figure 93 shows a chart of the resistance during the execution of a test.

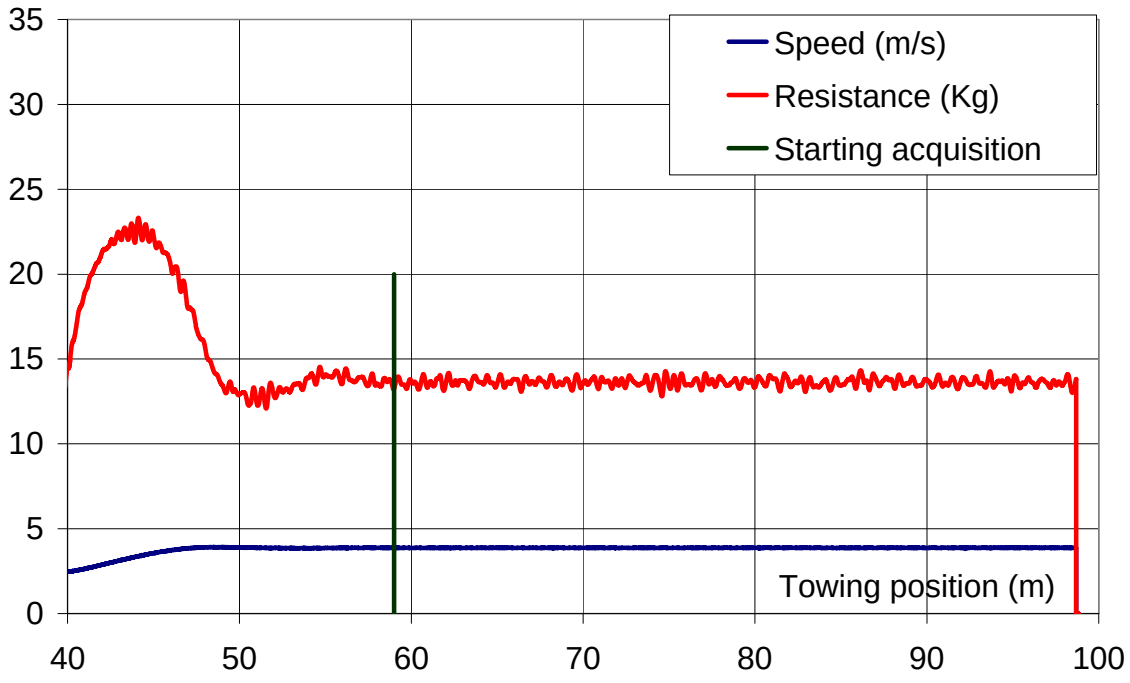

Figure 93 – Resistance and speed of C0301 hull

Density and viscosity are measured indirectly through the measurement of the temperature, as recommended in the ITTC procedures.

The thermometer used during the tests allows a precision of ± 0.5°C in a range of temperatures between -5 and 50°C.

Speed is measured with a wheel of 600.000 mm circumference connected to an encoder making 600 pulses in a single complete turn, this means that 1 mm movement of the tank will correspond to an encoder pulse. The speed measurement implies that the time is calculated with an 80 MHz clock. This

technique allows reaching a high precision of the measurement, since the relative error is equal to the inverse of the square root of the number of calculations (since it's possible to use an estimation of the errors according to the Poisson distribution). Formula 12 contains the linear expression used for the estimation of systemic errors and it is the result of an evaluation made with a measured base.

12 estimation of the maximum errors in speed measurement:

B_v = 5.586 e-4 V - 8.87 e -5

For the calculation of the uncertainty errors, Bs, linked to the geometry of the model, reference is made to the ITTC 7.5-02-02-02 procedure and to the standard manufacturing of the models provided for in the ITTC 7.5-01-01-01 procedure.

The maximum error Bs is given by the quadratic sum of the two components Bs1 and Bs2.

The first refers to the maximum error on the surface, depending on the precision of the model manufacturing, while the second refers to the errors made when assessing the test displacement.

The above mentioned ITTC procedure implies a 1 mm manufacturing uncertainty, this means a maximum error of 2 mm is accepted on length and width by floating and a maximum error of 1 mm by draught. The following values marked with subscripts are those comprised of the error :

$L_{WL}' = L_{WL} + 0.002$; $B_{WL}' = B_{WL} + 0.002$, $T' = T + 1$

Therefore, the estimation of the volume comprised of the error will be as follows:

$\nabla' = C_B B_{WL}' L_{WL}' T'$

Inducing an error in the wetted surface equal to $S - S'$ with

$S' = C_S \sqrt{\nabla' L'_{WL}}$

The increase of the volume implies a draught reduction:

$\Delta T = (\nabla' - \nabla)/A_{WP}$

That will induce a reduction of the wetted surface equal to $S'' = 2L_{WL} * \Delta T$

The value of Bs1 can be calculated as follows:

$Bs1 = S' - S - S''$

The error caused by the displacement measurement is strictly linked to the accuracy of the scale employed to weigh the model and the one used to weigh the ballast (in case a gauged ballast is not available) The maximum error on the displacement will be equal to the quadratic sum of the maximum error of each single weighing of the ballast. The difference between the nominal displacement and the displacement comprised of the error, divided by the density and the area of the waterplane allows an evaluation of the draught variation and the consequent wetted surface variation, induced by the error on the displacement.

$\Delta T = (\Delta' - \Delta) / \rho A_{WP}$

$Bs2 = 2LWL * \Delta T$

whereby

$Bs^2 = Bs1^2 + Bs2^2$

These procedure has been applied for a 121 kg displacement with the C954 hull and the calculation of the C_T coefficient has reported errors of less than 1%.

11.2 Arrangement and preparation of the models for tests and related errors

The models shall be adequately arranged before performing the towing tests.

The main operations to be carried out when starting an experimental test on a new model consist basically in the application of

- Bearings for the guides of the models
- inclinometers
- R47 positioning (or the load cell).

Then, the models are ballasted and trimmed using the distance of the the waterplane from the deck of the model as reference point, conventionally designed parallel to the zero trim waterplane at rest.

This makes it possible to evaluate the trim and the heel without using electronic devices and by measuring the draught of the model, whose value is then compared to the data resulting from the calculations of the hydrostatics.

Once positioned the model for the test and set the equipment on, the trims given by the inertial inclinometers are then recorded so to have an objective point of reference for the following tests (the recorded value won't be useful if the inclinometers are separated from the model); the tests can then be performed.

For the kind of test selected also the error that can be made in the positioning of the interceptor is taken into account. It is thus required to repeat the test several times in order to assure the repeatability of the data.

Below are some comparisons between the data related to resistances and trims repeated for the C954 hull:

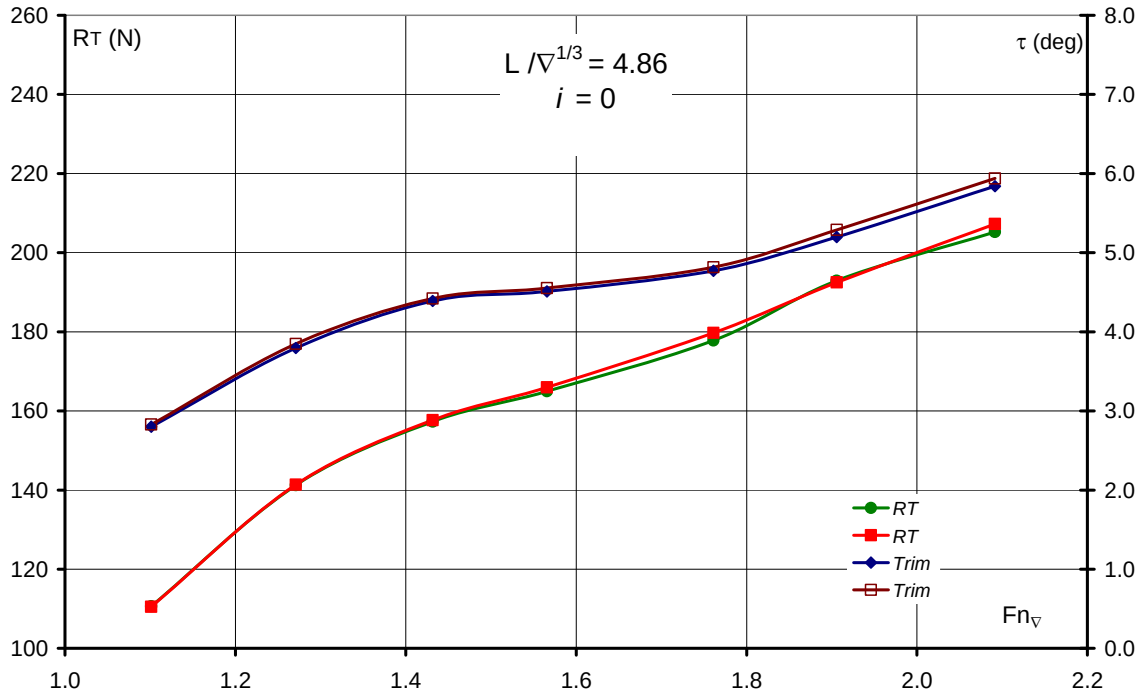

Figure 94 – Repeatability of towing tests, bare hull

The chart in Figure 94 shows the trend of resistances and trims for a towing run and its repetition; the test has been performed after having rearranged the model.

The most critical situation of this hull is the one related to the tests with a proven interceptor dimension of i = 1 mm; with this kind of arrangement it is very likely to make a big percentage mistake in the positioning. The biggest difficulties in the repetition of the tests have been encountered under these conditions; they are represented in the chart below.

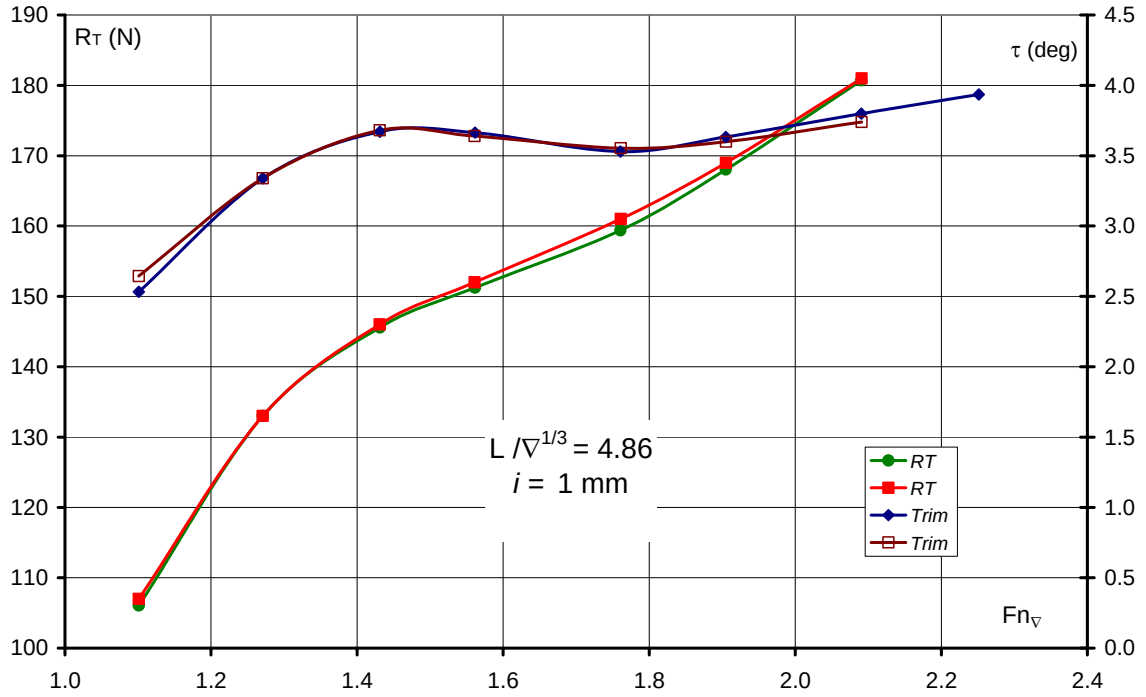

Figure 95 – Repeatability of the towing tests, i = 1 mm

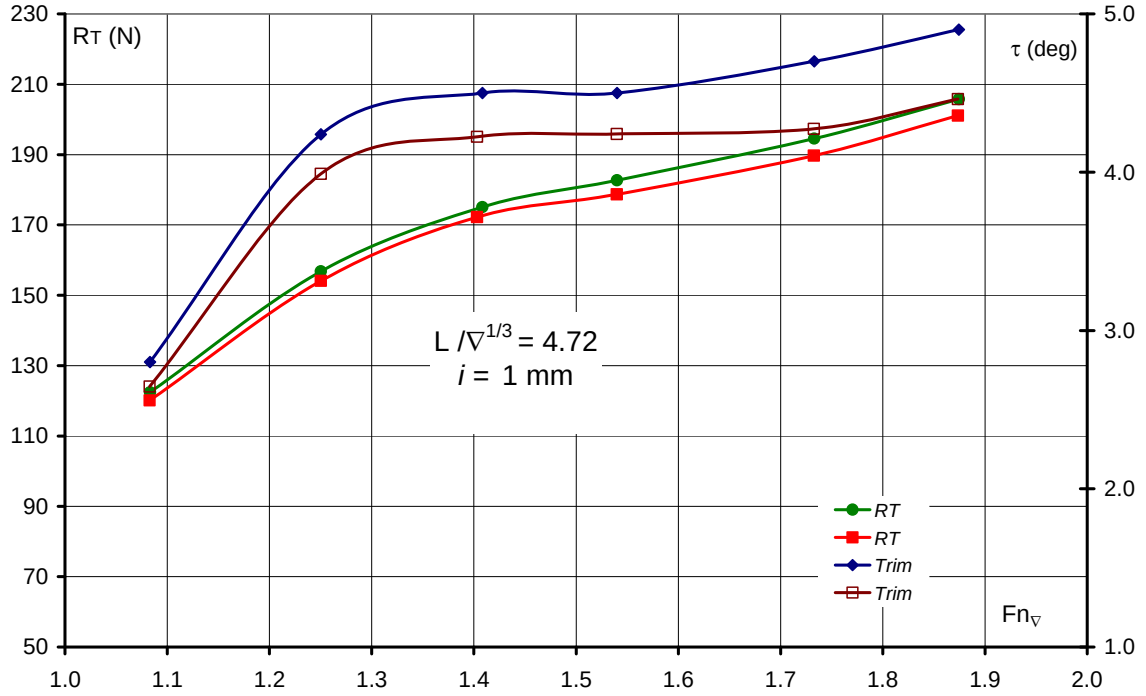

Figure 96 – Repeatability of the towing tests, i = 1 mm

The charts in Figure 95 and Figure 96 compare the runs repeated some days later. In both loading conditions alongside with the usual arrangement procedures, the interceptor has been unmounted and rearranged. The first

chart doesn't show any significant difference, in the second one the error in the positioning of the device has been measured, before performing the repeated test, at -0.35 mm (bigger than the max error allowed). In this case both the resistance and the trim during the repeated test result to be relevantly smaller, according to the data presented in the next paragraph. What observed so far, shows that the positioning of the device is a sensitive issue for the resistances and trims.

11.3 Estimation of the errors in the interceptor positioning.

The interceptor is a thin plate jutting few millimetres out of the stern of the model; it's thus really important to position the device in the best way possible. In order to assess the severity of an error in the positioning of interceptor on a C954 hull, a polynomial of sixth degree has been created, giving the resistance with varying dimension of the interceptor *i and* values of $L/\nabla^{1/3}$ = 4.86 and Fn_{∇} = 1.73, for *i* ranging between 0 and 4.2 mm :

13 towing resistance of the C954 hull with the interceptor varying for $L/\nabla^{1/3}$ = 4.86 and Fn_{∇} = 1.73, *i* 0 ÷ 4.2 mm.

$$Rx = 0.2517\, i^{6} - 3.515\, i^{5} + 17.86\, i^{4} - 38.72\, i^{3} + 31.19\, i^{2} - 16.02\, i + 204.1 \quad (N)$$

$$\frac{\partial Rx}{\partial i} = 1.510\, i^{5} - 17.57\, i^{4} + 71.44\, i^{3} - 116.2\, i^{2} + 62.38\, i - 16.02$$

The error on resistance caused by the interceptor can be synthesized as follows:

14 Maximum error on resistance induced by the positioning of interceptor:

$E_{Rx}(i) = \left|\frac{\partial Rx}{\partial i}\right| e_i$ where e_i is the maximum error due to the positioning of interceptor.

The esteemed maximum error allowed for the positioning of the interceptor is e_i = 0.2 mm

The table shows the relative values in terms of resistance:

Table 12 – Error induced by positioning

e_i = 0.2 mm	
i mm	E_{Rx}
0.4	0.5%
0.8	1.1%
1.2	1.8%
1.6	2.2%
2.0	2.0%
2.4	1.2%
2.8	0.5%
3.2	0.1%
3.6	0.3%
4.0	0.7%
4.2	0.7%

An analysis of the maximum error induced by the positioning of interceptor on a C0301 hull for Fn_∇ comprised between 1.3 and 2.5. and *i* between 0 and 5, L_{CG}/L_{WL} = 0.368 has been carried out. In order to perform the evaluation a polynomial in two variables has been formulated. The following is the kind of polynomial chosen to formulate the data in an accurate and not extremely complicated way:

$$Rx = A_5(Fn_\nabla)i^5 + A_4(Fn_\nabla)i^4 + A_3(Fn_\nabla)i^3 + A_2(Fn_\nabla)i^2 + A_1(Fn_\nabla)i + A_0(Fn_\nabla)$$

with

$$A_i(Fn_\nabla) = a_{i3}\,Fn_\nabla^3 + a_{i2}\,Fn_\nabla^2 + a_{i1}\,Fn_\nabla + a_{i0}$$

That for convenience will be expressed with the vectors and the matrix defined below:

$$\mathbf{(FN_\nabla)}^T = \{1\ FN_\nabla\ FN_\nabla^2\ FN_\nabla^3\};$$

$$\boldsymbol{i}^T = \{1\ i\ i^2\ i^3\ i^4\};$$

$i_i^T = \{0\ 1\ 2i\ 3i^2\ 4i^3\ 5i^4\}$;

$$A = \begin{matrix} 9.021E\text{-}02 & -3.321E\text{-}03 & -1.278E\text{-}01 & 1.037E\text{-}01 & -2.877E\text{-}02 & 2.590E\text{-}03 \\ 2.568E\text{-}02 & 1.960E\text{-}02 & 2.076E\text{-}01 & -1.721E\text{-}01 & 4.816E\text{-}02 & -4.353E\text{-}03 \\ 7.757E\text{-}03 & -1.621E\text{-}02 & -1.209E\text{-}01 & 9.948E\text{-}02 & -2.773E\text{-}02 & 2.502E\text{-}03 \\ -1.881E\text{-}03 & 1.086E\text{-}03 & 2.570E\text{-}02 & -2.000E\text{-}02 & 5.478E\text{-}03 & -4.905E\text{-}04 \end{matrix}$$

Whereby the polynomial can be expressed as the product of the vectors: $F_{N\nabla}$ and i and of the matrix **A**.

15 Polynomial formulation of the resistance of C0301 hull with i varying for L_{CG}/L_{WL} = 0.368

$Rx = (F_{N\nabla})^T A\ i$

Whose partial derivative to i is:

$$\frac{\partial Rx}{\partial i} = (F_{N\nabla})^T A\ i_i$$

Than the error has been evaluated as $E_{Rx}(i) = \left|\frac{\partial Rx}{\partial i}\right| e_i$

The table below lists the relative errors induced by the positioning of the interceptor in the abovementioned field test.

Table 13 – Error induced by positioning

$F_{n\nabla}$	i	Rx	E_{Rx}	$F_{n\nabla}$	i	Rx	E_{Rx}
	mm	N			Mm	N	
1.31	0	133	0.0%	1.31	3	121	1.0%
1.47	0	139	0.0%	1.47	3	126	1.0%
1.61	0	144	0.0%	1.61	3	128	1.1%
1.81	0	150	0.0%	1.81	3	133	1.1%
1.96	0	156	0.0%	1.96	3	136	1.2%
2.15	0	163	0.0%	2.15	3	143	1.0%
2.48	0	173	0.0%	2.48	3	160	0.4%

Fn_∇	i	Rx	E_{Rx}
1.31	1	127	0.9%
1.47	1	133	0.9%
1.61	1	135	1.0%
1.81	1	140	1.1%
1.96	1	143	1.1%
2.15	1	148	1.0%
2.48	1	157	0.4%

Fn_∇	i	Rx	E_{Rx}
1.31	4	119	1.0%
1.47	4	124	1.0%
1.61	4	127	1.1%
1.81	4	132	1.2%
1.96	4	136	1.2%
2.15	4	146	1.0%
2.48	4	172	0.4%

FN_∇	i	Rx	E_{Rx}
1.31	2	123	0.9%
1.47	2	128	1.0%
1.61	2	130	1.0%
1.81	2	135	1.1%
1.96	2	138	1.1%
2.15	2	144	1.0%
2.48	2	157	0.4%

FN_∇	i	Rx	E_{Rx}
1.31	5	118	1.0%
1.47	5	123	1.0%
1.61	5	126	1.1%
1.81	5	132	1.2%
1.96	5	137	1.2%
2.15	5	148	1.0%
2.48	5	179	0.3%

To calculate the values of matrix A a minimum constrained optimization problem has been formulated:

16 minimum constrained optimization problem for the calculation of the coefficients of matrix **A**:

$$\begin{cases} \min_A \Psi \\ |y_i - \hat{y}_i| \le \delta \end{cases} \qquad \Psi = \|\mathbf{y} - \hat{\mathbf{y}}\|^2$$

Where vector **y** represents the set of experimental values and **ŷ** represents the set of solutions to the equation **15** with the experimental data.

The method is reported in Annex I

11.4 Scale effect related to the interceptor

The values reported in previous chapters refer to a model scale. When transferring the values in full scale some errors are made due to the scale effects typical of the kind of test in object.

As widely known, when correlating the towing tank tests through the ITTC'57 procedures, the identity of the Froude number $Fn = V/(gL)^{0.5}$ is

obtained. That is the adimentional coefficient quantifying the intensity of the gravitational forces compared to the inertial ones.

The interceptor works, as said, on the pressure field on the bottom of hull close to the transom. It is made up of a thin plate whose height is smaller than the boundary layer, both in full scale and model scale. Considering, for instance, the models object of study and referring to the Prandtl formulas related to flat plates and turbulent flow, the dimension of the boundary layer obtained will range from 35 to 40 mm. Considering a scaling factor equal to 6, adequate to the tested models (with reference to the data bank shown in Annex II), the thickness of the boundary layer will range from 90 to 110 mm. The interceptor dimensions tested in model scale range from 1 to 5 mm (6 ÷ 30 mm in full scale).

Generally speaking, if we consider the model of boundary layer for a flat plate described with the formulas 21 and a constant Froude's law, the law of variation of the boundary layer in function of the scaling factor is thus obtained:

$\delta = 0.373\ L\ Rn^{-1/5}$ whereby

$\delta_s / \delta_m = L_s / L_m\ (Rn_m / Rn_s)^{1/5}$

The scale factor is $L_s / L_m = \lambda$ and, as the Froude's law suggests, $Vs/Vm = \lambda^{0.5}$

Where magnitude with subscript s refer to ship dimensions and subscript m to model dimensions.

In this way it is possible to obtain what follows:

17 boundary layer thickness scaling factor:

$$\delta_s = \delta_m\ k\lambda^{0.7}$$

Where k is a constant value considering the different viscosity values. Typically 0.85 ÷ 1.45

Also the boundary layer momentum thickness will follow the same law.

As mentioned in [4] the effects of the interceptor on the behaviour of the hulls in different scale are probably correlated with the boundary layer thickness, so in order to avoid scale effects the scaling factor needed is λ instead of $k\lambda^{0.7}$.

The k value, with standard viscosity, is 0.995 and since the exponent 0.7 is very close to 1, it can be considered significant to perform towing tank tests to evaluate the effects of this kind of device. This is frequently done in industrial application.

11.5 Problems connected to the constrained trim and draught tests

The constraint trim tests described in previous chapters, were elaborated in order to calculate resistance and draught of the model with different arrangements of interceptor and with equal trim. This kind of tests can be performed in two different ways:

- Constraining the model to a desired trim and evaluating the Lcg position through a torque measurement.
- Performing different tests allowing the model to freely change trims and draught and varying Lcg up to the desired trim.

The trim tests and the constrained draught and trim tests are useful to evaluate not only the Lcg variations but also the lift variations due to the device.

This kind of tests too can be performed either by constraining the model and measuring forces and moments or changing weight and position of the centre of gravity up to achieving the reference arrangement.

Procedures implying constraints on the degree of freedom make it possible to identify the desired point in one single run; while the second method requires quite long repetitions particularly for the trim tests and the

constrained draught and trim tests. In these procedures several runs may be required in order to identify a single point and a highly sensitive experimenter in order to identify the desired condition.

This second procedure has been chosen, although it's execution is more complex, for two reasons:

- Trims, draughts and resistances can be evaluated with R47, which is renowned for its reliability and is the device used for the tests in object.
- Constraining the model doesn't allow to compensate the gradient of the rails, which though a limited one, can cause several evaluation errors in the calculation of the lift.

So, in order to avoid this kind of errors, a curve has been studied allowing the compensation all along the length of the gradient of the rails, as shown below.

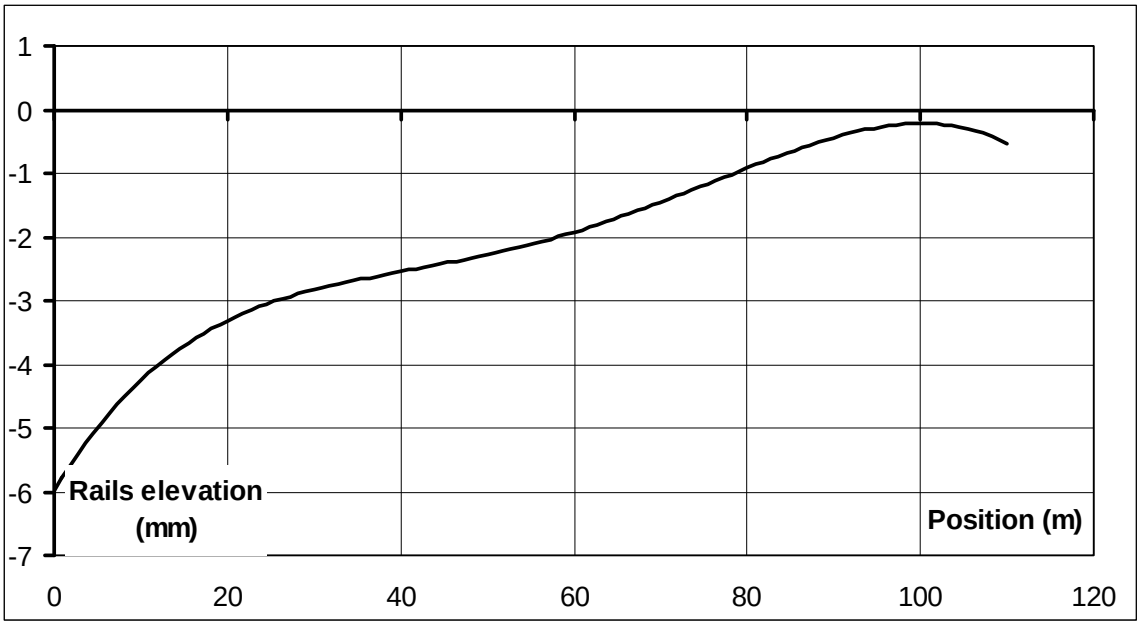

Figure 97 – Rails elevation

12. Displacement hulls.

Due to the hull geometry, the lower speed and, usually, length-displacement ratio on the displacement hulls the actions of the high lift devices are non significant. Nevertheless the interceptors are nowadays often installed on these ships. In order to evaluate the effectiveness of these devices in this field, at the DIN a towing tank tests program is now at the very first stage.

In particular, three models, whose geometrical coefficients and ratios are shown in the table below, have been tested in a typical luxury yacht speed range.

	C 1102/3	C 1103	M 8603
L/B	4.23	4.12	4.43
$L/\nabla^{1/3}$	5.72	5.28	5.45
C_P	0.64	0.64	0.62
C_B	0.43	0.53	0.45
B/T	3.54	3.44	3.74
Forward bulb	Yes	Yes	Yes

The figures below show the good effectiveness of the interceptors also if strictly evaluated as trim controller. Obviously these data have to be compared with the performances of other trim controllers without high lift effects. A consistent and reliable benchmark is available in [9]

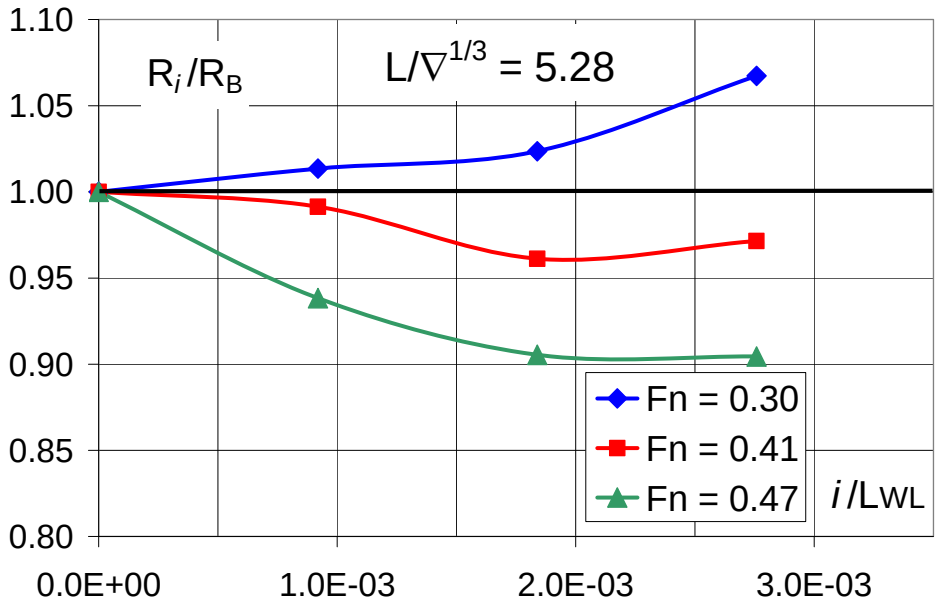

Figure 98 – Effectiveness of interceptor on model C 1103.

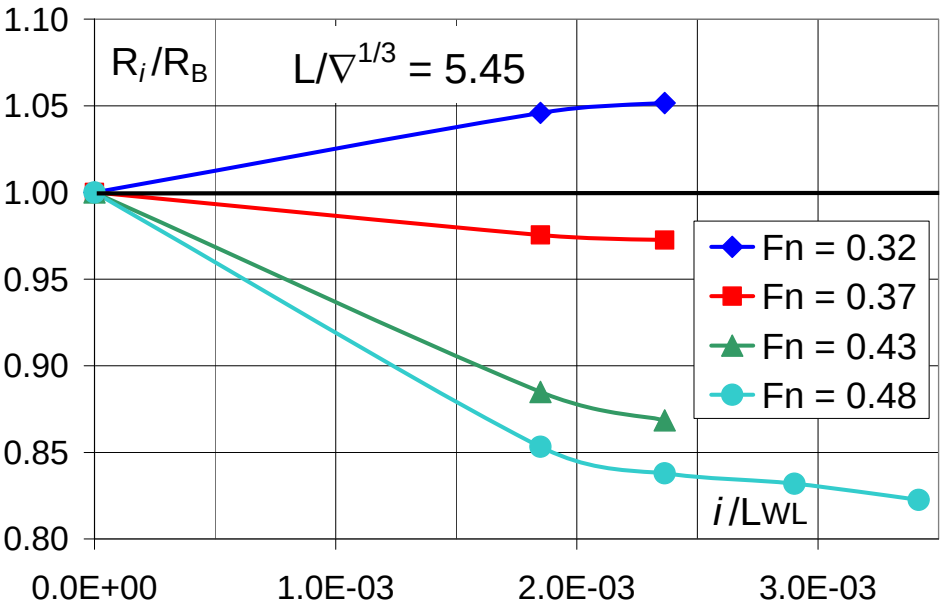

Figure 99 – Effectiveness of interceptor on model M 8603

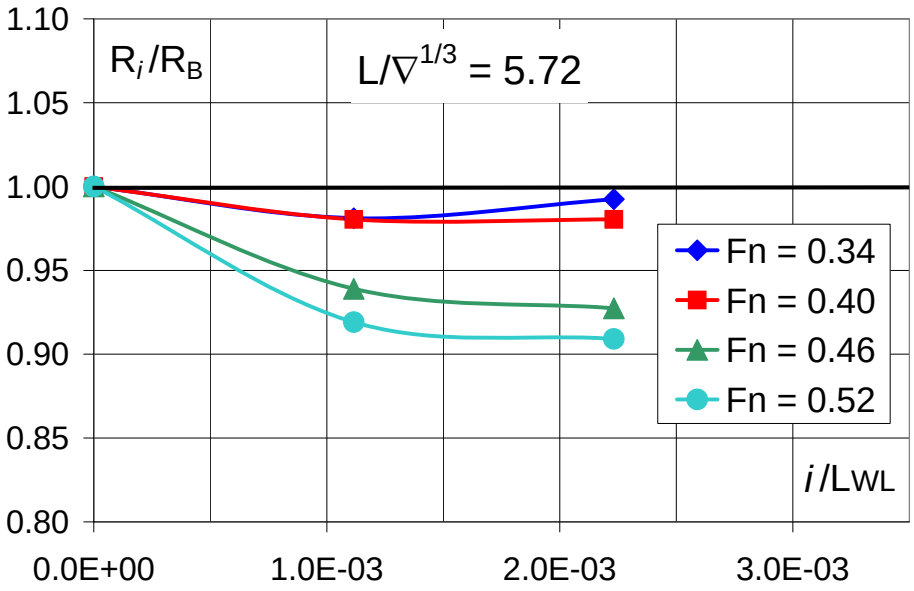

Figure 100 – Effectiveness of interceptor on model C 1102/3

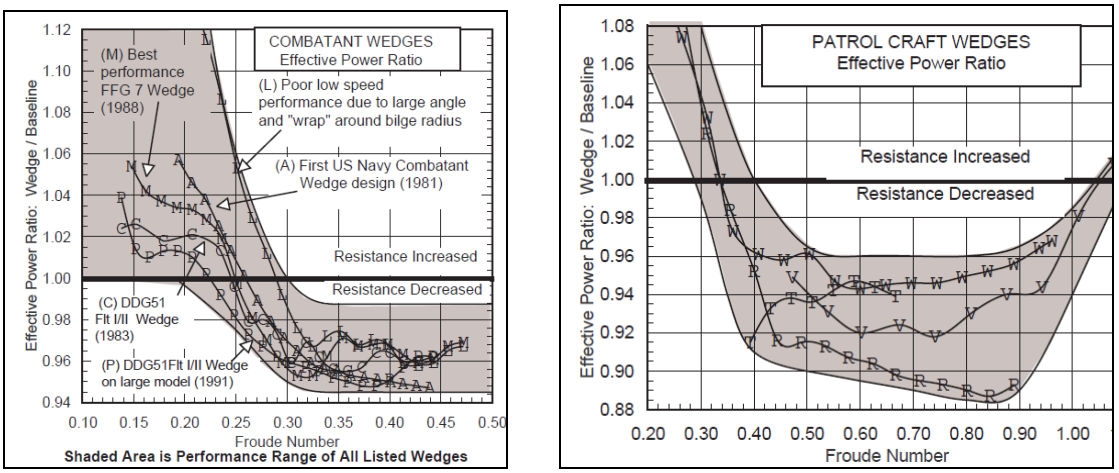

Figure 101 – Figure from Karafiath et al [9]

Comparing the data, with the same Fn range, it can be observed that the interceptors work significantly better than wedges or flaps with Fn > 0.4 .

13. Conclusions

The results obtained have contributed to the formation of an extensive experimental database, also related to several forms of bottom systematically varied.

The large number and the representation of the data allow the transfer of results in project applications, facilitating design activities in the sizing and placement of these devices.

The study allowed to divide and quantify the actions of the interceptor into two components: the trim correction and the high lift generation. Knowledge, even quantitative, of the two components, has promoted the creation of two different non-conventional and innovative systems DIS and SI. The data obtained from experiments on these devices showed great potential for improvement in terms of effectiveness, even taking into account the already excellent performance of conventional devices. Therefore, unconventional interceptors seem to have a future in high speed applications.

Reassuming the considerations expounded can be observed that:

- $\Rightarrow$ performance can be improved by varying appropriately, in an integrated manner, Lcg and the size of the Interceptor;

- $\Rightarrow$ deadrise angle has a strong influence on interceptors' effectiveness: great β implies significant reductions of high lift effect and, consequently, increasing of resistance;

- $\Rightarrow$ the Fn_{∇} range of best performances of the devices are quite not dependent on β values ($1.9<Fn_{\nabla}<2.3$);

⇒ the split interceptor has shown a good effectiveness in a wider range of speed: it seems to be a competitive alternative (in terms of resistance) to the *i*–variable interceptors;

⇒ DIS has generate the best overall performances; comparing the results with a bare hull at same Lcg, it reaches more than 25% of resistance reductions;

⇒ the effectiveness of the interceptors is not only confirmed as trim controller (*i.e.* useful to correct wrong Lcg positions) but is quite effective also comparing it to bare hull performances at best Lcg position;

⇒ first evaluations on interceptor's effectiveness in displacement hull field have been shown the good performance of the device.

Future work on this research will clarify the physical model of interceptors fixed on displacement hull and it will contribute to study in depth the performances of unconventional configurations.

State of the art

The article by Dawson and Blount [2] deals with the practical planning of ships focusing on the trim control. The article contains charts representing an important reference point for the planning of the trend of curvature radius of the Buttoks

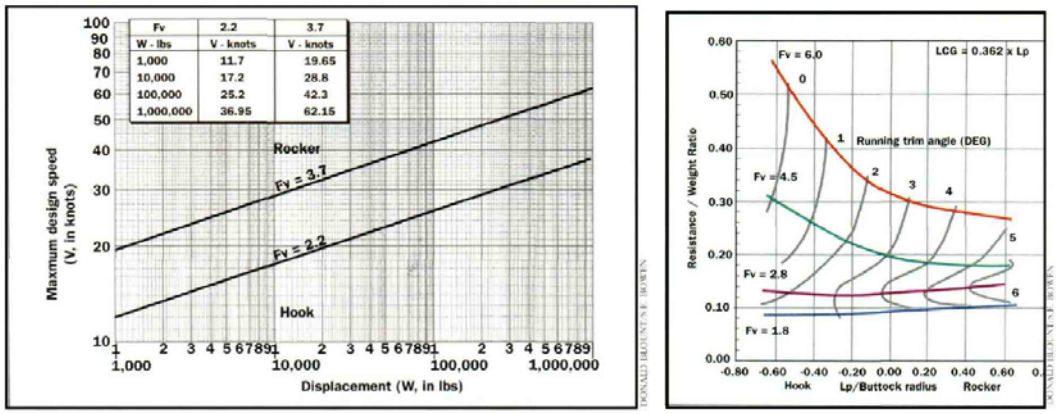

Figure 102 – Figure from Dawson and Blount [2]

The authors also provide an empiric formula to calculate the trimming moment and the following corrective formula to evaluate the effects of interceptor by an equivalent flap.

18 Dawson and Blount Formula to calculate the equivalent interceptor:

$d = Lc \sin\alpha_i$; $\alpha_i = 0.175\ \alpha_t + 0.0154\ \alpha_t^2$

Where d is the interceptor dimension in inches è, Lc is the length of the equivalent flap and α_t is the angle of the equivalent flap in degree (< 15°).

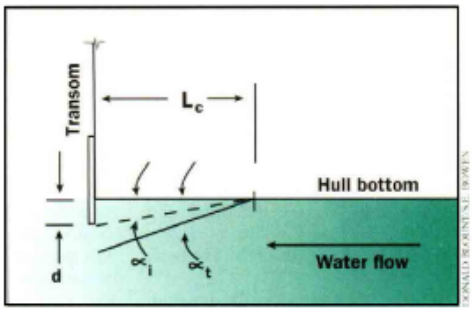

Figure 103 – Figure from Dawson and Blount [2]

Once calculated the equivalent flap it's than possible to calculate the lift and drag with the 19, as already proposed by Savitsky & Brown (1975), once the forces of the trim corrector are known the new trim can be evacuate with 20.

19 Formulas proposed by D & B to evaluate the forces exerted on the flap:

$L = 0.125\ A\ \alpha_t\ V^2$; $D = 0.0052\ L\ \alpha_t \tau$

20 D & B Formula to evaluate the trimming moment:

$M = (W/10{,}000)^{\frac{3}{4}}\ (Lp/Bpx)\ [-1{,}500 + (490\ (Lp/\nabla^{1/3})^2)/(Lp/Bpx)$

Where W is the displacement in pounds , Lp e Bpx are the length and the width cast between the edges and expressed in inches and ∇ is the volume in square feet.

In 2003 a general study on the hydrodynamic functioning of interceptors has been published by S. Brizzolara [3]. This work develops a 2D interceptor model applied to a flat plate. The aim is to give a reference point during the hydrodynamic planning of interceptors based on a simplified model. The field object of the study is the one of big speed ships, that very often show the transom sterns, particularly fitted for this kind of device. The analysis has been carried out on a CFD 2D RANSE model, using the k-ε as Reynolds turbulence model for high numbers.

The model considers an upstream speed range parallel to the plate and following the classical models of boundary layer. The work gives the trend

of the pressure coefficient Cp on the plate and the interceptor with a varying L/*h* ratio (where L is the length of the plate and *h* is the interceptor dimension) with Rn = 1.38 × 10^9 . In this work the author relates the highest value of the pressure coefficient not only to the interceptor height but also to the ratio between height and the boundary layer thickness of the device. Furthermore, a practical model for the prediction and comparison with the actual units is introduced.

2005 Brizzolara e Molini [4] published a further evolution of the work introducing a simplified potential flow mathematical model of the interceptor solved with a transformation of Schwartz-Cristofel;

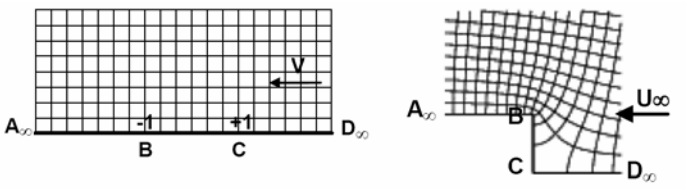

Figure 104 – From Brizzolara e Molini [4]:transformation of Schwartz-Christofel for the solution of the potential model (bottom step.)

The solution is obtained through the transformation, of the semiplane ζ (on the left) to the physical plane z (on the right)

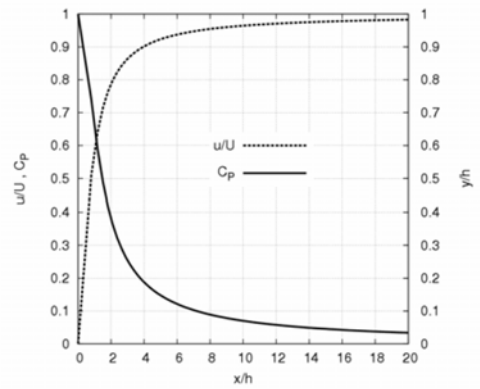

Figure 105 – From Brizzolata 2005: trend of the pressure coefficient and of tspeed in the potential solution.

In order to match the boundary layer momentum thickness and the lift the survey on CFD 2D has been developed; as already in the previous article the upstream speed range refers to the classical model of boundary layer:

the speed range considered follows a distribution as under formula 21, for the boundary layer momentum thickness the classical Prandtl model has been used

21 Speed distribution u/U, boundary layer thickness δ, e equivalent thickness of the momentum, ϑ:

a) $u/U = (y/\delta)^{1/7}$; $\delta = 0.373\ L\ Rn_L^{-1/5}$; c) $\vartheta = 0{,}0363\ L\ Rn_L^{-1/5}$

Where u is the speed modulus within the boundary layer , U is the speed at infinity, y the distance from the plate and L the length of the plate.

In this work, the speed range has been changed by defining a lift variation law as follows:

$L_{b.L} \propto 1 / \vartheta^{4.15 \div 4.3}$

Then, a 3D model flat plate has been created where the device has been set; the data conveyed contain not only information on pressure and lift coefficients, but also on the boundary effects of the device.

2009 S. Brizzolara together with D. Villa published a third work presenting a comparison between flap and interceptor; in this case the flat plate model used up to then was abandoned and a prismatic hull model has been adopted with a 14.6 degrees, 12 m long lift. Finally, the formula proposed by D&B (formula 18) has been used introducing new coefficients calibrated on CFD model.

22 Brizzolara Formula to evaluate the equivalent interceptor and the lift:

$\alpha_i = 0.102\ \alpha_t + 0.0134\ \alpha_t^2$; $L = 0.9344\ \alpha_t\ AV^2$

The values are expressed following the International reference system.

Brizzolara confirms the parabolic trend of α_i towards α_t , changes the coefficients based on a different data base.

An article recognised as one of the most meaningful is "Study on the Compound Effects of Interceptor with Stern Flap for two Fast Monohulls With Transom Stern" [7]. In this study an experimental analysis of the effects of interceptor and flap is proposed, alongside with a configuration combining the two devices, that hasn't shown giving particularly significant results. The data refer to experimental tank tests on two units models: a 20 m long unit, tests in the naval tank of the National Taiwan University and the another 29.5 m long tank tested at the HSVA. The study has reported that an adequate configuration of trim correctors can provide big results in terms of trims and resistance reduction. The study shows the highest effectiveness areas both for the flaps and interceptors and identifies for flaps a condition with $Fn_{\nabla} > 3$ and for interceptors the best working conditions in a speed field ranging between $2 < Fn_{\nabla} < 3$.

2006 on the occasion of the SEA-MED another experimental paper on interceptors has been presented by Mancini and Morioni by the title "Experimental evidences on functioning and use of Intruder". This experimental study has been carried out at the naval tank of the INSEAN and it represents a contribution to the lacking experimental literature on the effects of the device. The paper identifies the best advantages dimensions of the device both in terms of buoyancy length and of calculation of relative speeds when the device offers the best performances ($1 < Fn_{\nabla} < 2.5$). The experimental test carried out in this study highlights a clear advantage obtained by putting the hull down by the stern and setting the device.

As already mentioned in the introduction paragraph, widespread are also industrial applications of this device with a speed range different from the usual one of dynamic lift crafts. 2005 Markku Kanerva from Delta Marine,

at Meriliikenne ja Ympäristö 8.-9.12.2005 Hanasaari, Espoo introduced a work entitled "Energy Saving in Ships" where some solutions for the reduction of hull resistance are described. Among the others, there is a particularly effective solution is the one combining Ducktail-interceptor on the hull of a big fast ferry with low relative speeds of Fn 0.30 ÷ 0.40.

Manufacturing Comanies:

- LA.ME. Nautica
- MIDI- MSI Maritime Dynamics
- Humphree
- Volvo

Licenses

- Olofsson "ARRANGEMENT FOR DYNAMIC TRIM CONTROL OF RUNNING TRIM AND LIST OF A BOAT" US6006689- 28 dic 1999

This license provides the classical configuration of interceptor.

- Steven Loui et al. "VENTILATED FLOW INTERRUPTED IN STEPPED HULL" US20080156246 3 giu. 2008.

This licence presents a device similar to that o fan interceptor set by the step.

Loui et al. In license US7845301B2, US20080210150, US7380514 describe other configurations and positions of the device previously introduced.

Symbols

C_L lift coefficient = lift/$0.5\rho SV^2$

C_P pressure coefficient = $P/0.5\rho V^2$

C_T total resistance coefficient = $R_T/0.5\rho SV^2$

C_R residual resistance coefficient = $R_R/0.5\rho SV^2$

C_F frictional resistance coefficient = $R_F/0.5\rho SV^2$

Fn Froude Number = $V/(gL_{WL})^{0.5}$

Rn Reynolds number = VL_{WL}/ν

ν_s salt water viscosity

ν_0 fresh water viscosity

ρ_s salt water density

ρ_0 fresh water density

U_{CT} total error

P_{CT} precision limit

B_{CT} bias limit

C_B block coefficient

C_p prismatic coefficient

C_S wetted surface coefficient

CG centre of mass

ΔG rising of CG

A_{WP} water plane area

i interceptor height

y forward interceptor height

Ly forward interceptor longitudinal position

Lcg longitudinal position of CG

L_{WL} waterline length

τ_s trim at rest

β deadrise angle

R_T total resistance

R_{T_i} total resistance with interceptor applied

R_R residual resistance

R_F frictional resistance

Acronyms:

BPE Best Performance Envelope

DIN *Dipartimento di Ingegneria Navale di Napoli*

DIS Double Interceptor System

ITTC International Towing Tank Conference

SI Split Interceptor

Annex I

The optimization techniques are used to find out a set of parameters $\mathbf{x} = \{x_1, x_1, \ldots, x_n\}$ where vector $\mathbf{x}$ represents the target variable whose optimum value is pursued.

In the most simple cases this means looking for a maximum or a minimum of a function of the target variable $f(\mathbf{x})$, defined as target function. In the most complex cases the target function can be subject to equation relations $g_i(\mathbf{x}) = 0$ (i = 1,...,n), or inequality $h_i(x) = 0$ (i = 1,...,m) or limit parameters x_l, x_u.:

The general problem, can thus be expressed as follows:

$$\begin{cases} \min_x f(x) \\ h_i(x) = 0 \\ g_i(x) \le 0 \end{cases}$$

The method can be solved through the Karush-Kuhn-Tucker (KKT) equation:

$$\nabla f(x_0) + \sum_{i=1}^{m} \mu_i \nabla g_i(x_0) + \sum_{i=1}^{l} \nu_i \nabla g_i(x_0) = 0$$
$$\mu_i g_i(x_0) = 0, \mu_i \ge 0, i = 1, \ldots, m$$

First, the SQP (sequential quadratic programming) has to be solved in order to obtain the variations of $\mathbf{d}$ vector, where $\mathbf{d}$ is the vector of decreasing directions and $\mathbf{x}^{(k+1)} = \mathbf{x}^{(k)} \alpha\mathbf{d}$ is defined as line search.

SQP is thus as follows:

$$P(d) = F(x^{(k)}) + \nabla F^T\left[x^{(k)}\right] \cdot d + \frac{1}{2} d^T \cdot H^{(k)} \cdot d$$
$$h_i\left[x^{(k)}\right] + \nabla h_i^T\left[x^{(k)}\right] \cdot d = 0 \qquad i = 1, N$$
$$g_i\left[x^{(k)}\right] + \nabla g_i^T\left[x^{(k)}\right] \cdot d \le 0 \qquad i = 1, M$$

It represents an approximation of the problem where the target function is expressed in quadratic form and the relations are linearised.

H rappresents the hessian matrix of the KKT equation:

$$H = \nabla^2 F + \sum_{i=1}^{M} \mu_i \nabla^2 g_i(x_0) + \sum_{i=1}^{N} \nu_i \nabla^2 g_i(x_0)$$

The method used is called Quasi Newton, it defines the down direction as follows:

$\mathbf{d} = -Q\nabla F$

where Q i san approximation of the hessian matrix, using the BFGS (Broyden-Fletcher-Goldfarb,-Shanno) method.

The method used is taken from the study [21]

Below are reported the percentage differences between the experimental data and the value obtained from the polynomial formulation:

Fn_{∇}	*l*	HULL RESISTANCE	ERROR OF THE POLYNOMIAL
	mm	N	
1.31	0	133	0.2%
1.47	0	139	0.4%
1.61	0	144	0.1%
1.81	0	150	0.3%
1.96	0	156	0.3%
2.15	0	163	0.4%
2.48	0	173	0.1%
1.31	1	127	0.2%
1.47	1	133	0.4%
1.61	1	135	0.0%
1.81	1	140	0.2%
1.96	1	143	0.2%
2.15	1	148	0.3%
2.48	1	157	0.1%
1.31	2	123	0.1%
1.47	2	128	0.4%
1.61	2	130	0.1%
1.81	2	135	0.2%
1.96	2	138	0.0%
2.15	2	144	0.1%
2.48	2	157	0.0%
1.31	3	121	0.2%
1.47	3	126	0.3%
1.61	3	128	0.1%
1.81	3	133	0.1%
1.96	3	136	0.1%
2.15	3	143	0.2%
2.48	3	160	0.0%
1.31	4	119	0.1%
1.47	4	124	0.2%
1.61	4	127	0.2%
1.81	4	132	0.1%
1.96	4	136	0.5%
2.15	4	146	0.4%
2.48	4	172	0.1%
1.31	5	118	0.0%
1.47	5	123	0.1%
1.61	5	126	0.0%
1.81	5	132	0.1%
1.96	5	137	0.0%
2.15	5	148	0.0%
2.48	5	179	0.0%

Annex II

name	type	year	shipyard	LOA	L_{WL}	B	T	B/T	L/B		displ.	$L/\nabla^{1/3}$		Vs max	Vs cruice	Fnv max	Fn_{∇} cruice	Fn max	Fn cr	Origin
				m	m	m	m				t			Kn	Kn					
47-foot CG4700	sar	1997		14.1		4.2	1.2	3.5	2.91		20	4.466		27	20	2.70	2.00	1.27	0.94	art. sname transactionvol.98
RB-01	sar	2003	Lung-teh	19		5.6	1.1	5.09	2.94		43	4.662		25	21	2.20	1.85	1.01	0.85	speed at sea feb'03
Gad Rausing	sar	2003	SSRS staff	20			0.9		N.A.			N.A.		36.7	32	N.A.	N.A.	1.45	1.26	DIN Database
karft	sar	2002	Brodosplit	18.2		5.9	1.6	3.69	2.67			N.A.			24	N.A.	N.A.	N.A.	0.99	ship&boat nov. '02
kegki	sar	2002	Madenci	17					N.A.			N.A.		30		N.A.	N.A.	1.28	N.A.	speed at sea feb.'03
Van Koss	sar	2003		23					N.A.			N.A.		25		N.A.	N.A.	0.92	N.A.	speed at sea feb.'03
16.5	sar	1996		16.5					N.A.		28.4	4.649		20		1.89	N.A.	0.87	N.A.	DIN Database
Lysekil	pilot	1996		16					N.A.		24	4.768				N.A.	N.A.	N.A.	N.A.	ship&boat jul/aug'97
14.6	pilot	1996		14.6					N.A.			N.A.		25	20	N.A.	N.A.	1.15	0.92	ship&boat ottobre '97
Virginia'pilot	pilot	1996	Gladding hearn	15.4		5.1			2.62			N.A.		25	22	N.A.	N.A.	1.12	0.99	ship&boat gen/feb. '97
Dicovery class	pilot	1993	Engelear	21		6.3	1	6.3	2.89		33	5.628		28		2.58	N.A.	1.08	N.A.	ship&boat gen/feb. '97
Strait falcon	pilot	1997	camarc	16		4.8			2.89		27	4.585		21	18	2.00	1.71	0.93	0.79	DIN Database
17.2	pilot	2000	camarc	17.2		4.6	0.8	5.75	3.24			N.A.		35	32	N.A.	N.A.	1.49	1.36	ship&boat gennaio/feb. 2000
22.7	pilot	2001		22.7		6			3.28			N.A.		26		N.A.	N.A.	0.96	N.A.	DIN Database
cp 265	patrol boat	2001	Rodriquez	25		5.76	0.94	6.13	3.76			N.A.		34		N.A.	N.A.	1.20	N.A.	ship&boat aprile. 2001
15	pilot	1994		15		4.2	1.33	3.16	3.10		22.6	4.561		19		1.86	N.A.	0.87	N.A.	DIN Database
sar	sar	2000	vittoria	15	12.8				N.A.		20	4.677		41		4.10	N.A.	1.88	N.A.	DIN Database
P100	patrol boat	1999	vittoria	17.4	15				N.A.		21	5.392		44		4.37	N.A.	1.87	N.A.	DIN Database
RIB	sar	1995	vittoria	16.4	14.1				N.A.		23	4.917		70		6.85	N.A.	3.06	N.A.	DIN Database
P66	patrol boat	1992	vittoria	16	13.8				N.A.		16	5.432		51		5.30	N.A.	2.26	N.A.	DIN Database
Eiswette	sar	1990		23.2		5.5			3.66		30	6.419		20		1.87	N.A.	0.73	N.A.	DIN Database
Otto Schulke	sar	1990		18.9		4.3			3.81		25	5.557		16		1.54	N.A.	0.65	N.A.	DIN Database

name	type	year	shipyard	LOA m	L_{WL} m	B m	T m	B/T	L/B	disl. t	$L/\nabla^{1/3}$	Vs max Kn	Vs cruice Kn	Fnv max	Fn_{∇} cruice	Fn max	Fn cr	Origin
Paul Denker	sar	1990		16.8		4			3.64	25	4.939	15		1.45	N.A.	0.65	N.A.	DIN Database
Skomvaer III	sar	1990		19.5		5.8			2.91	34	5.175	26		2.38	N.A.	1.04	N.A.	DIN Database
Aril	sar	1990		14		4			3.03	28	3.963	20		1.89	N.A.	0.94	N.A.	DIN Database
Bill Jinkins	sar	1990		17.1		5.2			2.85	27	4.900	35		3.33	N.A.	1.49	N.A.	DIN Database
17.6 M Lifeboat	sar	1990		17.7		4.6			3.34	25	5.204	16		1.54	N.A.	0.67	N.A.	DIN Database
15 M Lifeboat	sar	1990		15.2		4.6			2.86	20	4.814	16		1.60	N.A.	0.72	N.A.	DIN Database
Watson	sar	1986		14.3		3.9	0.84	4.64	3.18	24.5	4.233	9		0.87	N.A.	0.42	N.A.	DIN Database
Clyde	sar	1986		21.6		4.6			4.07	35	5.677	11		1.00	N.A.	0.42	N.A.	DIN Database
Arun	sar	1986		16.3		5.2	1.5	3.47	2.72	31.5	4.437	18		1.67	N.A.	0.79	N.A.	DIN Database
Barnet	sar	1986		15.8		4.1	1.05	3.9	3.34	28.5	4.447	9		0.85	N.A.	0.40	N.A.	DIN Database
Thames	sar	1986		15.3		4.4	1.15	3.83	3.01	29	4.281	18		1.69	N.A.	0.81	N.A.	DIN Database
Solent	sar	1986		14.4		4.3	1.05	4.1	2.90	28.5	4.053	9		0.85	N.A.	0.42	N.A.	DIN Database
Oakley	sar	1986		14.8		4.3	1.05	4.1	2.98	31.5	4.029	9		0.84	N.A.	0.41	N.A.	DIN Database
Tyne	sar	1986		14.3		4.3	1.07	4.02	2.88	26	4.150	17.5		1.68	N.A.	0.82	N.A.	DIN Database
64'FLB	sar	1990		19.5		4.3	0.93	4.62	3.93	27.5	5.554	17.5		1.66	N.A.	0.70	N.A.	DIN Database
Trent	sar	1992		14		4.6	1.15	4	2.64	28	3.963	27		2.56	N.A.	1.27	N.A.	DIN Database
Severn	sar	1990		17		5.6	1.4	4.09	2.63	38	4.347	25		2.25	N.A.	1.07	N.A.	DIN Database
Canot 1	sar	1990		17.6		4	0.93	4.3	3.81	22.5	5.359	22		2.16	N.A.	0.93	N.A.	DIN Database
Canot 2	sar	1990		15.5		4	0.71	5.63	3.36	20	4.909	21		2.10	N.A.	0.94	N.A.	DIN Database
15.1	sar	1995		15.1		4.7	1.7	2.76	2.78	38	3.861	10		0.90	N.A.	0.45	N.A.	DIN Database
J.F.	sar	1995		15.6		4.8	0.85	5.65	2.82	16	5.322	35		3.64	N.A.	1.56	N.A.	DIN Database
16m	sar	1995		16.2		5.2	1.65	3.15	2.70	25	4.763	34		3.28	N.A.	1.49	N.A.	DIN Database
300A	sar	1995		15.8		5.2	1.4	3.71	2.63	29.5	4.396	21		1.97	N.A.	0.93	N.A.	DIN Database
Res Cruiser	sar	1995		18.9		4.3	1.26	3.41	3.81	30	5.229	16		1.50	N.A.	0.65	N.A.	DIN Database
US 1 Surf Res.	sar	1995		14.6		4.2	1.3	3.33	3.01	18.3	4.763	27		2.74	N.A.	1.25	N.A.	DIN Database
D'star D-mark	pilot	1995		14.7		4.6			2.77	18.5	4.778	37		3.75	N.A.	1.70	N.A.	DIN Database
Voyager	pilot	1995		18.6		6.3			2.56	29.3	5.187	28		2.63	N.A.	1.15	N.A.	DIN Database

name	type	year	shipyard	LOA	L_{WL}	B	T	B/T	L/B	disl.	$L/\nabla^{1/3}$	Vs max	Vs cruice	Fnv max	Fn_{∇} cruice	Fn max	Fn cr	Origin
				m	m	m	m			t		Kn	Kn					
Scirocco	offshore provider			15.1		6.3	0.9	7	2.08		N.A.	23	19	N.A.	N.A.	1.04	0.86	DIN Database
Tiger	pilot			11.9	10.6	4.1	0.6	6.83	2.59	10.8	4.756	33	26	3.66	2.88	1.66	1.31	DIN Database
St.ursula	Patrol boat			16.76		4.9			2.98	17.7	5.529	32	28	3.27	2.86	1.38	1.21	DIN Database
Pilot 790	Patrol boat			16.9	13.25	4.6	0.90	5.11	2.88	22.5	4.655	37	32	3.63	3.14	1.67	1.44	DIN Database
Carabinieri classe 800	Patrol boat			17		5.0	1.9	2.7	2.95	25.9	4.939	35	25	3.36	2.40	1.50	1.07	DIN Database
Eiswette	Rescue Fleet			23.3		5.6			3.58	66	4.956		20	N.A.	1.64	N.A.	0.73	DIN Database
Theo Fischer	Rescue Fleet			23.1		6.0			3.34	80	4.609		23	N.A.	1.83	N.A.	0.84	DIN Database
H. J. Kratschke	Rescue Fleet			18.9		4.3			3.81	35	4.967		16	N.A.	1.46	N.A.	0.65	DIN Database
FF70	fire fighting		vittoria	23	20.6				N.A.	70	4.957	34	22	2.76	1.79	1.23	0.80	DIN Database
Express 4	fast crew utility		SBF, Australia	20.8	18.77	4.8	1.1	4.49	3.91		N.A.	26	25	N.A.	N.A.	0.99	0.95	DIN Database
Jelfar	fast ferry		Wuhan Nanhua	18	16.028		0.8		N.A.	23	5.590	22.5		2.20	N.A.	0.92	N.A.	DIN Database

Annex III

Resistance dynamometer with transducers for measurement of the alteration draught and trim R 47 – KEMPF & REMMERS GMBH * HAMBURG

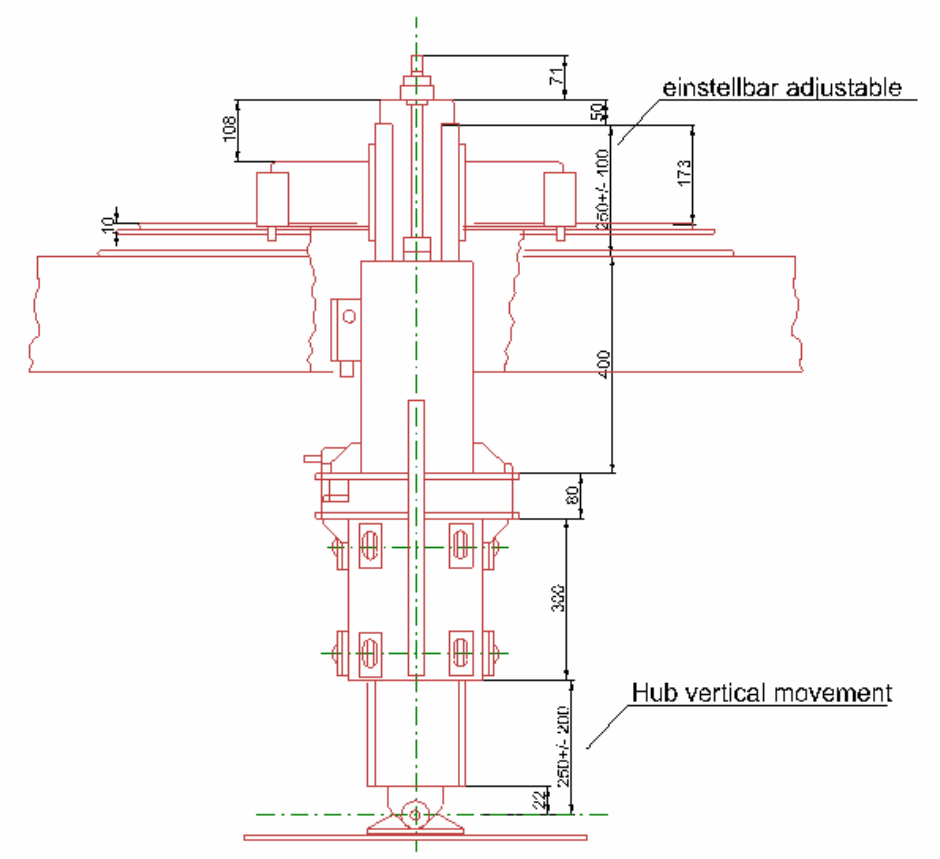

References

References are divided into 5 different subparagraphs:

- Main References.
- Related Pubblication.
- Autor References.
- Reference Book.
- ITTC recomanded procedures and Guidelines- Testing Metods

The first paragraph lists the main reference bibliography, whose contents are described in the previous chapters.
The secondo paragraph lists other publications about the subject of the thesis.
The third one lists the author's publications on the subject.
The fourth and fifth paragraphs quote the reference publications containing the general knowledge and the main ITTC procedures related to tests carried out.

Main References

[1] Savitsky D. 1964 "Hydrodynamic design of planing hulls", Marine Tecnology, 1, 1, pp 71-95

[2] Dawson D, Blount D.L. "Trim Control" Professional Boat Builder N°75, feb-mar 2002, pp. 140-149

[3] S. Brizzolara "Hydrodynamic Analisys of Interceptors With Cfd Metods" Proceedings FAST 2003, Ischia, Italy

[4] . S Brizzolara, A. Molini (2005). "Hydrodynamics Of Intercepors: A Fundamental Study", Proceedings ICMRT 2005, Int. Conference on Maritime Research and Transportation. Ischia (Naples), Italy. (vol. 1).

[5] S .Brizzolara, D. Villa "A Systematic Cfd Analysis Of Flaps / Interceptors Hydrodynamic Performance" Proceedings 10th International Conference on Fast Sea Transportation (FAST 2009), Athens, October 2009.

[6] A.Mancini, A. Morioni "Riscontri Sperimentali sul Funzionamento e l'Utilizzo dell'Intruder" Proceedings SEA-MED 2006, Messina, July 2006

[7] J.F.Tsai, J. L. Hwang and S.K. Chou "Study on the Compound Effects of Interceptor with Stern Flap for two Fast Monohulls With Transom Stern" Proceedings FAST 2003, Ischia, Italy

[8] Markku Kanerva "Energy Saving in Ships" Meriliikenne ja Ympäristö 8.-9.12.2005 Hanasaari, Espoo

[9] G. Karafiath , D .Cusanelli, and Lin C. Wen, "Stern Wedges and Stern Flaps for Improved Powering – U.S. Navy Experience", The Society of Naval Architects and Marine Engineers, 1999 Annual Meeting Preprints

Related publication

[10] Dina H. Kowalyshyn (AM), and Bryson Metcalf (V) "A USCG Systematic Series of High Speed Planing Hulls "Transaction SNAME 114, 2006

[11] S. Bruckner , C. Ighina, A. McKay, A. Migali, A. Sverchkov, Krylov "Experimental Evaluation of the Effect of Interceptor and Side Keels on the Longitudinal Stability of a Stepped Hull"

[12] D. Savitsky & P. W. Brown "Procedures for Hydrodynamic evaluation of planing hulls in smooth and rough water" Proceeding of Hampton Road Section, SNAME November 1975

[13] J. Almeter, "Avoiding Common Errors in High-Speed Craft Powering. Predictions" proceedings HIPER'08, Naples 18th-19th September 2008.

[14] M.J. Hughes "Seakeeping Simulations for High-Speed Vessels with Active Ride Control Systems" ", proceeding, HPER '10 Melbourne, Fl USA 13-15 ott 2010

[15] D. Savitsky M. Morabito "Surface Wavw Conturs Associated With the Forebody Wake of Stepped Planing Hulls" Marine Tecnology Vol 47, No1 January 2010

[16] C.P.Van Dam; D.T. Yen; Vijgen, P. (1999). "Gurney flap experiments on airfoil and wings". Journal of Aircraft(0021-8669) 36 (2): 484-486.

Autor References:

[17] F. De luca, C. Pensa, A. Pranzitelli "Valutazione Sperimentale e Numerica del Funzionamento degli Interceptor", proceeding, SEA-MED 2010, Messina, Italia 2 luglio 2010.

[18] F. De Luca, C. Pensa, A. Pranzitelli "Experimental and Numerical Investigation on Interceptors' Effectivenes", proceeding, HPER '10 Melbourne, Fl USA 13-15 ott 2010.

[19] F. De Luca, C. Pensa "Experimental data on Interceptors' Effectiveness", proceedings, 9th symposium on High Speed Marine Veicles Napoli, Italia 25-27 maggio 2011 pp.7

[20] F. De Luca, C. Pensa "Influence of deadrise angle and interceptors' shape and position on resistance reduction" proceedings, First International Symposium on Naval Architecture and Marittime 24-25 October 2011, Yildiz Technical University, Istanbul, Turchia.

[21] F. Balsamo F. De Luca C. Pensa "A New Logic for Controllable Pitch Propeller Management", proceeding, 14th International Congress of International Maritime of the Mediterranean, Genova, Italia 13-16 sett. 2011

Reference Books

E.V. Lewis "Principles of Naval Architect vol 2", SNAME

Frank M. White, "Fluid Mechanics 4th Edition" McGraw-Hill

Katz & Plotkin "Low Speed Aerodynamics" McGraw-Hill

ITTC recommended procedures and Guidelines- Testing Metods

High Speed Marine Vehicles Resistance Tests	ITTC 7.5-0-05-01
Model Manufacture Ship Models	ITTC 7.5-01-01-01
Resistance Uncertainty Analysis	ITTC 7.5-02-02-02